United States
Environmental Protection
Agency

Environmental Sciences Research
Laboratory
Research Triangle Park NC 27711

EPA-600/4-78-041
July 1978

Research and Development

EPA

Flow Structure and Turbulent Diffusion Around a Three-Dimensional Hill

Fluid Modeling Study on Effects of Stratification Part I. Flow Structure

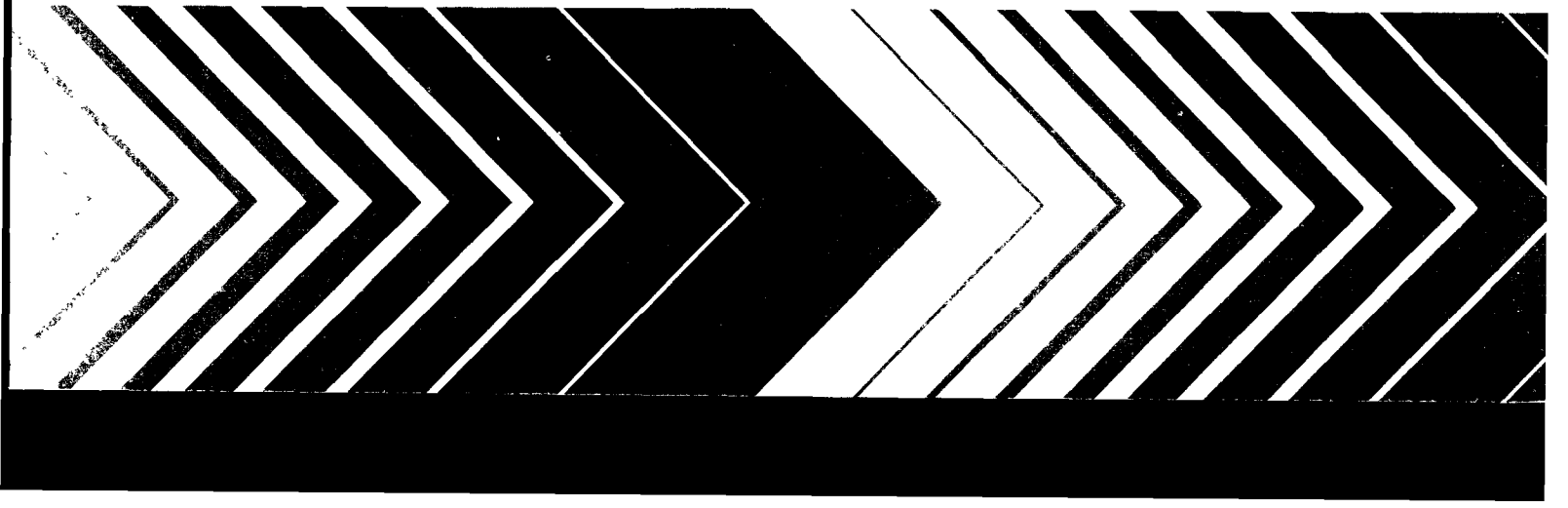

RESEARCH REPORTING SERIES

Research reports of the Office of Research and Development U S Environmental Protection Agency, have been grouped into nine series These nine broad categories were established to facilitate further development and application of environmental technology Elimination of traditional grouping was consciously planned to foster technology transfer and a maximum interface in related fields The nine series are

1 Environmental Health Effects Research
2 Environmental Protection Technology
3 Ecological Research
4 Environmental Monitoring
5 Socioeconomic Environmental Studies
6 Scientific and Technical Assessment Reports (STAR)
7 Interagency Energy-Environment Research and Development
8 Special Reports
9 Miscellaneous Reports

This report has been assigned to the ENVIRONMENTAL PROTECTION TECHNOLOGY series This series describes research performed to develop and demonstrate instrumentation, equipment, and methodology to repair or prevent environmental degradation from point and non-point sources of pollution This work provides the new or improved technology required for the control and treatment of pollution sources to meet environmental quality standards

This document is available to the public through the National Technical Information Service Springfield Virginia 22161

EPA-600/4-78-041
July 1978

FLOW STRUCTURE AND TURBULENT DIFFUSION AROUND A THREE-DIMENSIONAL HILL

Fluid Modeling Study on Effects of Stratification

Part I. Flow Structure

by

Julian C.R. Hunt
Department of Applied Mathematics
and Theoretical Physics
University of Cambridge
Cambridge, England CB3 9EW

William H. Snyder
Meteorology & Assessment Division
Environmental Sciences Research Laboratory
U.S. Environmental Protection Agency
Research Triangle Park, NC 27711

and

Robert E. Lawson, Jr.
Northrop Services, Inc.
Research Triangle Park, NC 27709

ENVIRONMENTAL SCIENCES RESEARCH LABORATORY
OFFICE OF RESEARCH AND DEVELOPMENT
U.S. ENVIRONMENTAL PROTECTION AGENCY
RESEARCH TRIANGLE PARK, NC 27711

DISCLAIMER

This report has been reviewed by the Environmental Sciences Research Laboratory, U.S. Environmental Protection Agency, and approved for publication. Mention of trade names or commercial products does not constitute endorsement or recommendation for use.

William H. Snyder is a physical scientist in the Meteorology and Assessment Division, Environmental Sciences Research Laboratory, U.S. Environmental Protection Agency, Research Triangle Park, North Carolina. He is on assignment from the National Oceanic and Atmospheric Administration, U.S. Department of Commerce.

ABSTRACT

This research program was initiated with the overall objective of gaining understanding of the flow and diffusion of pollutants in complex terrain under both neutral and stably stratified conditions. This report covers the first phase of the project; it describes the flow structure observed over a bell shaped hill (polynomial in cross section) through neutral wind tunnel studies and stably stratified towing tank studies. It verifies and establishes the limits of applicability of Drazin's theory for flow over three-dimensional hills under conditions of small Froude number. At larger Froude number, a theory is developed, and largely verified, to classify the types of lee wave patterns and separated flow regions and to predict the conditions under which they will be formed. Flow visualization techniques are used extensively in obtaining both qualitative and quantitative information on the flow structure around the hill. Representative photographs of dye tracers, potassium permanganate dye streaks, shadowgraphs, surface dye smears, and hydrogen bubble patterns are included. While emphasis centered on obtaining basic understanding of flow around complex terrain, the results are of immediate applicability by air pollution control agencies. In particular, the location of the surface impingement point from an upwind pollutant source can be identified under a wide range of atmospheric conditions. Part II, to be printed as a separate report, will describe the concentration field over the hill resulting from plumes released from upwind stacks and will further quantify the results obtained in Part I.

This report covers a period from April 1, 1977, to March 31, 1978, and work was completed as of March 31, 1978.

CONTENTS

FIGURES

TABLES

SYMBOLS

b	horizontal half-width of hill perpendicular to flow direction
$[B]$	flow region at base of hill when $F<<1$
D	depth of towing tank or channel
$\mathcal{D}$	diffusivity of heat or salt
$f(r)$	height of hill as a function of the radius
F	Froude number $\equiv U/Nh$
F_L	Froude number $\equiv U/NL$
g	acceleration due to gravity
h	height of hill
H_s	stack height or height of streamline far upstream of hill
$[H_1]$	flow region below top of hill when $F<<1$
$[H_2]$	flow region above top of hill when $F<<1$
L	half-length of hill at half-height $[=R_o(h/2)]$
L_o	half-length of hill in x-direction
n_o	distance of streamlines from z=0 axis far upstream of hill
n_s	distance of streamlines from surface of hill
N	Brunt-Väisälä frequency $[=(g(d\rho/dz)/\rho)^{1/2}]$
$\{N\}$	node point
$\{N'\}$	half-node point
p	pressure
$\hat{p}$	perturbation pressure
P	perimeter of ellipsoidal hill on x=0
P_i	singular points of surface shear stress
r	radial coordinate in horizontal plane
$R_o(z)$	radius of hill
S	speedup factor $[=U_{max}/U_\infty(h)]$
$\{S\}$	saddle point
$\{S'\}$	half-saddle point
$[T]$	flow region at top of hill when $F<<1$

U_{max}	maximum velocity over hill
U_r	horizontal velocity in r-direction
U_θ	horizontal velocity in θ-direction
U_∞	upstream velocity, constant with elevation
$U_\infty(z)$	upstream velocity, varying with elevation
W	vertical velocity
x	horizontal, streamwise coordinate
y	horizontal, spanwise coordinate
z	vertical coordinate
z_i	elevation of plume impingement point (height of maximum concentration)
α_B	coefficient denoting thickness of [B]
α_T	coefficient denoting thickness of [T]
β_o	speedup integral (Eq. 3.13)
Δ	vertical deflection of streamline
θ	angle of "longitude" in (r,θ,z) system
λ	aspect ratio of hill $(=b/L_o)$
Λ	wavelength of lee wave
ρ	density
$\rho_o(z)$	upstream density profile
Σ_N	number of node points
Σ_S	number of saddle points
Ψ	streamline
$\{\}^{(a)}$	attachment point
$\{\}^{(s)}$	separation point

ACKNOWLEDGEMENTS

JCRH is grateful to his research student Dr. P.W.M. Brighton for teaching him so much about stratified flow over obstacles and to Dr. Phillip Mason of the Meteorological Office (U.K.) for an enlightening conversation about lee waves. We are grateful to Messrs. Roger Thompson and Daniel Dolan for help with the photographs, to Messrs. Lewis Knight, Leonard Marsh, and the late Karl Kurfis for help with running the experiments and to Miss Tameria Bass for typing the manuscript. Financial support for JCRH was provided through an appointment as Associate Professor, Department of Geosciences, N.C. State University, through EPA Grant R804653.

1. INTRODUCTION

The flow patterns and velocity distributions around three-dimensional hills need to be better understood before one can even interpret measurements, let alone make reasonable predictions of the dispersion of pollution from sources in this kind of complex terrain. The aspects of the structure of these stratified flows that most affect dispersion are:

(a) Whether streamlines from upwind impinge on the hill, go round[1] the hill, or go over the top;

(b) The size and location of internal hydraulic jumps and the region of the separated or recirculating flow in the lee of the hill, as the stratification varies; and

(c) The effects of heating and cooling of the surface.

Existing theory (see Sect. 3) and observations of air flow over mountains (Queney et al., 1960) all indicate that, when the stratification is strong enough, the air flows in approximately horizontal planes around the topography (see Figure 1). This observation is used in estimating surface concentrations caused by upwind sources of pollution in the EPA Valley model (Burt and Slater, 1977). But hitherto there has been little firm laboratory or atmospheric data as to how strong the stratification must be for any given streamline starting below the top of the hill to pass round rather than over the hill. A criterion for this changeover to occur is suggested in Sect. 3 on the basis of the low-Froude number theory of Drazin (1961), which the experiments described in Sect. 5 confirm. As a scale for comparison between these and other measurements of the increase in wind speed over three-dimensional hills in neutral or weakly stratified flows, we summarize the results of potential flow calculations of the wind speed and streamline displacement over ellipsoidal hills in neutral flow.

---

1. The adverb "round" is used in the sense of following a circular path, whereas "around" is used in the sense of nearby or about.

It is well known that a small amount of stratification can have a strong effect on the separated flow downwind of bluff obstacles such as hills or escarpments (see, for example, Scorer, 1954, 1968). In the case of two-dimensional hills, the separation behind hills with moderate slopes can be suppressed, but "rotors", in which there is reverse flow, may be found farther downwind as part of the lee wave pattern. Internal hydraulic jumps are found downwind of hills with moderate or large slopes in which the streamlines jump abruptly upwards, the horizontal component of velocity decreases, and a large amount of energy is dissipated. Despite its practical importance to air pollution dispersion and aeronautics, the distinctions and connections among these phenomena are still far from clear, even in the case of two-dimensional hills. There has not even been a laboratory study of two-dimensional flows where all these phenomena occur, although some valuable insights were provided by the wind tunnel study of Kitabayashi et al. (1971) and the aircraft observations of Connell (1976) around Elk Mountain, Wyoming. If the slope of the hill is small enough, separation may occur without hydraulic jumps. For that case, Brighton (1977) has, for the first time, calculated and confirmed experimentally, in a stratified water channel at Cambridge, the dependence of laminar separation on Froude number for two-dimensional hills.

In this report, we describe laboratory studies of the flow patterns, with particular emphasis on the separated flow regions and the internal hydraulic jumps, around an axisymmetric, three-dimensional hill. A fourth order polynomial shape has been studied in a large stratified towing tank (2.4 x 1.2 x 25 m), in a small, stratified towing tank (0.20 x .10 x 2.0 m), and in an unstratified wind tunnel.

The method we adopt for analyzing and presenting a large quantity of flow visualization data of this kind is to first locate the points where the surface shear stresses are zero or where the velocity in a cross section through the flow is zero. These points are then characterized in terms of whether they are separation or attachment points and, more unusually, in terms of their topological nature as saddle points or node points, because topological theory (Hunt et al., 1978) shows that the number of saddle points must equal the number of node points. This provides a kinematic check on the inferred flow from the flow visualization data. This minimal attempt at systematizing visualization data provides a more concrete basis for qualitative comparisons

between (a) full scale and model scale observations of the flow around hills and (b) the theory and experiment.

Some quantitative results are also obtained from the flow visualization experiments: namely, at low Froude number, the vertical deflection of streamlines; at moderate to large Froude numbers, the distance of streamlines from the surface of the hill and the connection between the lee waves and the separated flow downwind of the hill; and at all Froude numbers, the increase in velocity or speedup over the hill.

As Scorer has pointed out, laboratory studies of stratified flows tend to overemphasize the effect of the upwind stratification rather than the equally, perhaps more, important effects of the local heating and cooling of the surface of the hills. These effects are not only local but may also have a large effect on the flow by inhibiting or promoting separation (Scorer, 1968, p. 113; Brighton, 1977). There have been some attempts to heat the surface of model terrain, but more to simulate fumigation of elevated plumes than katabatic or anabatic winds (Liu and Lin, 1976). Any comparison between full scale and model experiments, where such thermally generated winds are not simulated, must be made with great caution.

The main objective of Part I of this report is to elucidate, by theory and experiment, the structure of the flow, the velocity field, and the pattern of the streamlines of the stably stratified and neutral flow over a model hill, so that the concentration measurements described in Part II can be understood. Secondly, we hope that some general conclusions can be drawn about stably stratified flows around three-dimensional hills; and thirdly, we hope that these experiments will act as a stimulus for further experimental, theoretical, and computational investigations of these flows.

2. CONCLUSIONS

1. A flow structure to describe stably stratified flow over three-dimensional hills was developed in sections from physical scaling laws, some primitive analyses, and analogy with two-dimensional hills. The experiments broadly confirmed the general predictions about the flow structure, the important features of which are summarized below:

(a) When $F<<1$ (say $F<0.3$ for hills with moderate slope), the flow is approximately horizontal except in narrow regions at the top [T] and bottom [B] of the hill. These regions have thicknesses of about Fh, and streamlines starting in region [T] tend to pass over the top of the hill. A small lee wave or internal hydraulic jump may be found on the lee side of the hill in region [T]. Below region [T] the flow separates on the lee side of the hill, where a mainly horizontal recirculating flow is found. However, there is some vertical mixing caused by streamlines, deflected downwards by about hF^2 outside the wake, entering the wake and reverting to their original height.

(b) When F is of the order of 1 but not very much less than 1 (say >0.3), then it is less useful to think in terms of perturbations from the asymptotic state of $F\to 0$. Rather, it proves better to think in terms of the response of the flow over the hill to the wavelength Λ of the lee wave pattern set up by the hill. Experiments on a number of shapes of hills show that there is a range of the Froude number F_L based on the length of the hill, in which $2L\lesssim\Lambda\lesssim 5L$, where the lee wave is neither so long as to allow the boundary layer to separate (supercritical flow), nor so short as to force the lee wave to generate a rotor on the lee face (subcritical).

(c) When F is not much greater than 1, say, of the order of 1.5 or greater, overall, but not in detail, the flow structure around the hill becomes similar to that of neutral flow. But far downstream the stratification may have a strong effect, even when F is as large as 10.

2. The potential effects of the stratification on a plume from an upwind source are summarized below. The implications for surface concentrations will be further amplified in Part II.

(a) The stronger the stratification, the narrower will be the vertical width and the wider will be the horizontal width of the plume. If the plume starts below the hill top, yet goes over the top, it will pass very close to the hill surface and be further contracted in the vertical and expanded in the horizontal.

(b) The criterion for determining whether the plume will impact on the hill surface and go round the sides or go over the top is, roughly, $H_s=h(1-F)$, where H_s is the dividing streamline height, h is the hill height, and F is the Froude number characterizing the stratification. If the plume height (upstream) is smaller than this streamline height, it will impact on the hill surface; otherwise, it will go over the top.

(c) In moderately stratified flow (say, $0.4<F<1.5$), if the plume height is larger than $h(1-F)$, but not much larger than $h(1+F)$, the plume can still pass down the lee side of the hill very close to the surface.

(d) Although no sources were placed downwind of the hill, it is evident from the mainly horizontal recirculation patterns observed there in strongly stratified flows ($F<0.3$) that a downwind plume below $h(1-F)$ would also impinge on the hill surface. For weaker stratifications, plumes could also be brought rapidly to the ground as a result of the lee waves (descending streamlines) and rotors induced by the hill.

(e) From conclusions 1(a) and 2(c), we arrive at the "2-1/2 times rule", long ago established from neutral wind tunnel studies of flow from stacks close to obstructions and amply demonstrated as adequate from field observations (mostly from the lack of complaints!) over many years.

3. Since our experiments were all conducted in an approach flow without shear, the application of the results of modeling to the atmosphere has to be more than usually justified. Turbulent unstratified flows around bluff bodies all have much the same structure of separation regions, singular points, etc., for large variations in the approaching shear because the body's own wake flow has such a strong controlling effect (Hunt et al., 1978). The actual position of upstream vortices can be changed, but the structure of the wake flows are remarkably similar. Thus, in a stratified flow where the stratification somewhat "decouples" the flow at different heights, as one can see exactly when $F<<1$ (Eq. 3.1), the effect of the upstream shear on the flow structure is likely to be small. But, of course, quantitative results such as the coefficient α_T defining the thickness of the [T] region, or the speed-up factor S will be considerably influenced; we do not even know yet whether they will be increased or decreased!

4. A more fundamental limitation of our experiments may be the fact that they were conducted in finite depth tanks. The approximate argument of Sect. 3.2 suggests that the effect of the finite depth on three-dimensional lee waves is not very marked. Investigation of the lee wave pattern in the large tank may help elucidate this question. Experiments are certainly needed in stratified flows where the density gradient varies with depth, as it always does in the atmosphere; but we hope that the general ideas about the relation between the wavelengths of lee waves Λ and the horizontal length scale of the hill L may still be useful for estimating when, where, and what kind of separated flows will occur.

3. REVIEW OF THEORY

3.1 Small Froude Number Theory

The only theory giving quantitative results for stratified flow around a three-dimensional mountain or hill which is not merely a small perturbation of a plane surface is that due to Drazin (1961), which has been extended and largely confirmed experimentally by Riley et al. (1976) and Brighton (1978). The theory is valid asymptotically as the Froude number $F(=U_\infty(h)/Nh)\to 0$, where $U(h)$ is the upstream velocity at the level of the top of the hill, N is the Brunt-Väisälä frequency (i.e., proportional to the square root of the density gradient), and h is the height of the hill (see Figure 2a). The essential results from our present understanding of the theory are these:

(a) The fluid moves approximately horizontally in two regions: $[H_1]$, above the plane $z=0$ and below the summit of the hill, and $[H_2]$, above the summit (see Figure 2).

(b) Regions [B] and [T] exist at the base and the top of the hill with thicknesses $\alpha_B Fh$, and $\alpha_T Fh$[1], where the α's are factors of order one and depend on the shape of the hill. (We assume that the α's are 1.0 unless otherwise stated, and that the extent of [T] is symmetrical above and below the summit.) In these regions, the flow is not constrained to move horizontally.

(c) In the lee of the hill there may be a wake in which the flow also moves approximately horizontally, but the streamlines in the wake do not emanate from the same levels upstream.

(d) In $[H_1]$, to the first approximation as $F\to 0$, the horizontal velocity $U_H=(U_r,U_\theta)$ is described by potential theory; for example, if the mountain is axisymmetric about the z axis, with a radius $R_0(z)$, and if the wake is ignored,

---

1. Note that $Fh=U_\infty/N$, so if α_B and α_T are independent of F, the thicknesses of [B] and [T] may be independent of the hill height h.

$$U_r = U_\infty(z)(1 - R_0^2(z)/r^2)\cos\theta, \text{ and} \qquad (3.1a)$$

$$U_\theta = -U_\infty(z)(1 + R_0^2(z)/r^2)\sin\theta \quad . \qquad (3.1b)$$

Riley et al. (1976) showed how the effect of the wake can be estimated by using free streamline potential theory.

(e) It follows from Eqs. 3.1 that the horizontal pressure gradients in $[H_1]$ vary with z due to U_∞ and R_0 variations, and, consequently, the vertical pressure gradient $(\partial p/\partial z)$ is perturbed. For example, on the stagnation line this perturbation (denoted by $\partial\hat{p}/\partial z$) is negative because dR_0/dz is negative. In strongly stratified flows, the perturbation pressure gradient is balanced by perturbations to the density gradient, which are produced by vertical displacements $\Delta(r,\theta)$ of streamlines starting from upstream. Generalizing Drazin's theory to allow for variations in U(z), Brighton (1978) showed that

$$\Delta(r,\theta) = -(\partial\hat{p}/\partial z)/[g\ \partial\rho_0/\partial z], \text{ or} \qquad (3.2)$$

$$\Delta(r,\theta) = -\frac{1}{2N^2}\left\{\frac{\partial}{\partial z}\left(U_\infty^2 - (U_r^2 + U_\theta^2)\right)\right\} \quad .$$

For the simple flow given by Eqs. 3.1,

$$\Delta(r,\theta) = -\frac{1}{N^2}\left\{\frac{dU_\infty^2(z)}{dz}\ \frac{R_0^2}{r^2}\left(\cos 2\theta - R_0^2/2r^2\right)\right.$$

$$\left. + \frac{U_\infty^2}{r^2}\ \frac{d(R_0^2)}{dz}\ \left(\cos 2\theta - R_0^2/r^2\right)\right\} \quad . \qquad (3.3)$$

The mean vertical velocity W is the time rate of change of Δ of a fluid particle, so that

$$W = \left(U_r\frac{\partial}{\partial r} + \frac{U_\theta}{r}\ \frac{\partial}{\partial\theta}\right)\Delta(r,\theta) \quad . \qquad (3.4)$$

Note that $W/U_\infty(h)$ is of $O[F^2 \times (\text{local slope})]$. The deflection of a typical streamline Ψ_{H1} is shown in Figures 2b and c. Note that for

all shapes of obstacles

$$\Delta(r,\theta) = W = 0 \qquad (3.5)$$

at the upwind stagnation line.

(f) Streamlines in $[H_2]$, such as Ψ_{H2}, are not deflected.

(g) As a consequence of the result (b), streamlines such as Ψ_T in Figure 2b pass through region T and therefore over the top if they originate upstream at a height

$$H_s > h(1 - F) \quad . \qquad (3.6)$$

3.2 Lee Waves and Separation

When the Froude number is of the order of 1, then $h \sim U/N$; in other words, the length of waves (e.g., lee waves) set up in the stratified flow by the hill are of the same order as the height of the hill, and they can then begin to control the flow (See Figure 3).

Either an exact or an order of magnitude analysis of stratified flow over two-dimensional hills with moderate slopes shows that the character of the flow depends primarily on the ratio of the wavelength of the lee waves ($2\pi U/N$) to the total length ($2L_0$) of the hill, rather than the height. The reason is that streamlines and isopycnals are deflected by the hill by a distance of order h (i.e., h is characteristic of the amplitude of the waves) up to a height above the hill of the order of $2L_0$ (rather than h), producing a change in potential energy of the order of $ghL_0 \partial\rho/\partial z$; the change in kinetic energy is of order $\rho U_\infty^2 h/L_0$, and so the dimensionless ratio determining the flow must be $(U_\infty/(L_0 N))$. This ratio is proportional to the wavelength of a lee wave ($2\pi U_\infty/N$) divided by the length of the hill L_0.

Some general conclusions about the way this ratio determines the flow can be drawn from the recent analytical and experimental work of Brighton (1977), the computational work of Sykes (1978) on laminar flow over two-dimensional hills, and the general observations of Scorer (1968). It appears that when the stratification is such that $2\pi U_\infty/N \simeq 2L_0$, separation of the flow over a rounded hill will be suppressed, if it can be, at any Froude number. (Clearly, for very steeply sided hills separation always occurs.) But if these two lengths differ considerably from each other,

separation must occur on hills of moderate slope. If $2L_0 >> 2\pi U_\infty/N$ (i.e., $F << 1$), separation is controlled by the pressure distribution produced by the lee wave pattern, and, if $2L_0 << 2\pi U_\infty/N$ (i.e., $F >> 1$), separation on the lee slope of the hill is controlled by the boundary-layer flow.

It is useful to designate the highest Froude number at which separation is first suppressed as the critical Froude number for separation, $F_{crit(s)}$, and to describe flows for which F is greater than or less than $F_{crit(s)}$ as super- or subcritical, respectively. (Normally, these terms are used to denote the existence or nonexistence of waves; hence the suffix s for separation.)

In practice any experiment has to be conducted in a flume or towing tank of finite depth D. In that case, the lee wave pattern can be quite different, as may be seen in the case of two-dimensional hills by comparing the computed streamlines of Huppert (1968) for a semicircular hill in an infinite fluid, and of Davis (1969) in a finite channel (or see Turner, 1973, pp. 61-62). Brighton (1977) has shown theoretically how, for laminar flow over two-dimensional hills with low slopes, separation is determined by the Froude number based on the depth of the tank F_D, and the Froude number $F_L (> F_D)$ based on a suitable length L of the hill, such as the semi-length at the half height. When $F_D < 1/\pi$ (i.e., $F_L < D/(L\pi)$), the hill triggers off standing internal waves which have a wavelength $\Lambda = (2\pi U_\infty/N)(1-F_D^2\pi^2)^{-1/2}$ and which produce separation under a rotor a distance of order Λ downstream of the hill. It appears from Brighton's analysis of flow over hills with low slopes that the downslope acceleration produced by this internal wave effectively suppresses separation on the hill while promoting it farther downstream. As the stratification is further increased, or F_D is reduced, Λ may become small enough that $\Lambda \simeq 2L$, in which case separation once again occurs on the downstream slope of the hill. This time it is produced by the internal wave, not the boundary layer. One might describe this Froude number as the lower critical Froude number. Thus, separation on hills with low slopes is suppressed for the range of F_L given by

$$(2/2\pi)(1 - \pi^2 F_L^2 L^2/D^2)^{-1/2} < F_L < D/L\pi \quad . \tag{3.7a}$$

For such a hill, $D/(L\pi)$ is the critical Froude number. This theory was confirmed by experiment in a small stratified flume at Cambridge on a hill with maximum slope of 0.3. (See Figures 3a, b, and d.).

When the hill has a moderate but not large slope, the internal wave motion may not be strong enough to suppress the separation on the hill until $\Lambda \sim 2L_o$, the overall length of the hill. This is similar to the case of an infinite fluid, where the separated flow can also be suppressed when $\Lambda \sim 2L_o$. Brighton's calculations suggest that the critical wavelength $\Lambda \sim 5L$ (See Figure 3c). Consequently, we might expect that, for a <u>moderate slope</u>, separation is suppressed only over a narrow range of wavelengths, namely,

$$2L < \Lambda \lesssim 5L, \tag{3.7b}$$

or

$$0.3 = 2/(2\pi) \lesssim F_L(1 - \pi^2 F_L^2 L^2/D^2)^{-1/2} \lesssim 5/2\pi = 0.8 \quad . \tag{3.7c}$$

Thus, if $L \ll D$, the critical Froude number is about 0.8, and the lower critical Froude number is about 0.3. The flow over the sharp-edged triangular hill used by Davis (1969) roughly satifies this inequality.

Can these ideas be applied to three-dimensional hills? The definitive theoretical calculation of Crapper (1959) of an infinite stratified flow over an axisymmetric hill with small slope shows that the lee waves:

(a) have a wavelength in the flow direction of about $2\pi U/N$,

(b) are confined in the spanwise (y) direction to a strip of width 2L (rather than in a wedge like shipwaves as was thought at first (Queney et al., 1960)),

(c) do not decrease significantly with height (z) above the hill, and

(d) can have a greater amplitude than those of a two-dimensional hill.

These results suggest that:

(a) The lee waves created by a three-dimensional hill must be just as much affected by the depth of the flume or tank as those of a two-dimensional hill. But the side walls are not likely to have much effect, provided the width of the tank is somewhat greater than $2L_o$, which it must be to avoid the normal "blockage" effects.

(b) We can estimate the streamwise wavelength Λ of three-dimensional waves in a tank of depth D (assuming D>>L) by assuming the spanwise wavelength over an axisymmetric hill is about 2L and using the linearized wave equation (e.g., the Boussinesq form of Crapper's Eq. 31); then

$$\Lambda \simeq \frac{2\pi U}{N} \left\{ \frac{1 - (1 + L^2/D^2)\, F_L^{\,2}/4}{1 - F_L^{\,2}/4} \right\} \simeq \frac{2\pi U}{N} \left(1 - \frac{L^2 F_L^{\,2}}{8D^2}\right), \qquad (3.8a)$$

if $F_L^{\,2}/4 \ll 1$.

(c) Since lee waves over a three-dimensional hill are just as strong, they should be able to suppress separation just as much as they do over a two-dimensional hill.

(d) Assuming that the general criterion for the suppression of separation is also $\Lambda \simeq 2L_o \simeq 5L$ for three-dimensional hills, then it follows from Eqs. 3.7c and 3.8a that separation on the lee side of a hill with moderate slope will be suppressed when

$$0.3 \lesssim F_L(1 - F_L^{\,2}L^2/8D^2) \lesssim 0.8 \quad . \qquad (3.8b)$$

3.3 Kinematic Theory

Although little dynamical theory exists that predicts the velocity and streamline pattern of stratified flow over hills, some useful kinematic theory provides a limitation on the large number of possible streamline patterns which can be drawn from a limited amount of experimental information. (See Lighthill, 1963, and, for the most recent results, Hunt et al., 1978.)

When identifying and examining the "singular" points on the surface of the hill and the surrounding plane where the shear stress is zero, there are advantages in describing these points in terms of their topological characteristics such as saddle {S} or node {N} points, rather than in the usual fluid dynamical categories of separation and attachment points, which are here denoted by superscripts $\{\}^{(s)}$ and $\{\}^{(a)}$. Figure 4 shows examples of these singular points. The main advantage is the topological constraints on the total number of saddle points (Σ_S) and node points (Σ_N).

For any shape of hill (provided that it does not have any holes through the middle, which a building might have), the surface flow pattern inferred from the observations must satisfy:

$$\Sigma_S - \Sigma_N = 0 \quad . \tag{3.9}$$

Another advantage of this approach is that, by identifying the positions of singular points, one provides a more succinct way of describing the flow (as opposed to defining the whole streamline pattern). One experiment can be more easily compared with another, and computations can also be tested this way.

The mean streamline pattern in a plane y=constant can also be analyzed in terms of the topological properties of the points where the mean velocity in the plane is zero, denoted by the letters, {S}, {N}. However, half saddles {S'} and half nodes {N'} also have to be defined where the singular point is on the surface (See Figure 4c.) The flow pattern must now satisfy

$$(\Sigma_S + \tfrac{1}{2}\Sigma_{S'}) - (\Sigma_N + \tfrac{1}{2}\Sigma_{N'}) = 0 \quad . \tag{3.10}$$

There is an additional constraint in deriving the flow pattern in stratified flows. If the diffusivity D of heat (if temperature stratified) or salt (as in our towing tank experiments) is small enough (i.e., $D/(Uh)<<1$), if the turbulent mixing in the wake is weak, and if the velocity, pressure, and density distributions far downstream are the same as upstream, then fluid particles starting at a height z upstream must return to a height z downstream. This implies, where mean streamlines and mean particle paths (from upstream sources) are close together (only true in weak turbulence), that no streamline starting at height z>0 can be the streamline which attaches to the plane z=0 at the downstream attachment point, as will become clearer in Sect. 5.

3.4 Estimating the Velocity and Streamline Displacement over the Hill in Neutral Flow

For flow over a three-dimensional hill, a useful way of estimating the increase of velocity and, of greater importance in pollution studies, the displacement of streamlines relative to the surface, is to consider potential flow over an ellipsoid (see Figure 5a). For an ellipsoid described by

$$\frac{x^2}{L_o^2} + \frac{y^2}{b^2} + \frac{z^2}{h^2} = 1, \qquad (3.11)$$

Milne-Thompson (1960, p. 518) has proven (in fact he quotes the result in an examination question!) that the surface velocity is the same at all points on the central plane of the ellipsoid (x=0), is a maximum, and is given by

$$U = U_{max} = 2U_\infty/(2 - \beta_o), \; V = W = 0, \qquad (3.12)$$

where

$$\beta_o = \left(\frac{L_0}{h}\right)\left(\frac{b}{h}\right)\int_0^\infty \frac{du}{((L_0/h)^2 + u)^{3/2}((b/h)^2 + u)^{1/2}(1 + u)^{1/2}} \; . \qquad (3.13)$$

The upwind flow U_∞ is uniform with height. We shall define the term "speed-up" as

$$S = U_{max}/U_\infty, \text{ or } S = U_{max}/U_\infty(h) \; . \qquad (3.14)$$

From Eq. 3.12, we can first find how the transverse aspect ratio of the hill ($\lambda = b/L_0$), i.e., the ratio of its horizontal width perpendicular to the wind to its length parallel to the wind, affects the speedup S. We shall assume for convenience that $h = L_0$. Evaluating the integral in Eq. 3.13 with the help of Gradshteyn & Ryzhik (1965, p. 78),

$$\beta_o = 1 + \frac{1}{\lambda^2 - 1} - \frac{\lambda}{(\lambda^2 - 1)^{3/2}} \ln\left(\lambda + \sqrt{\lambda^2 - 1}\right), \qquad (3.15)$$

whence as

$$\lambda = b/L_o \to \infty, \; \beta_o \to \left(1 - \frac{\ln(2\lambda) - 1}{\lambda^2}\right) , \qquad (3.15b)$$

so that

$$S \sim 2\left(1 - \frac{\ln(2\lambda) - 1}{\lambda^2} \; . \; . \; .\right) \; . \qquad (3.15c)$$

Thus if $\lambda \simeq 10$, S=1.96; the speedup is reduced by 2% below the value of an infinitely long circular cylinder. When $\lambda \to 1$, $\beta_o \to 2/3(1+0(\lambda-1))$, so that $S \sim 3/2$, the speedup over a sphere.

Thus if $\lambda \simeq 10$, S=1.96; the speed-up is reduced by 2% below the value of an infinitely long circular cylinder. When $\lambda \to 1$, $\beta_0 \to 2/3(1+0(\lambda-1))$, so that $S \sim 3/2$, the speed-up over a sphere.

If the wind is parallel to the longest side of the hill, or if the flow over a spherical hill separates, so that the effective length of the hill in the direction of the wind increases, then, assuming h=b, and $\lambda<1$,

$$\beta_0 = \lambda^2 \left[-\frac{2}{(1-\lambda^2)} + \frac{2}{(1-\lambda^2)^{3/2}} \ln[(1+\sqrt{1-\lambda^2})/\lambda] \right] ; \quad (3.16a)$$

when $\lambda \to 1$, $\beta_0 = 2/3$ as before, and when $\lambda \ll 1$,

$$\beta_0 \sim \lambda^2 [\ln(4/\lambda^2) - 2], \quad (3.16b)$$

so that $\beta_0 \to 0$, and $S \to 1$ as $\lambda \to 0$, i.e., there is no increase in velocity over the hill.

From the graphs presented in Figures 5b and c, we note that if $\lambda \simeq 2.5$, the speed-up is 1.75, i.e., half-way between a cylinder and a sphere. If $\lambda \sim 0.6$, the speed-up is half-way between that of a sphere and undisturbed flow.

To estimate the magnitude of the distance of streamlines from the surface of the ellipsoid, we define an average displacement $\overline{n}_s$ of a surface streamline in the plane x=0. (See Figure 5a.) Far upstream, these streamlines all touch an ellipse with minor axis n_0 and major axis $(b/h)\, n_0$ in the y-direction. (By far upstream we mean that $|x|$ is very much greater than whichever is the largest of b, h or L_0.) Then, by flow continuity

$$\overline{n}_s U_{max} P = \left(\frac{b}{h}\right) \frac{\pi}{2} n_0^2 U_\infty, \quad (3.17)$$

where P is the perimeter of the semi-ellipsoid on the plane x=0.

$$P = 2b\, E(90^o/\alpha), \quad (3.18a)$$

where E(/) is a complete elliptic integral of the second kind, and $\alpha = \sin^{-1}((b^2 - h^2)^{1/2}/b)$, (b>h) (Abramowitz & Stegun, 1965, pp. 590-592). To within 10%, P can be approximated by

$$P = 2L_0\lambda[\pi/2 - \sin^{-1}(\sqrt{1 - 1/\lambda_1^2})(1 - 2/\pi)], \text{ where } \lambda_1 = b/h \quad (3.18b)$$

whence, if $h=L_0$ ($\lambda=\lambda_1$), as $\lambda \to \infty$, $P \to 2L_0\lambda = 2b$; as $\lambda \to 1$, $P \to \pi L_0$.
If $b=h$ when $\lambda<1$,

$$P = \pi h = 2\pi L_0/\lambda \quad . \quad (3.18c)$$

Thus, from (3.17), the ratio of the distance of a streamline from the ellipsoid over the central plane to its distance upstream is, when $\lambda \geq 1$:

$$\frac{\bar{n}_s}{n_0} \simeq \frac{\pi\lambda_1 n_0 (2 - \beta_0)}{8L_0\lambda[\pi/2 - \sin^{-1}(\sqrt{1 - 1/\lambda_1^2})(1 - 2/\pi)].} \quad (3.19a)$$

Thus, in the limit $\lambda \to \infty$ (assuming $L_0=h$); since $\beta_0=1$,

$$\bar{n}_s/n_0 = (\pi/8)(n_0/L_0). \quad (3.19b)$$

When $\lambda \to 1$, $\beta_0 \to 2/3$, and

$$\bar{n}_s/n_0 = n_0/(3L_0) = n_0/(3h). \quad (3.19c)$$

When $\lambda<1$, with $\lambda_1=1$

$$\bar{n}_s/n_0 = \frac{n_0(2 - \beta_0)}{4h} = \frac{n_0 U_\infty}{2hU_{max}} \quad (3.20a)$$

so that, in the limit $\lambda \to 0$,

$$\bar{n}_s/n_0 = n_0/(2h). \quad (3.20b)$$

The practical implication of (3.19b), (3.19c), and (3.20b) is that, for a wide range of shapes (where $h=b$ or L_0), the ratio $\bar{n}_s/n_0$ is roughly 1/2 to 1/3 of the initial ratio of the streamline height to the hill height.

However, if the hill's width is very much greater than L_0, one may be interested in the ratio of $\bar{n}_s$ to n_0, where n_0 is calculated when $b = (\lambda L_0) >>x>> L_0$. In this case $\bar{n}_s U_{max} P \simeq 2bn_0 U_\infty$, where $\lambda >> 1$, so that

$$\bar{n}_s/n_0 = 1/2(1 - O(1/\lambda)), \quad (3.21)$$

which is the two-dimensional result.

4. APPARATUS

4.1 Large Towing Tank

The experiments were conducted in both towing tanks and in the wind tunnel of the EPA Fluid Modeling Facility. Details of the experimental apparatus are shown in Figures 6 to 10. The large towing tank is 1.2 m in depth, 2.4 m in width, and 25 m in length (Figure 6a). It has an aluminum framework, and the sides and bottom are lined with acrylic plastic for viewing purposes. A towing carriage allows models to be towed the length of the tank at variable speeds. Rails on the side walls of the tank support the carriage across the tank. (See Figure 6, or for additional details, Thompson and Snyder, 1976.) The carriage is pulled by cables driven by a motor at the end of the tank. The lowest reasonably uniform speed that can be attained is about 5 cm/s, and the highest is about 50 cm/s.

Coupled with the tank is a filling system (similar to that described by Pao et al., 1971) that allows the tank to be filled with an arbitrary stable density profile using salt water (specific gravity from 1.0 to 1.2). The filling system is composed of a brinemaker, five large tanks, and numerous pumps and valves as shown in Figure 6b. The filling operation is started with the tank empty. Saturated salt water (sodium chloride) is pumped continuously from tank A through valve 5, pump 1, and valve 27 into head tank F, with the overflow returning to tank A through valve 19. Similarly, fresh water is pumped from tank C through valve 4 and pump 2 into head tank G, with overflow returning to tank C through valve 22. This procedure maintains a constant pressure on the mixing valve, which proportions the amounts of fresh and salt water going into the towing tank. Four longitudinal tubes extending the length of the towing tank are manifolded to the supply line at one end. These longitudinal tubes are supported approximately 3 mm above the floor and contain 3 mm holes spaced approximately 15 cm apart. These tubes, then, distribute the water along the floor of the towing tank. Initially, a 4-cm

layer of fresh water is pumped into the tank. The mixing valve is adjusted to admit a small amount of salt water which is to be mixed with the fresh water in the supply line. A 4-cm depth of this mixture is then admitted to the towing tank. This mixture, being heavier, flows under the fresh water, lifting it. This procedure is repeated, each time increasing the specific gravity of the mixture, until the tank is full. Since the specific gravity of the mixture and the layer depths are variable, it is possible to produce nearly any stable density profile shape. The specific gravity of the mixture is monitored with a Princo Densitrol specific gravity indicator (Model W 747) mounted on a bypass on the supply line.

The final density profiles were measured by withdrawing samples from various depths in the tank and measuring their specific gravity with precision hydrometers or an electronic balance. Figure 6c shows one of the density profiles measured during this set of experiments and compares it with another measured after 13 days and more than 15 tows of the hill through the tank. The initial profile is quite linear with a Brunt-Vaisala frequency of $N=1.33$ rad/s. The later profile shows only a slight erosion of the gradient near the surface, i.e., the top 8 cm of water is near neutral in stability, with the bulk of the water matching the original stratification.

4.1.1 Polynomial hill

The model hill was made of 6 mm acrylic plastic sheet by vacuum molding onto a wooden former. Ideally, the shape was to be a fourth order polynomial [$f(r)=h/(1+(r/L)^4)$] that would avoid sharp gradients at the top of the hill (similar to a Gaussian shape), but would decay reasonably rapidly as r became large, in order that the hill would fit onto the baseplate. Due to imperfect construction techniques, the final shape was closer to

$$f(r) = h\left[\frac{1.04}{1+(r/L)^4} - \frac{0.083}{1+[(r-r_1)/L_1]^2} - 0.03\right], \quad (4.1)$$

where $h=L=22.9$ cm, $r_1=20.3$ cm, and $L_1=7.6$ cm. This equation describes the shape of the hill to within $\pm$ 2 mm. The maximum slope was about 1.0.

This hill was mounted on a flat baseplate, which was constructed of acrylic plastic attached to a framework of rectangular aluminum tubing. This framework was in turn suspended from the carriage through four jackscrews, which permitted leveling of the baseplate on the water surface. The hill was thus towed upside down across the water surface. The baseplate was immersed approximately 4 mm for each tow. Details of the model are provided in Figure 7. A sketch of the hill mounted on the baseplate is provided in Figure 7a. The upstream edge of the model was bevelled at 45^{o} in order to reduce the abruptness of the step. Twenty-eight sampling ports (i.d.=1.6; o.d.=2.4 mm) were fixed on the surface of the hill along each of the radial lines $\theta=180^{o}$, -165^{o}, -90^{o}, and 0^{o} (see Figure 7b, c and d). These sampling ports were not flush with the surface, but protruded a distance of 2.5 mm from the surface to simulate a full scale sampler height of, say, 3 m. On a full scale hill, surface roughness and convection would diffuse a plume to the ground if the plume were a small distance above it; on the ultra-smooth model hill at much lower Reynolds number, surface roughness and convection were absent, so that flush surface measurements might indicate zero surface concentrations in highly stable flows. This may have occurred in some of the model towing experiments at Flow Research (Liu and Lin, 1975).

Figure 7d defines the coordinate system. The origin (right-handed system) is on the baseplate directly under the top center of the hill.

4.1.2 Flow visualization

As part of our study of the flow over the polynomial hill, dye was emitted isokinetically from a "stack" of 0.635 cm o.d. The stack was bent through 90^{o} parallel to the flow to avoid any cross-stream momentum in the effluent. It was located 91.8 cm (4h) upstream of the hill center and 97.9 cm downstream of the platform's leading edge (see Figure 7c). The stack height H_s was varied from 0 to 1.2 hill heights. The effluent used was blue food dye (Warner Jenkinson No. 393) diluted with the proper amount of salt water to obtain a neutrally buoyant plume of 1 part dye and 15 parts salt water. The density of this dye solution was made equal to the local density of the static fluid at the emission height of the stack.

The effluent was pumped into the stack through a positive displacement pump (Fluid Metering Inc. Model RP-D) from a large graduated cylinder. A damper downstream of the pump, in addition to flexible tubing, minimized pulsations in the flow from the stack. The flow rate was preset and also double-checked during each test.

In other tests, dye was released from the surface sampling ports on the windward and leeward hill lines (θ=180^{o}, 0^{o}) to study the surface flow patterns, or alternately, through an injection rake emitting dye at 11 levels above ground at the stack position to study the centerplane streamlines. To ensure that the dye solution at each port or tube would have the same density as the static fluid at the same height as the dye port with the hill stationary, salt solution was drawn through each port into small jars by application of vacuum pressure to a second tube fixed into the lid of the jars (see Figure 8). Small amounts of concentrated dye were then added to each of the jars. Four different colors of dye were used in an alternating pattern for the surface ports to distinguish different levels. Then, with the carriage moving, the "vacuum" tank was pressurized, forcing the dye/salt solution back through the ports into the flow around or upstream of the hill. Color photographs (see Figure 11) and motion pictures were taken of the surface releases using this process at Froude numbers of 0.2, 0.4, 0.9, and 1.7. Black and white photographs of the upstream multilevel dye release were taken at Froude numbers of 0.2, 0.4, 1.0 and 1.7.

The multicolored dye solution, the streamers from the upstream multilevel injection tubes, and the plumes from the upstream stacks were photographed using 35mm cameras from the side and bottom of the towing tank (top view of the hill). The photographic and lighting arrangements are sketched in Figure 8. Both cameras used Kodak Tri-X film, shutter speeds of 1/125 s, and f/8 aperture settings. Back diffusive lighting for the side views was provided by a fluorescent light panel. This panel consisted of six 2.4 m long fuorescent tubes (75 W each) mounted on a white backboard and a 3 mm x 1.2 m x 2.4 m sheet of white, translucent acrylic plastic placed between the tubes and the towing tank to diffuse the light. Reflective lighting for the top views was provided by banks of fluorescent tubes placed just under the floor of the towing tank. Each of these banks contained three 76 cm and two

51 cm long fluorescent tubes (total wattage: 130 W/bank) and covered an area 72 x 118 cm. These banks lined the outside thirds of the floor of the towing tank over its entire length (see Figure 8). The model and baseplate were painted white to provide a suitable background against which to photograph the dye. For the side views of the multicolored dye experiments, the still camera, motion picture camera, and the diffusive light panel were attached to the carriage and towed with the hill. For top views and side views of the plumes from the upstream stack, all the cameras and the light panel were stationary relative to the towing tank. The refraction of light by the salt solution resulted in some distortion and blurring of the photographs, so that quantitative information was sometimes difficult to derive directly from the photographs.

To obtain a better understanding of the surface flow patterns, granules (2- to 3-mm diameter) of potassium permanganate ($KMnO_4$) were cemented to the hill surface. These granules dissolved rather slowly as the hill was towed through the tank, yielding bright purple streamers indicating the surface flow patterns. Whereas the technique was highly useful for the intended purpose, it was undesirable from a number of viewpoints: (a) After a few minutes of contact with the water, the $KMnO_4$ stained the model surface a dark brown, making the dye streamers difficult to distinguish from the brown surface stains in the black and white photographs. At towing speeds in excess of about 15cm/s, the streamers were exceedingly difficult to photograph because they became too thin. To the eye, however, they were easily distinguishable. (b) The $KMnO_4$ colors the entire water body in a short amount of time, making further visualization more difficult. It can be neutralized with sodium sulfite, and the resulting precipitate filtered out; whereas this could be useful for filtered recirculating water channel, it was not feasible in our stratified tank. (c) It is a strong oxidizer; it reacts with numerous materials used in the construction of the tank and is somewhat hazardous to handle. (d) It is tedious and cumbersome to apply and cleanup in a tank as large as ours.

Because the streamers and the dye from the multilevel injection tubes were difficult to photograph at the higher tow speeds (higher Froude numbers), the tank was filled with a much weaker stratification ($N \sim 0.5$ rad/s as opposed to ~ 1.3 rad/s) so that surface flow and centerplane streamline patterns

could be photographed at high Froude numbers and low towing speeds. This provided an additional benefit in that it provided an opportunity to observe, at least to a limited extent, the variation of the flow patterns with Reynolds number alone (see Sect. 5.4). Photographs of the surface flow patterns are presented in Figure 12.

Shadowgraphs (see Figure 13) were also photographed using a 35mm camera placed 9 m from the viewing screen. The light source for the shadowgraphs was a 750 W lantern slide projector, placed 9 m from the model centerline. A large sheet of translucent drafting paper was taped to the sidewalls of the tank for a viewing screen.

4.1.3 Measurement of plume impingement points and streamline deflections

One series of tests was run at Froude numbers of 0.2, 0.4, 0.6, and 0.8 and stack heights of 0.2, 0.4, 0.6, and 0.8 hill heights in order to determine (a) whether the plume went over the hill or around it, (b) the impingement point z_i, defined as the height of the maximum concentration on the 180^0 line (upstream centerline on the hill surface), and (c) the streamline deflection at $\theta=-90^0$. Samples were drawn during the tow simultaneously through all the surface ports using the sampling system described previously (Figure 8). The collected sample jars were then visually inspected to determine which contained the highest concentration of dye (generally an easy task).

The multilevel dye injection photographs (Figure 14) were also analyzed to obtain streamline deflections over the top of the hill.

4.2 Small Towing Tank Experiments

The disadvantage of the large stratified towing tank is that the residual flow takes about an hour to settle down, and it takes at least 2 hours to change a model. Consequently, if some quick qualitative experiments using a number of differently shaped models are required, or if the models need to be withdrawn from the fluid often, a small tank is desirable. Another advantage is that hydrogen bubble visualization experiments can be more easily conducted when there is not a large volume of refracting fluid to distort the image, as happens in the large tank.

These are some of the reasons for also using a small stratified towing tank 2.0m x 0.20m x 0.10m deep in these experiments. The tank was filled by the usual "two-tank" method of Oster and Yamamoto (1963), with a stratified salt solution having specific gravity varying from 1.0 at the surface to as much as 1.2 at the bottom. Model hills were mounted on a baseplate suspended from a carriage driven by a cable and electric motor similar in principle to that of the large tank (see Figure 9a). The practical speed range was 5 to 25 cm/s. The model hill and baseplate could be lowered into the tank and fixed simply by fastening two nuts. The polynomial hill used here had about the same shape as the large hill; its height was 2 cm.

4.2.1 Surface stress patterns

Shear stress patterns were observed on the surfaces of several model mountains by a technique similar to the surface oil flow technique commonly used in wind tunnel studies. The technique itself consisted of coating the models with a gelatinous solution of dye and KNOX brand gelatin (100 cm^3 blue liquid dye to 10 g gelatin). The models were then clamped into place on the towing carriage and drawn through the tank (about 2 m distance). As shown in Figure 12c, the dye was sheared away in regions of high stress and tended to collect along the stagnation areas, leaving a visual record of the surface flow patterns.

This technique is fraught with difficulties, making its use less satisfactory than the corresponding wind tunnel technique using zinc oxide powder and oil. Because the residual motion of the water destroyed the surface pattern after towing ceased, it was essential to photograph the pattern during the last instant of the tow. The consistency of the dye/gelatin mixture was critical; if the solution was too gelatinous, no pattern formed; if it was too thin, the dye was quickly diluted and washed away. Temperature also played a role in obtaining proper consistency. A solution temperature of 30 ^{o} to 32 ^{o}C permitted uniform surface coating of the gelatin mixture for towing in the water at 24 ^{o} to 25 ^{o}C. Finally, as the gelatin slowly dissolved, the dye separated from the surface with the flow at the separation points; these dye streaks, away from the surface, although weak, were superimposed on the surface flow patterns in the photographs.

4.2.2 Hydrogen bubble technique

A hydrogen bubble wire system (Schraub et al., 1965) was developed to study the streamline pattern and the velocity field on the centerline of the hills (see Figure 9a). The wire was 6 cm long and fixed 5.5 cm from the leading edge of the baseboard. The wires used in this study were 0.025-mm diameter chromel thermocouple wires. Several other types and diameters were tried, but most produced poor bubble quality (i.e., large bubbles which rapidly rose to the surface) or were rapidly contaminated. Time markers were produced by pulsing the voltage applied to the wires, generating distinct lines of bubbles. To generate uniformly spaced bubble streaks, the wire was kinked by running it between two small gears (Clutter and Smith, 1961). This provided a very uniform spacing of streaks, but was usable only at speeds in excess of about 8 cm/s because of problems with bubble rise. The bubbles that formed on the wire tended to be swept back to the apex of the kink and coalesce before they were swept off by the flow. Even finer wire would have been helpful in this case. Current flow through the wire was also found to be significant in altering the bubble size, lower current producing smaller bubbles.

The power supply used (see Figure 9b) was a general purpose unit with output voltage of 15 to 30 V at 1 A maximum current. It could be used in the continuous mode or pulsed to provide time markers. The oscillator section provided variable pulse rate and pulse width. The output current was adjustable over a wide range, which was found to be important in adjusting bubble size. Provision for reversing polarity was also included for cleaning purposes. Polarity reversal removed any contaminants that had been electrolytically deposited. Photographs of the pulsed bubble patterns are shown in Figure 15.

The lighting and photographic arrangement used is shown in Figure 9c. Backlighting was used to illuminate the bubbles. This consisted of two 750 W studio lights arranged at an angle of 25^{o} to the test section. A flat black background was placed immediately behind the test section to provide adequate contrast for the illuminated bubbles. Photographs were recorded with a 35mm camera equipped with a 135mm lens to reduce distortion due to parallax. Tri-X film was used with an aperture setting of f/5.6 and exposure time of 1/250 s.

Velocities were obtained from the photos by determining the distance between successive bubble streaks. This was accomplished by digitizing the centerpoints of successive streaks, then computing the straight line distance between the two points. Conversion of the measured distances to velocity values was accomplished by scaling the measured displacements by the displacement of a set of reference streaks located in the free stream upstream of the model. It was assumed that these freestream reference points represented the actual towing speed for the streamline.

While many photographs were taken, not all were of sufficiently good quality for analysis. The poor quality photographs were mostly at low velocities where bubble rise was a serious problem. Also, as the bubbles rose they tended to cling to the model and coalesce, forming bubbles large enough to alter the flow patterns (cf. Figure 15a). In some of the photographs, bubble quality was not good enough to allow for complete analysis, though the gross flow pattern was quite visible.

4.3 Wind Tunnel Experiments

The identical polynomial hill used in the towing tank was also used in the wind tunnel for flow studies under neutral stability conditions. The EPA Meteorological Wind Tunnel (Thompson and Snyder, 1976) has a test section 3.7 m wide, 2.1 m high, and 18.3 m long (see Figure 10a). The air speed in the test section may be varied from 0.5 to 10 m/s. The flow uniformity in the core (outside the wall boundary layers) is good, i.e., deviations from the average flow speed are less than 1% across the test section at 3 m/s. The turbulence intensity is typically 0.5% at this speed.

The hill was placed such that its apex was 424 cm from the entrance to the test section (Figure 10b).

4.3.1 Velocity measurements

Turbulence measurements were made with Thermo-Systems Model 1054A anemometers in conjunction with Model 1243-20 cross-film (boundary layer style) probes. The output signals from the anemometers were digitized at the rate of 1000 samples/s and linearized and processed on a PDP 11/40 minicomputer. Sampling (averaging) times of 1 min were found to yield reasonably repeatable results.

Probes were calibrated next to a pitot tube in the free stream flow in the test section of the wind tunnel. A computer program calculated the parameters (A, B, and α) to yield a "best fit" to Kings law, $E^2=A+BU^{\alpha}$, from the six input calibration points. Other programs calculated the average velocity U, the longitudinal and vertical turbulence intensities $(\overline{u^2})^{1/2}$ and $(\overline{w^2})^{1/2}$, the Reynolds stress $\overline{-uw}$, and the flow angle, $\phi=\tan^{1}(U_1-U_2)/(U_1+U_2))$, where U_1 and U_2 are the mean velocities indicated by film numbers 1 and 2, respectively. Because the hot-film was sensitive to ambient temperature drift, the sampling program was set up to correct for temperature drift according to $E^2=(A+BU^{\alpha})(T_f-T_{new})(T_f-T_{cal})$, where T_f, T_{new}, and T_{cal} are the film, new room, and calibration temperatures, respectively (Bearman, 1971).

The Reynolds stress measurements were corrected for errors due to sensor yaw response using the correction factor graphed in Figure 10c. This correction factor was obtained by measuring shear stress profiles in a pipe flow apparatus over a range of velocities from 2 to 17 m/s. The resulting profiles were extrapolated to the wall of the pipe, and the value obtained was compared with the wall shear stress calculated from the measured pressure drop along the length of the pipe. The ratio of the measured wall shear stress to the extrapolated value was then used as the Reynolds stress correction factor. It was found to be dependent upon both velocity and the geometry of the sensor support; hence, the correction in Figure 10c is specific to the boundary layer style probe. A comparison of the transverse and longitudinal components of turbulence intensity measured in the pipe flow apparatus showed good agreement with those measured by other investigators, hence, no corrections were applied to those measurements.

4.3.2 Flow visualization

A paraffin oil-fog generator (Kenney Engineering Model 1075SG) was used to produce smoke for the qualitative flow visualization studies. In this generator, paraffin oil is aspirated onto a heating element which creates a fine oil-fog. A separate air supply then carries the smoke into the wind tunnel.

One phase of this study involved visualization of smoke emitted from the stack upstream of the hill. Plume centerlines were traced from photographs at various stack heights in order to obtain an idea of the centerline streamline pattern over the hill. Photographs were also taken of the smoke being emitted at low speed through the surface sampling ports to obtain an idea of the surface flow pattern. Finally, drops of titanium tetrachloride were placed at various positions on the hill surface. This created a dense white smoke which was also helpful for understanding the surface flow pattern.

5. PRESENTATION AND DISCUSSION OF RESULTS

5.1 Presentation of Results

Figures 11 through 16 present the visualization photographs. Figure 11 shows the flow patterns observed from the injection of tracers through the surface ports, multicolored dye in the towing tank, and smoke in the wind tunnel. Figure 12 shows the surface shear stress patterns observed from the gelatin/dye solution in the small towing tank and from the potassium permanganate in both the large and small tanks. The shadowgraphs of Figure 13 show the change in the location of the separation point downstream of the hill as the Froude number changes. Figure 14 shows the streamers from the multilevel injection tubes upstream of the hill and tracings of smoke plume centerlines from the wind tunnel tests. The speedup over the top of the hill and the downstream lee wave patterns are illustrated in the hydrogen bubble photographs of Figure 15. Figure 16 shows how plumes from upwind stacks impinge on the hill surface and/or go round the hill, depending on the Froude number.

Figure 17 presents the quantitative measurements of the flow structure with and without the hill in the wind tunnel. We have attempted to collate all the observations by drawing the surface shear stress patterns and the mean centerline streamline patterns for a number of different Froude numbers in Figure 18. The classification of the surface singular points, denoted by P_i, are tabulated in Table 1.

The plume impingement height is plotted as a function of the source height and the hypothesis $F=1-H_s/h$ is shown to be valid in Figure 19. A streamline pattern over Elk Mountain, Wyoming, is presented in Figure 20 for a crude comparison with the present observations. Figure 21 shows the displacement of streamlines above the hill top as a function of Froude number.

TABLE 1: CLASSIFICATION AND LOCATION OF SINGULAR POINTS ON POLYNOMIAL HILL

Froude No.	P_1 (x,y)	P_2 (x,y)	P_3 (x,y)	P_4 (x,y)	P_5 (x,y)
0.2	$\{S'\}^{(s)}$ (-2.4,0)	$\{N'\}^{(a)}$ (-.4,0)	$\{S'\}^{(s)}$ (.4,0)	$\{N'\}^{(s)}$ (3.4,0.9)	$\{S'\}^{(s?)}$ (5.8,0)
0.4	$\{S'\}^{(s)}$ (-1.8,0)	$\{N'\}^{(a)}$ (-1.0,0)	$\{S'\}^{(s)}$ (1.0,0)	$\{N'\}^{(s)}$ (2.4,0.5)	$\{S'\}^{(s)}$ (3,0)
1.0			$\{S'\}^{(s)}$ (0.5,0)	$\{N'\}^{(s)}$ (1.2,0.4)	$\{S'\}^{(a)}$ (1.6,0)
1.7			$\{N'\}^{(s)}$ (0.4,0) $\{S'\}^{(a)}$ (0.8,0) $\{S'\}^{(s)}$ (1.2,0)	$\{N'\}^{(s)}$ (1.8,0.7)	$\{S'\}^{(a)}$ (3.4,0)
∞			$\{S'\}^{(s)}$ (-0.3,0) $\{N'\}^{(a)}$ (0.2,0) $\{S'\}^{(s)}$ (0.6,0)	$\{N'\}^{(s)}$ (1.3,0.7)	$\{S'\}^{(a)}$ (3.5,0)

Notes: (i) Singular points denoted by P_i are shown in Figure 18.

(ii) {S'}, half-saddle point; {N'}, half-node point; $\{\}^{(a)}$, attachment point; $\{\}^{(s)}$, separation point.

(iii) Coordinates of P_i are given relative to the center of the hill and are normalized in terms of the hill height, h.

(iv) The singular points P_3 may, in fact, be three singular points as found at F=1.7 and F=∞.

5.2 Qualitative Description of the Flow

At the lowest Froude number (F=0.2, Figures 11a, b, 12a, b, 13a, b, 14a, b, 16, and 18a), the flow is, in large measure, constrained to move in horizontal planes. In a narrow region near the top of the hill, the flow has enough kinetic energy to overcome the potential energy and, thus, to go over the top. In the middle region, $[H_1]$ of Figure 2, the plume rises slightly before it impacts on the surface, dips slightly from its upstream elevation as it goes round the sides, then rises again as it separates from the surface of the hill. Separation occurs as the flow goes round the sides at an angle of approximately 110^{o} from the upstream stagnation line. A slight hydraulic jump occurs just downstream of the top of the hill. The surface shear stress patterns show a symmetric pair of more or less vertically oriented vortices downstream causing an upstream flow on the centerline. The downstream dye release, however, shows the surface flow to be primarily perpendicular to the free-stream flow direction and to oscillate from one side to the other, broadly filling the wake with dye. There is only a very weak upslope component to the flow on the leeward slope. Frequently, different colors of dye, emanating from different elevations on the surface, would be observed flowing in opposite directions. This oscillation of the flow in the wake also caused the plumes upstream of the hill to oscillate from side to side at low frequency. (See, for example, Figure 14b, at a lower Froude number of 0.1.) A time sequence of photographs showed the plume (from a stack of height H_s=0.4h) oscillation to be irregular in amplitude and frequency. The lateral displacement of the plume impingement point reached as far as one-third the local hill radius on each side of the centerline at a Froude number of 0.2. There was a significant component of energy at a vortex shedding period of 33 s (calculated from the Strouhal number using the hill radius at the height of the stack), but, since this period differs with elevation and since the flows at different levels are not disconnected, some overall, apparently irregular, oscillation occurs.

A weak downslope flow on the windward centerline results in a weak, perhaps intermittent, horseshoe vortex; its location appears to move up and down the slope. Indeed, the streamers from the upstream multilevel

injection tube could be seen rolling up in vortices of one sign of circulation at one instant and of the opposite sign at the next. Because of the problems with bubble rise, the hydrogen bubble technique did not yield satisfactory results at this low Froude number.

At a Froude number of 0.4 (Figures 11c, d, 12a, b, 13d, 14a, b, 15a, and 18b), the flow has more energy to move in the vertical direction. The region where the flow goes over the top is now broader. At a stack height of only 0.6h, the plume is spread thinly to cover the entire upper half of the hill (Figure 16). In the middle region [H_1], as at the smaller Froude number, the plumes rise somewhat before they impact on the hill; they dip significantly, however, from their upstream elevation as they go round the sides and continue losing elevation, at least for some distance downstream. In going round the sides, the flow separates from the surface at about the same point as it did at the smaller Froude number (110^o). In going over the top, however, the flow does not separate until it is roughly half-way down the lee slope. The shadowgraphs (Figure 13d) show a strong hydraulic jump just downstream of this separation point. The height of this disturbance varied from 1.2 to 1.8 hill heights. The hydrogen bubble photographs from the small towing tank show a weaker hydraulic jump but illustrate the lee wave pattern more vividly.

The surface shear stress patterns again show a symmetric pair of vertically oriented vortices downstream causing an upstream flow on the centerline. These vortices, however, are smaller and closer to the base of the hill (rather than farther downstream). Dye release from the downstream ports again shows the surface flow to be perpendicular to the free-stream flow direction, to oscillate from side to side, and to broadly fill the (now narrower) wake. The motion picture film shows this more clearly.

The reverse flow down the windward slope is much more prominent, with the plume from any stack less than h/2 being rolled up into an intermittent horseshoe vortex. At a stack height of 0.2h, the location of the point of maximum concentration was lower in elevation than at the lower Froude number of 0.2.

At a Froude number of 0.6, separation begins near the downwind base of the hill, and the hydraulic jump peaks approximately two hill heights downstream of the hill center (see Figure 13f). At a Froude number of 0.8,

separation begins even farther downstream, and the hydraulic jump peaks somewhere beyond three hill heights downstream (Figure 13g).

At a Froude number of 0.9 (Figure 11e), all the flow in the centerplane goes over the top of the hill, but a plume starting on the ground-level centerline upstream of the hill would be broadly spread to cover nearly the entire hill surface. The flow goes down the leeward slope without separating. At a slightly higher Froude number (1.0), the hydrogen bubble photograph (Figure 15b) and the surface shear stress patterns (Figures 12b and c) clearly show separation at the top of the lee slope. However, neither the streamers from the multilevel injection tubes (Figure 14) nor the shadowgraph (Figure 13) make this separation bubble visible. Evidently, the flow is on the verge of separating from the top of the lee side of the hill; the existence or nonexistence as well as the size of the recirculating region is evidently critically dependent on the exact Froude number, the Reynolds number, and/or the precise upstream flow conditions.

As the Froude number is increased farther, the size of the recirculating region grows, and the wake dimensions grow laterally and vertically. At a Froude number of 1.7 (Figures 11f, 12, 13, 15c, and 18d), the flow separates just past the top of the hill, resulting in a large recirculating region on the leeward slope. Again, a plume starting at ground level on the upstream centerline would be spread broadly to cover the entire hill surface. This flow resembles neutral flow except that the streamlines are closer to the top of the hill and they lose elevation much faster in the wake of the hill.

Smoke visualization in the wind tunnel ($F=\infty$) showed the plumes to be spread broadly to cover the entire hill surface. Figures 11g and h show oil smoke being emitted through the sampling ports. From the release from the upwind ports, it may be seen that the flow speed is low on the lower half of the slope and fairly high on the upper half. The release from the downwind ports shows the flow to be up the slope, separating upstream of the hill center. Although these are instantaneous photographs, they are fairly representative of the average characteristics. Figures 11i and j show smoke being emitted from a puddle of titanium tetrachloride

at the downwind base of the hill. The large fluctuations in the flow field are evident, but the up-slope flow and separation at the top are fairly consistent. Also, the horseshoe vortex may exist intermittently low on the upwind slope (see Figure 12c).

Measurements of the velocity fields with and without the hill in place in the wind tunnel ($F=\infty$) are presented in Figure 17; included are mean velocity (speed as well as direction), local longitudinal and vertical turbulence intensity, and Reynolds stress profiles. The free stream speed U_∞ was 3 m/s. From the graphs, it may be seen that the boundary layer over the smooth tunnel floor was approximately 65 mm thick at the center of the hill (but in the absence of it). The free stream turbulence intensity was typically less than 0.5%. The filling out of the velocity profiles on the upwind slope of the hill and the overspeed regions on the top and side are evident.

The mean velocity vectors show quite significant vertical components as far as two hill heights upstream and up to twice as high as the hill itself. Directly above the hill and on the side, however, the vertical components are essentially zero. The abnormally high turbulence intensities at the upwind base of the hill are most likely caused by the abrupt step (6 mm) from the wind tunnel floor to the hill, only a short distance upstream from there. The very small turbulence intensities on the top and side of the hill are a result of the overspeed and extremely thin boundary layers at those points.

5.3 Comparison with Theory

From all the observations at low Froude number ($F<0.4$), we can see the validity of the theoretical description of the flow (given in Sect. 3) for the asymptotic region [H_1]. That is, the velocities are primarily horizontal, and the impinging streamlines are deflected downwards (unlike neutral flow where they mainly move upwards).

Unlike the smaller scale experiments of Brighton (1978), where the flow was everywhere laminar, a most important feature of these experiments is that the boundary layer on the surface of the hill is turbulent. Despite this, the low Froude number theory is approximately valid. This gives additional support to the validity of this scaling to the atmosphere,

where almost always the surface flow is turbulent.

Of great practical importance is the height z_i at which the plume impinges on the hill. The asymptotic theory when F<<1 predicts that when $H_s<h$, $z_i=H_s$. In Figure 19 we plot the values of z_i/h against Froude number (Figure 19a) and against H_s/h (Figure 19b). The latter figure and Figures 14a and 16 show rather convincingly, at least for this hill, that when $H_s>h(1-F)$ (our hypothesis of Sect. 3.1), the plume will touch or rise over the top of the hill. Note that if $h>H_s>h(1-F)$, the streamlines can pass down the lee side of the hill very close to the surface, as if the top of the hill was a hill of height (Fh) on a plane at z=h(1-F).

The photographs of surface dye releases also support the hypothesis that the summit region [T] has a thickness of Fh. Figures 11a and c show that dye from the ports moves upwards rather than horizontally or downward when z/h>0.82 for F=0.2, and z/h>0.61 for F=0.4, compared with predicted values of 0.80 and 0.60.

The maximum observed downward deflections at $\theta=90^o$ are compared in Table 2 with values computed from Eq. 3.3 using potential flow theory and from Eq. 3.2 using a free-streamline model for U_θ, following Riley et al.,(1976), which given a maximum value for U_θ/U_∞ of about 1.4 when $\theta=90^o$. H_s is the upstream height of the observed streamlines.

TABLE 2. COMPARISON OF OBSERVED AND CALCULATED STREAMLINE DEFLECTIONS.

Froude Number	H_s/h	$-\Delta/h$ @ $\theta=90^o$		
		Observed	Calculated (Eq. 3.3)	Calculated (Free streamline theory)
0.2	0.20	>0.15	0.25	
0.2	.40	.12	.17	0.08
0.2	.55	.16	.16	.08
0.2	.60	.21	.17	
0.2	.80	.08	.25	
0.4	.40	.12	.67	.32
0.4	.55	.10	.64	.32
0.4	.60	.38	.67	

When F=0.2, the observed vertical deflection in the middle region [H_1], is only slightly smaller than that calculated from Eq. 3.3, but about twice as large as that computed using the free-streamline model. The agreement is poor near the top of the hill in region [T] as was expected. When F=0.4, the deflections calculated from Eq. 3.3 are greater than the upstream height of the streamlines, which is, of course, absurd; the theory is obviously invalid at this Froude number. The free-streamline theory overestimates the deflections by a factor of two to three.

Riley et al. (1976) and Brighton (1978) investigated the flow around model hills that did not slowly widen at their base; their hills all had gradients greater than or equal to one near the base. The flow pattern produced by this type of hill is quite different from one whose gradient tends to zero near its base (i.e., $dR_0/dz \to \infty$ as $z/h \to 0$). This slope tends to produce a large deflection when $z/h < 0.1$. This shape of hill also produces a downflow on the upstream centerline of the hill, resulting in a large negative deflection at $\theta = 180^o$, whereas the theory predicts zero deflection on the upstream stagnation line. This is part of the explanation for the vortex on the lower upstream side of the hill seen in Figure 18a. This vortex exists in the base region [B] (see Figure 2a), where the asymptotic theory described in Sect. 3 is invalid. The vortex is necessary kinematically if the other singular point classifications in Figures 18a and b and Table 1 are correct.

Another possible explanation for the differences between theory and experiment is that the plume diffuses downwards more than upwards when $z/h < 1/2$ because Δ increases rapidly as z decreases when $z/h < 1/2$. It may be erroneous to assume that the center of the plume is the mean streamline through the source.

The surface shear stress lines and mean centerline streamlines are sketched in Figure 18. It must be remembered when viewing these figures and comparing them with the various photographs that the photographs are instantaneous pictures. Whereas we have tried to pick representative ones, the details may vary markedly from the average conditions. The sketches represent our best judgment of the mean patterns. It was not possible, for example, to show the oscillation in the wake at low Froude number or the oscillation of the plumes on the upwind side in the sketches.

Figure 18a and b show some aspects of the complicated separated flow in the rear of a bluff three-dimensional hill when F<1. The mainly horizontal motion around the hill region [H_1] induces a boundary layer motion on the hill which separates, much as on a circular cylinder. The angle of separation is about 110^0 from the upstream stagnation line. This compares to about 80^0 for a circular cylinder at the same Reynolds number of 10^4, or, since the surface flow is very turbulent, separation might occur at 100^0 or even 110^0.

When F=0.2, Figures 11a and 16 show that centerline streamlines in region [H_1] starting upstream at a height H_s (<h(1-F)), rise suddenly on meeting the three-dimensional separation streamline surface. This surface intersects the hill surface on the critical shear stress line through P_3. These centerline streamlines return approximately to their upstream level but also experience vertical mixing through a depth of about Δ. It would be misleading to describe this rise of the streamlines as a jump. However, the centerplane streamline over the top of the hill does experience a sudden vertical rise and strong vertical mixing which can reasonably be called a local internal hydraulic jump. The plan view of the wake shows vigorous horizontal mixing through the wake.

When F=0.4, there is a strong downflow on the lee side which develops into a huge wave or hydraulic jump whose height varies from 1.2 to 1.8h. This value is less than that found behind two-dimensional model hills. (e.g., Davis, 1969). Notice that the downstream wave or jump is highly curved and does not seem to extend laterally beyond the width of the hill. At lower Froude numbers, Brighton (1978) observed a curved trailing vortex rather than a jump.

As the Froude number is increased to about 1.0, the separated flow region is reduced even further in size (see Figure 11e and 18c). Note that since there can be no streamlines that start at a finite height upstream and end on a ground level attachment point (see Sect. 3.3), the streamline separating from P_3 reattaches at P_5. But since no surface streamline is observed to connect P_3 to P_5, the flow within the separated region is three-dimensional. At the nodal points, P_4, $P_4^{(i)}$, the surface flow swirls in, upwards, and eventually leaves downstream (Figure 12c). Downwind of P_5 one or more lee waves develop (Figure 15b). On the upstream side

we observe (Figure 14a) that streamlines emanating from a height H_s above about h/3 pass over the top, while those below that impinge onto the hill (the hypothesis of Sect. 3.1 for z_1 is not valid when $F \geq 0.5$).

The flow patterns shown in Figures 11 and 14 not only indicate the path of the center line of the plume but also the mechanisms controlling the width of the plume. Over the hill the vertical plume width is reduced by the streamlines converging in the vertical plane, and the horizontal width is amplified by the divergence in the horizontal plane. There is also an indirect effect due to the density gradient being increased by the convergence of the streamlines in the vertical plane. From the photographs it can be deduced that the vertical density gradient is about five times its upstream value, so locally N increases by five. For a plume starting upstream the latter effect mainly reduces the growth of the plume width (σ_z), while the former effect actually reduces the width of the plume. From the photograph in Figure 14, the distance between streamlines about 0.2h above the hill top is seen to be about half its upstream value; for comparison purposes it is worth noting that in neutral potential flow over a hemisphere, on a streamline 0.2 of a radius above the hill top, the vertical plume width is about 0.6 of its upstream value.

In Figure 20a the streamline pattern over Elk Mountain, Wyoming, estimated from aircraft observations by Marwitz et al. (1969) is shown for comparison with Figures 14 and 18c. The density distribution was different from that in our tank, there being a well-mixed layer below a fairly sharp inversion, but the gross Richardson number ($\simeq F^{-1/2}$) was about 1.0. It is interesting that these observations indicate that if $H_s/h > 1/3$ the streamlines pass over the hill top, as in our experiments; for a streamline starting at $H_s/h \sim 1.0$, these observations indicate that the distance n_s from the hill top to the streamline is 0.1h, whereas we found 0.2h (see Figure 21). Although these are of the same order the difference is significant and is probably due to the different upstream density gradient.

Figure 20b shows streamline computations by Marwitz et al. (1969) from a two-dimensional inviscid shallow water model; the model evidently gives some of the main qualitative features of uniformly stratified flows (probably only for $F \geq 1$). The surface streamline patterns shown in Figures

18c and d are similar to those inferred by Connell (1976) from his aircraft observations.

The main difference between the flow at Froude number 1.7 and neutral flow ($F=\infty$) is the location of the separation point on the top of the hill $P_3^{(a)}$ (Figures 18d and e and 12c). When F=1.7, P_3 is slightly <u>downwind</u> of the centerline, and, when $F=\infty$, P_3 is <u>upwind</u>. The character and location of the other singular points is approximately the same. Another difference is that the streamlines are closer to the top when F=1.7 (Figure 21).

The mean velocity and turbulence over the hill in neutral flow measured in the wind tunnel are shown in Figures 17a through e. Note particularly in Figure 17a that the speedup factor S over the hill is the same on the top as on the side of the hill, as would be expected by potential flow theory (Sect. 3.4). Defining S on the top as $S=U(1.03h)/U_\infty(h)$, we find S=1.27. To allow for the separated region in the lee of the hill, as a reference value we might compute S for an ellipsoid elongated in the direction of the flow such that h=b, and $L_0/h \simeq 3/2$; from Figure 5c, S=1.28, which suggests that the measured value is of the right order. The turbulence measurements indicate the thickness of the upwind boundary layer and how its thickness is reduced by the large negative pressure gradient over the hill. There is effectively very little turbulence outside the boundary layer.

Figure 21 shows the displacement of streamlines above the hill surface as a function of upwind streamline height, derived from the multilevel tracer injection photographs (Figures 14a and c). The neutral flow data from the towing tank and from the wind tunnel match fairly closely the upper limits predicted by potential flow theory (Eqs. 3.19 and 3.20), except for the larger values of H_s. The theory predicts $n_s \propto H_s^2$, but is obviously valid only when $H_s << h$.

Evidently because of the wake, the flow over this body more closely resembles that over one very long in the streamwise direction (compared to its width) than it does that over an axisymmetric body.

It is evident from the figure that as the stratification increases, the streamlines become much more closely packed. The implications for concentration will be discussed in Part II.

The data from the small towing tank consistently show smaller displacements than those from the larger facilities; this may be due to problems with bubble rise (the model was towed upside down) or it may be a Reynolds number effect (the small towing tank is 1/12th the size of the large tank).

How do the experimental flow patterns compare with the speculative predictions of Sect. 3.2 about the lee waves and the existence and position of separation? We first examine the nature of the separated flows at the four primary Froude numbers of our tests, and classify these as sub- or supercritical, according to the nature of the separation. For subcritical flows ($F_L < F_L^{crit}$) separation on the centerline of the lee slope is located where the flow in the downstream lee wave rotor leaves the surface, primarily an inviscid mechanism. For supercritical flows ($F_L > F^{crit}$), separation on the centerline is determined by the boundary layer behavior on the lee slope under the action of the pressure gradient outside the boundary layer, which may, of course, be affected by the lee waves. We conclude without any doubt that, when F=0.2 and 0.4, the separated flows are subcritical, and when F=1.0 and 1.7 the flows are supercritical; though in the larger tank, when F=1.0, the separated flow region is very small, and the flow is only just supercritical.

When $F \simeq F_L = 0.3$ separation does in fact occur on the lee side of the hill at about a value of x=L/2, the separation being caused by the rapid upward movement in the standing lee wave behind the hill. This corresponds approximately to the lower limit of F_L at which separation occurs downstream of the hill. Thus the observed lower critical Froude number of about 0.3 compares well with the rough estimate of 0.3 suggested in Eq. 3.8b. When F_L is less than the lower critical Froude number, then $F \ll 1$, and the lee waves have a small amplitude ($\sim U/N \sim hF$) and, near the hill, are confined to the [T] layer. This is the pattern observed when F=0.2.

Secondly, we can use the hydrogen bubble photographs in Figure 15a, b and c to estimate the wavelength Λ of the lee waves, to compare these with the natural wavelengths of the internal waves in the stratified flow, and to note the value Λ/L as the separated flow changes from a sub- to a supercritical character. We tabulate these parameters below:

TABLE 3: LEE WAVE ESTIMATES AND SEPARATED FLOW CLASSIFICATION

F_L	Theoretical (3-dimensional internal waves)	Measured (at about z=2h from Figs. 15a&b)	Character of separated flow	
	$\Lambda/L = 2\pi F_L$		Predicted (based on eq. 3.8b)	Observed
0.4	2.5	2.0 ± 0.5	subcritical	subcritical
1.0	6.3	6.0 ± 1.5	supercritical	supercritical

Note that : (a) in our experiments F_L=F because L=h, and (b) the ratio of the hill height h to that of the tank D is about 0.2 (for the large or small tank), so that the wavelength of the natural waves, given by Eq. 3.8b, is about equal to that of waves in an infinite medium, i.e. $2\pi U/N$.

5.4 Flow Variations with Reynolds Number

Most of the runs were done in the large towing tank at a fixed stratification ($N \sim 1.33$ rad/s), and in order to increase the Froude number, the towing speed was increased; this resulted in a corresponding increase in the Reynolds number. Systematic studies to examine the influence of Reynolds number on the flow patterns around the hill were not conducted. However, some experiments were done in the large tank with a weaker stratification ($N \sim 0.5$ rad/s), and also in the small tank, thus, yielding information at the same Froude number, but different Reynolds numbers. For example, at F=0.4, we have Reynolds numbers of 400 and 1900 from the small tank, 10,000 from the large tank with weak stratification, and 27,500 from the large tank with strong stratification. In the large tank, no variation with Reynolds number was observed; allowing for differences in visualization techniques and for slight differences in the shape of the hill and the absence of the "square flange" in the small tank, it is also safe to say that only slight variations of the flow patterns with Reynolds number

were observed. Our conclusions on the flow patterns were thus more heavily weighted by the results from the large tank. Extrapolations of these results to the atmosphere, where the Reynolds number may be several orders of magnitude larger is a much more serious question, and no apologies are offered. It has been shown by numerous authors that many of the flow patterns observed in the atmosphere, in particular lee waves and hydraulic jumps, can be simulated at much smaller Reynolds numbers (even considerably smaller than in the current experiments) in the laboratory.

REFERENCES

Abramowitz, M. and Stegun, I.A., 1965: Handbook of Mathematical Functions. 1st ed., Dover Publ., New York, N.Y., 1046 pp.

Bearman, P.W., 1971: Corrections for the Effect of Ambient Temperature Drift on Hotwire Measurements in Incompressible Flow, DISA Information, No. 11, p. 25-30, May.

Brighton, P.W.M., 1977: Boundary Layer and Stratified Flow over Obstacles, Ph.D. Thesis, Univ. of Cambridge, England.

Brighton, P.W.M. 1978: Strongly Stratified Flow Past Three-Dimensional Obstacles and Mesoscale Vortex-Streets in the Atmosphere, to be published in Q.J.R. Meteorol. Soc.

Burt, E.W. and Slater, H.H., 1977: Evaluation of the Valley Model, Preprints of AMS-APCA Joint Conf. on Appl. of Air Poll. Meteorology, Salt Lake City, Utah, Nov. 29-Dec. 2.

Clutter, D.W., and Smith, A.M.O., 1961: Flow Visualization by Electrolysis of Water, Aerospace Engr., v. 20, p. 24-27 and 74-76.

Connell, J.R., 1976: Wind and Turbulence in the Planetary Boundary Layer around an Isolated 3-D Mountain as Measured by a Research Aircraft, Int. Conf. on Mountain Meteorol. and Biometeorol., Interlaken, Switz., 28 pp., June.

Crapper, G.D., 1959: A Three-Dimensional Solution for Waves in the Lee of Mountains, J. Fluid Mech., v. 6, p 51.

Davis, R.E., 1969: The Two-Dimensional Flow of a Fluid of Variable Density over an Obstacle, J. Fluid Mech., v. 36, p 127.

Drazin, P.G., 1961: On the Steady Flow of a Fluid of Variable Density Past an Obstacle, Tellus, v. XIII, No. 2, p 239-51.

Gradshteyn, I.S. and Ryzhik, I.M., 1965: Table of Integrals, Series and Products, 4th ed., Academic Press, New York, N.Y., 1086 pp.

Hunt, J.C.R., Abell, C.J., Peterka, J.A. and Woo, H., 1978: Kinematical Studies of the Flows around Free or Surface Mounted Obstacles; Applying Topology to Flow Visualization, to be published in J. Fluid Mech.

Huppert, H.E., 1968: Appendix to paper by J.W. Miles, J. Fluid Mech., v. 33, p 803.

Kitabayashi, K., Orgill, M.M. and Cermak, J.E., 1971: Laboratory Simulation of Airflow and Atmospheric Transport-Dispersion over Elk Mountain, Wyoming, Fluid Dyn. and Diff. Lab. Report No. CER 70-71 KK-MMO-JEC-65, Colo. State Univ. Fort Collins, Colo., 90 p., July.

Lighthill, M.J., 1963: Laminar Boundary Layers, p. 48-88 (Ed. L. Rosenhead), Oxford Univ. Press.

Liu, H.T. and Lin, J.T., 1975: Laboratory Simulation of Plume Dispersion from Lead Smelter in Glover, Missouri, in Neutral and Stable Atmosphere, EPA-450/3-75-066, U.S. Environmental Protection Agency, Research Triangle Park, N.C., April, 47 pp.

Liu, H.T. and Lin, J.T., 1976: Plume Dispersion in Stably Stratified Flows over Complex Terrain; Phase 2, EPA-600/4-76-022, U.S. Environmental Protection Agency, Research Triangle Park, N.C., May.

Marwitz, J.D., Veal, D.L., Auer, A.H., Jr., and Middleton, J.R., 1969: Prediction and Verification of the Air flow over a Three-Dimensional Mountain, Tech. Rpt. No. 60, Natural Resources Res. Inst., Univ. of Wyo.

Milne-Thomson, L.M., 1960: Theoretical Hydrodynamics, 4th ed., Macmillan Publ. Co., New York, N.Y.

Oster, G. and Yamamoto, M., 1963: Density Gradient Techniques, Chem. Reviews, v. 63, p 257-68.

Pao, Y.H., Lin, J.T., Carlsen, R.L., and Smithmeyer, L.P.C., 1971: The Design and Construction of a Stratified Towing Tank with an Oil-Lubricated Carriage, Flow Research Rpt. No. 4, Flow Res., Kent, Wash., 31 p.

Queney, P., Corby, G.A., Gerbier, N., Koschmieder, H., and Zierep, J., 1960: The Airflow over Mountains, World Meteorol. Org. Tech. Note No. 34, Geneva, Switz.

Riley, J.J., Liu, H.T. and Geller, E.W., 1976: A Numerical and Experimental Study of Stably Stratified Flow around Complex Terrain, EPA-600/4-76-021, U.S. Environmental Protection Agency, Research Triangle Park, N.C., May.

Shraub, F.A., Kline, S.J., Henry, J., Runstadler, P.W., Jr., Littel, A., 1965: Basic Engr., v. 87, p 429-44.

Scorer, R.S., 1954: Theory of Airflow over Mountains, III: Air Stream Characteristics, Q.J.R. Meteorol. Soc., v. 80, p. 417-28.

Scorer, R.S., 1968: Air Pollution, Pergamon Press, New York, N.Y.

Sykes, R.I., 1978: Stratification Effects in Boundary Layer Flow over Hills, Proc. Roy. Soc. A. (in press).

Thompson, R.S. and Snyder, W.H., 1976: EPA Fluid Modeling Facility, Proc. Conf. on Envir. Modeling and Simulation, Cincinnati, Ohio, April 19-22, EPA-600/9-76-016, U.S. Environmental Protection Agency, Washington, D.C.

Turner, J.S., 1973: Buoyancy Effects in Fluids, Cambridge Univ. Press, Cambridge, England.

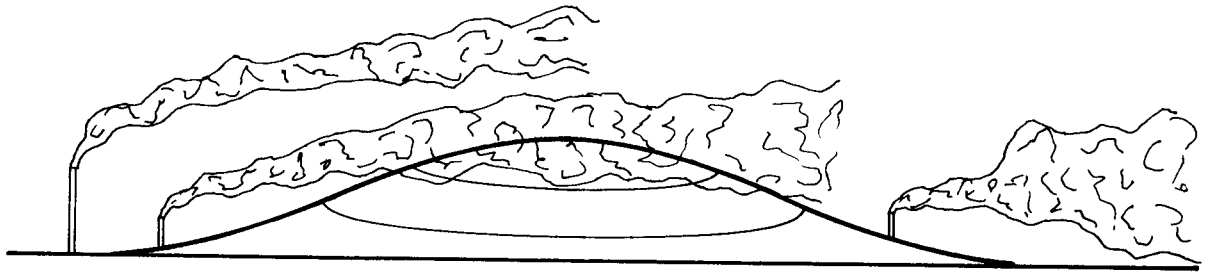

(A) NEUTRAL STRATIFICATION

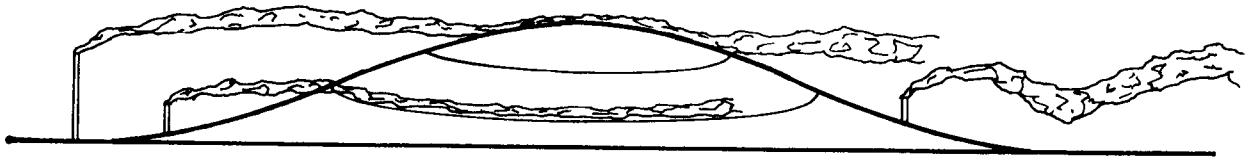

(B) STABLE STRATIFICATION

Figure 1. Sketch of plume behavior over three-dimensional hill in neutral and stable stratification.

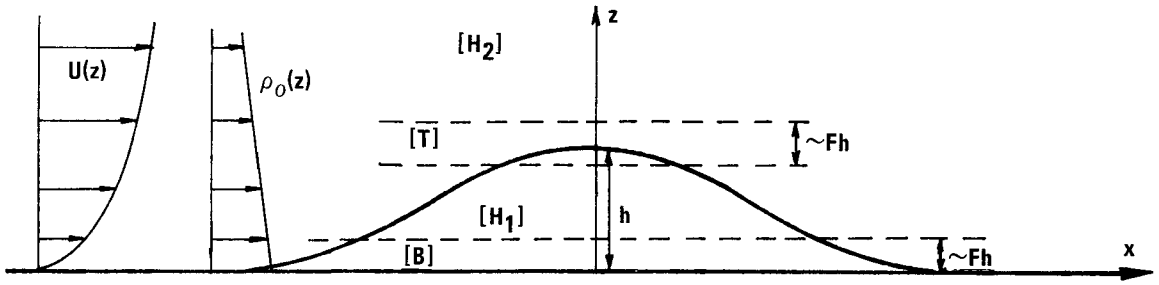

(A) DEFINITION OF REGIONS

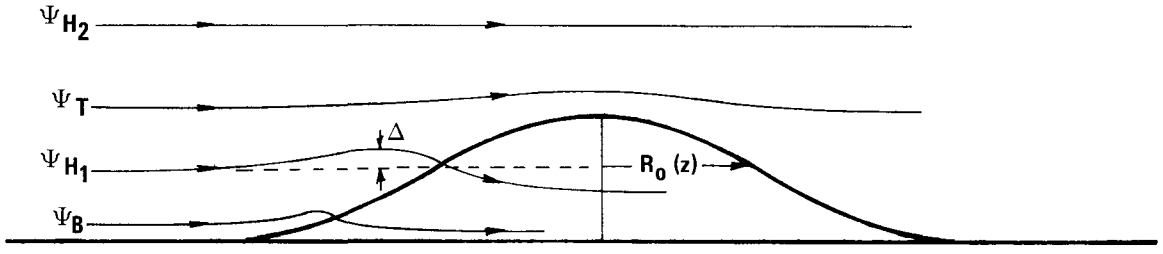

(B) STREAMLINE PATTERNS

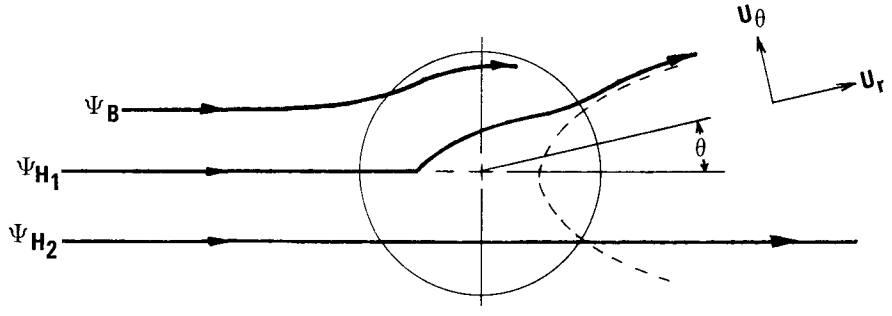

(C) PLAN VIEW

Figure 2. Small Froude number theory for flow over three-dimensional hills.

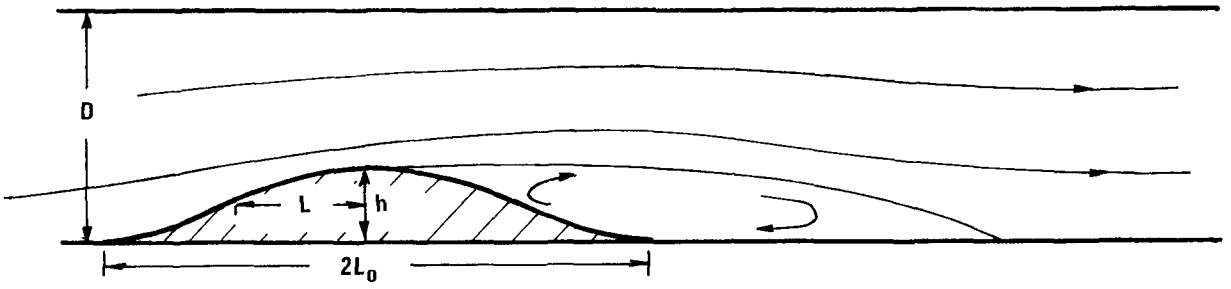

(A) SUPERCRITICAL FROUDE NUMBER; NO WAVES POSSIBLE. $F_L > D/(L\pi)$ SEPARATION IS BOUNDARY LAYER CONTROLLED.

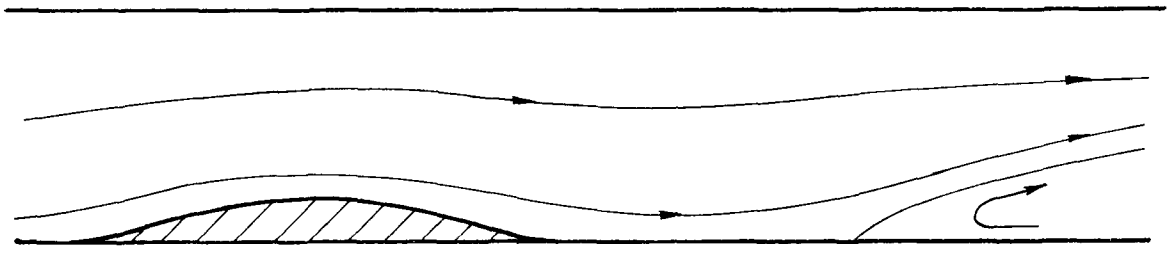

(B) HILL WITH LOW SLOPE; SUBCRITICAL FROUDE NUMBER; NO SEPARATION ON LEE SLOPE; SEPARATION CAUSED BY LEE WAVE ROTOR.
$(1/\pi)(1-\pi^2 F_L^2 L^2/D^2)^{1/2} < F_L < D/(L\pi)$.

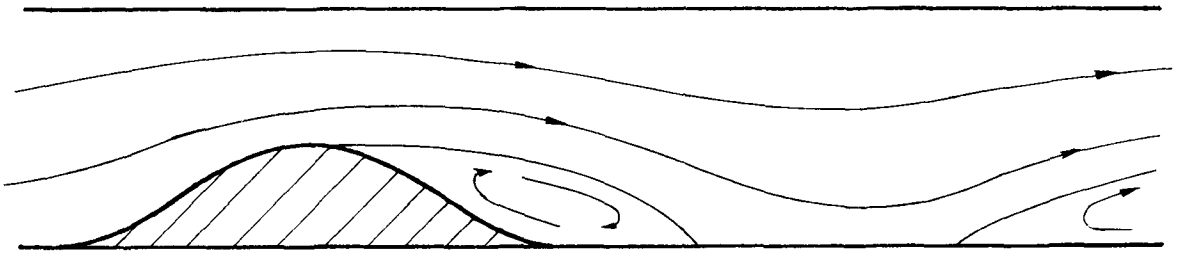

(C) HILL WITH MODERATE SLOPE; SUPERCRITICAL FROUDE NUMBER; BOUNDARY LAYER SEPARATION ON LEE SLOPE.
$5L \lesssim F_L < D/(L\pi)$.

(D) SUBCRITICAL FROUDE NUMBER; LEE WAVE INDUCED SEPARATION ON LEE SLOPE.
$F_L < (1/\pi)(1-\pi^2 F_L^2 L^2/D^2)^{1/2}$

Figure 3. Stratified flow over two dimensional hills in a channel. (Note: The critical Froude number is the highest Froude number at which separation on the lee slope can be suppressed.)

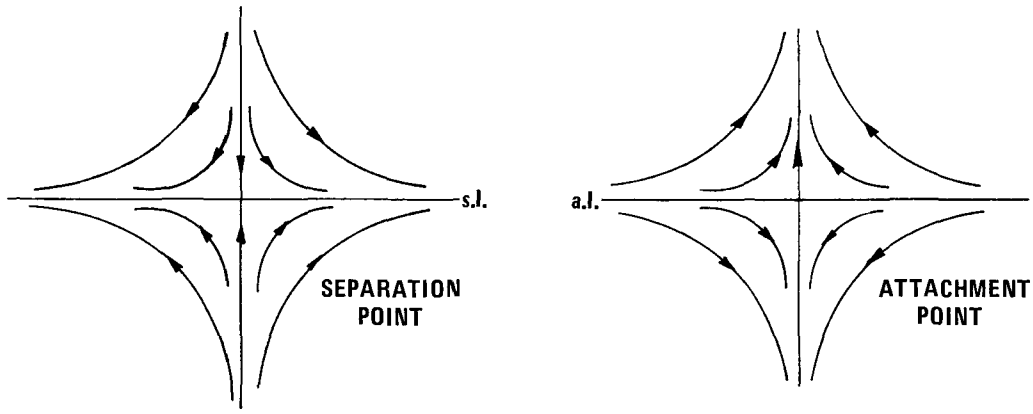

(A) SADDLE POINTS IN SURFACE SHEAR STRESS LINES.

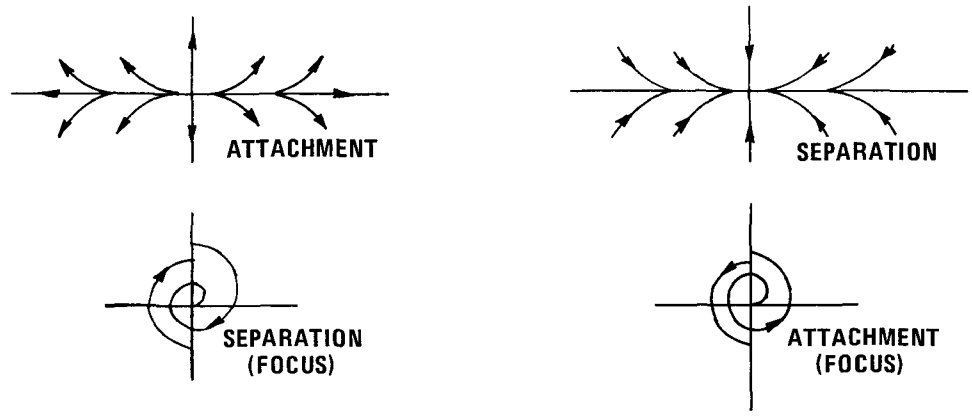

(B) NODE POINTS IN SURFACE SHEAR STRESS LINES.

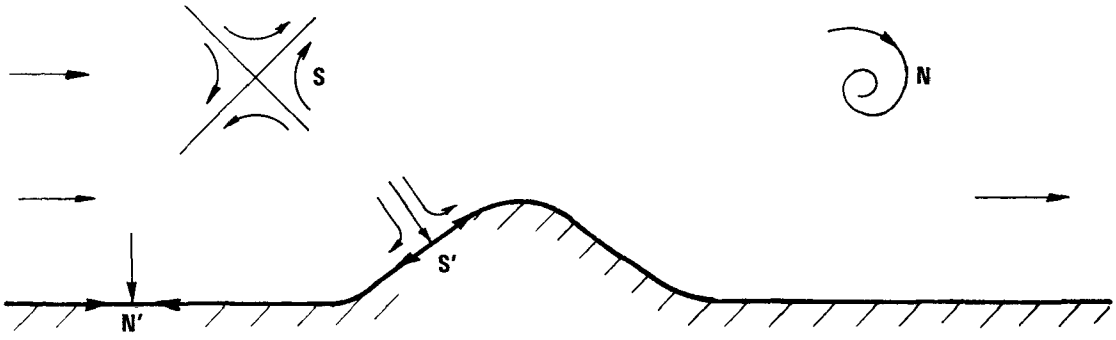

(C) SINGULAR POINTS IN THE MEAN STREAMLINE PATTERN. NOTE HALF NODES (N') AND HALF SADDLES (S') ON THE SURFACE.

Figure 4. Singular points of the surface shear stress lines and mean streamlines.

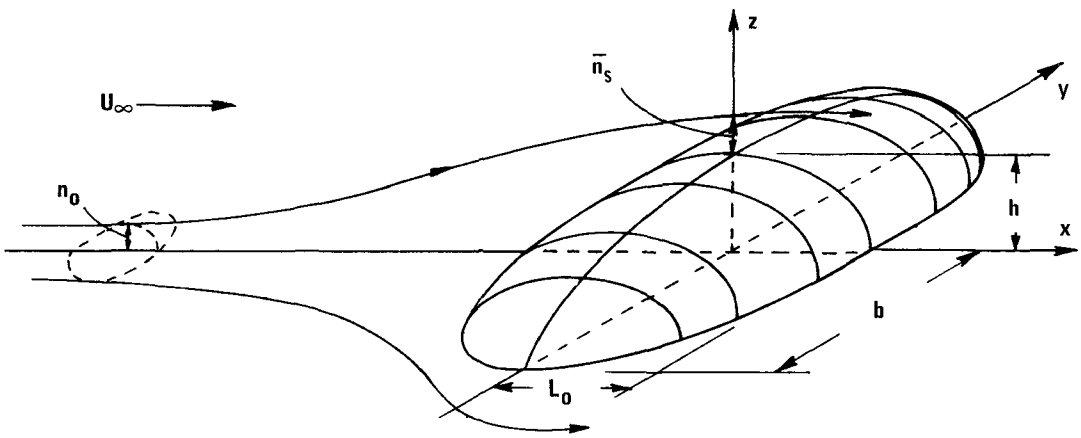

(A) COORDINATES AND NOTATION FOR ANALYSIS

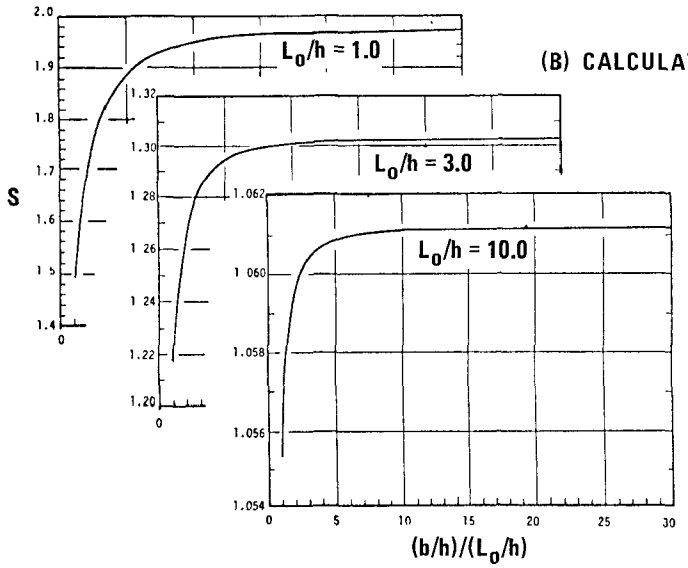

(B) CALCULATED SPEEDUP FOR $b \geqslant L_0$.

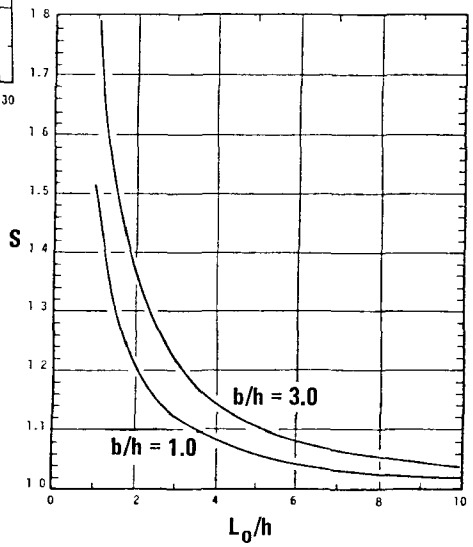

(C) CALCULATED SPEEDUP FOR $L_0 \geqslant h$.

Figure 5. Potential flow over an ellipsoidal hill.

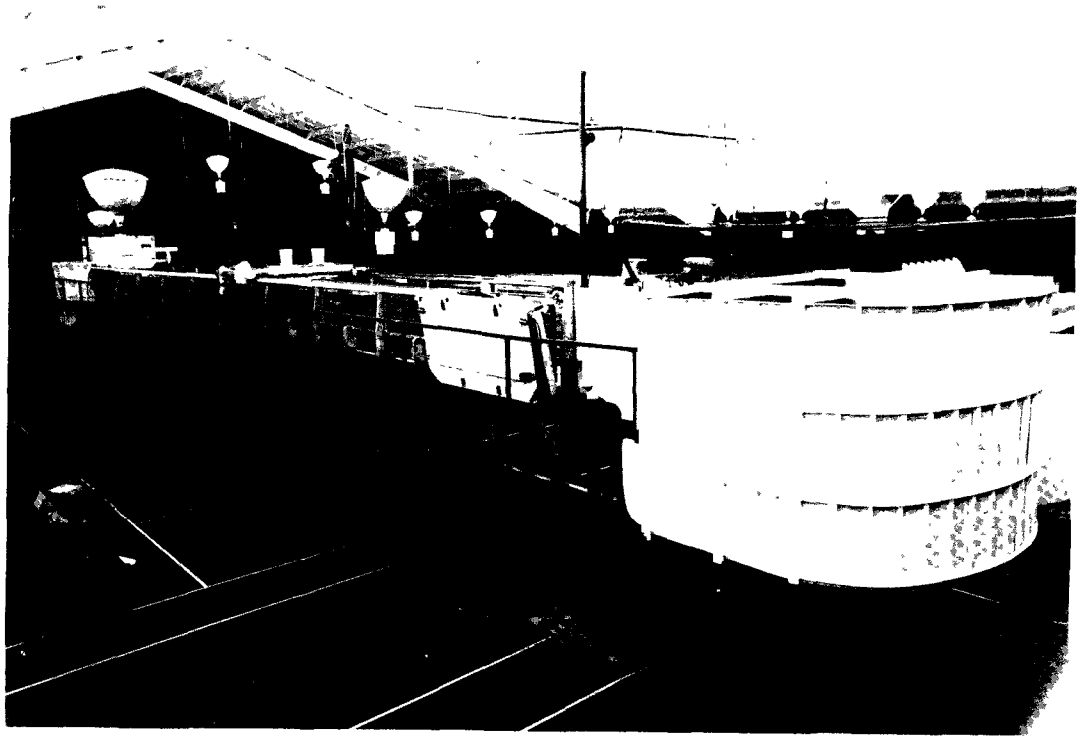

(A) THE EPA WATER CHANNEL/TOWING TANK.

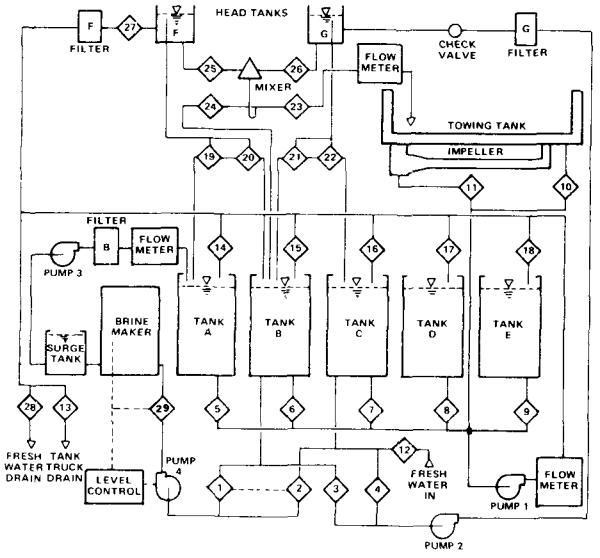

(B) THE FILLING SYSTEM.

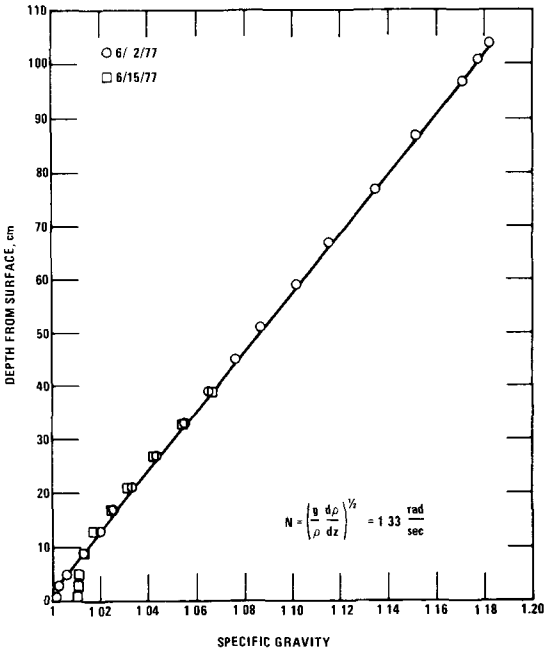

(C) TYPICAL DENSITY PROFILES

Figure 6. The large stratified towing tank.

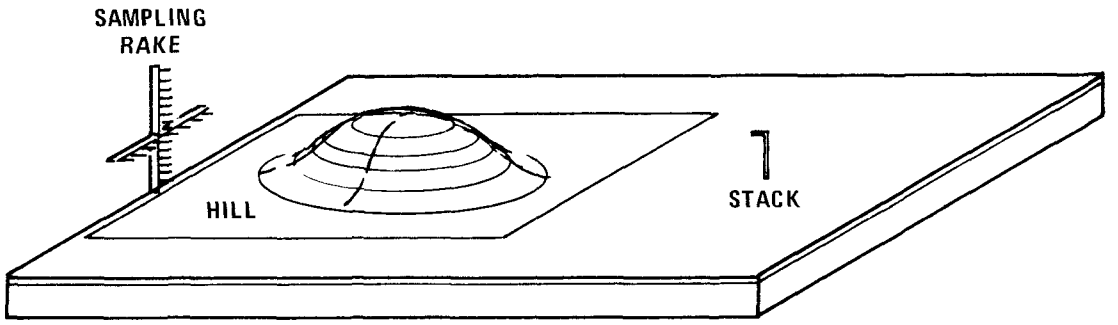

(A) SKETCH OF HILL ON BASEPLATE.

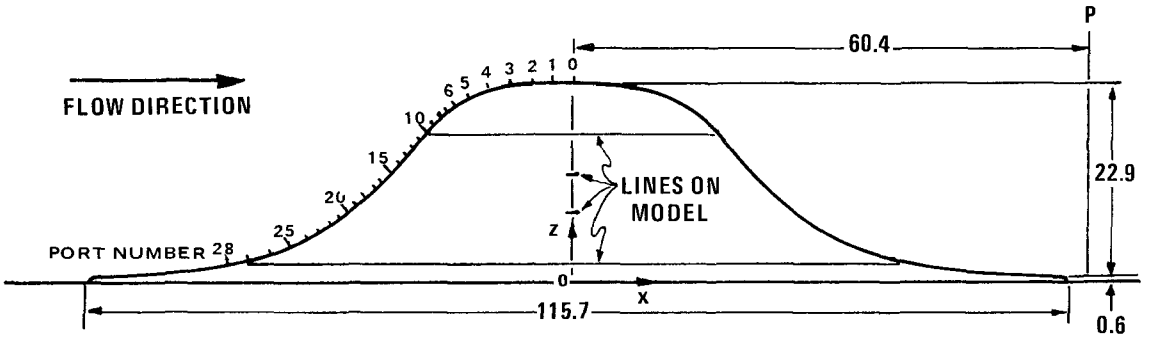

(B) PROFILE SHAPE OF HILL.

ALL DIMENSIONS IN cm.

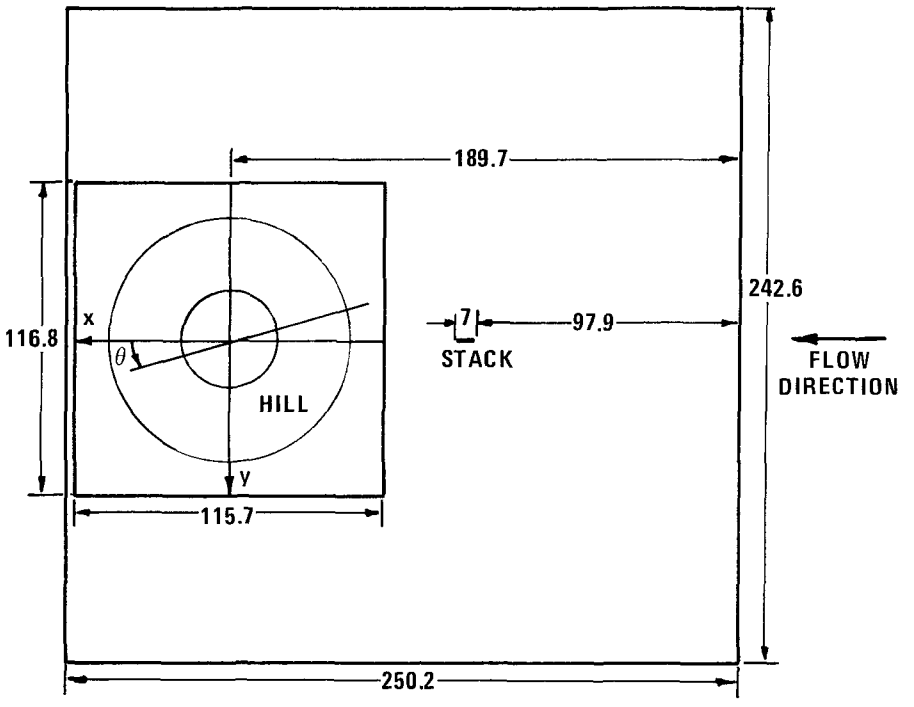

(C) PLAN VIEW OF HILL ON BASEPLATE.

Figure 7. Details of polynomial hill model.

POLYNOMIAL HILL - PORT LOCATIONS

ALL DIMENSIONS IN CENTIMETERS

TUBE NO.	x(0)	x(-90)	x(-165)	x(180)	y(0)	y(-90)	y(-165)	y(180)	z	s	TUBE NO	x(0)	x(-90)	x(-165)	x(180)	y(0)	y(-90)	y(-165)	y(180)	z	s
0	0	0	0	0	0	0	0	0	23 5	0											
1	+ 2 56	0	- 2.47	- 2.56	0	2 56	- 0.66	0	23.44	2.56	15	+21.76	0	-21.02	-21.76	0	21.76	- 5 63	0	10.79	26.69
2	+ 5.12	0	- 4.95	- 5.12	0	5.12	- 1.33	0	23.29	5 13	16	+22.68	0	-21.91	-22.68	0	22.68	- 5 87	0	9.98	27.98
3	+ 7 59	0	- 7 33	- 7.59	0	7.59	- 1.96	0	22 94	7.62	17	+23.59	0	-22.79	-23.59	0	23.59	6 11	0	9.04	29.22
4	+ 9.97	0	- 9.63	- 9 97	0	9 97	- 2.58	0	22.21	10.11	18	+24.51	0	-23.67	-24.51	0	24 51	- 6.34	0	8.25	30.42
5	+12.25	0	-11.83	-12 25	0	12.25	- 3.17	0	20.96	12.72	19	+25.51	0	-24.64	-25.51	0	25.51	- 6.60	0	7.46	31 71
6	+14 17	0	-13 69	-14 17	0	14.17	- 3.67	0	19.41	15.19	20	+26.61	0	-25.70	-26.61	0	26 61	- 6.89	0	6.66	33.07
7	+15 09	0	-14.58	-15.09	0	15.09	- 3.91	0	18.51	16.47	21	+27 61	0	-26.67	-27.61	0	27.61	- 7.15	0	5.98	34 28
8	+16.00	0	-15 45	-16.00	0	16 00	- 4 14	0	17.51	17.82	22	+28 71	0	-27.73	-28 71	0	28.71	- 7.43	0	5.30	35 57
9	+16.83	0	-16.26	-16.83	0	16.83	- 4 36	0	16.57	19.08	23	+29.81	0	-28.79	-29 81	0	29.81	- 7.72	0	4.68	36.83
10	+17.65	0	-17.05	-17 65	0	17.65	- 4.57	0	15.58	20 36	24	+30.91	0	-29.86	-30.91	0	30 91	- 8.00	0	4.13	38.06
11	+18.38	0	-17.75	-18 38	0	18 38	- 4.76	0	14.69	21 52	25	+33.28	0	-32.15	-33 28	0	33.28	- 8.61	0	3.10	40.65
12	+19 20	0	-18 55	-19.20	0	19.20	- 4.97	0	13.68	22.82	26	+35.66	0	-34.44	-35 66	0	35.66	- 9.23	0	2.18	43.16
13	+20.03	0	-19.35	-20 03	0	20.03	- 5.18	0	12 70	24.10	27	+38.13	0	-36.83	-38.13	0	38.13	- 9.87	0	1 62	45.72
14	+20.85	0	-20 14	-20.85	0	20.85	- 5 40	0	11 77	25.35	28	+40 60	0	-39.22	-40 60	0	40.60	-10.51	0	1 11	48.24

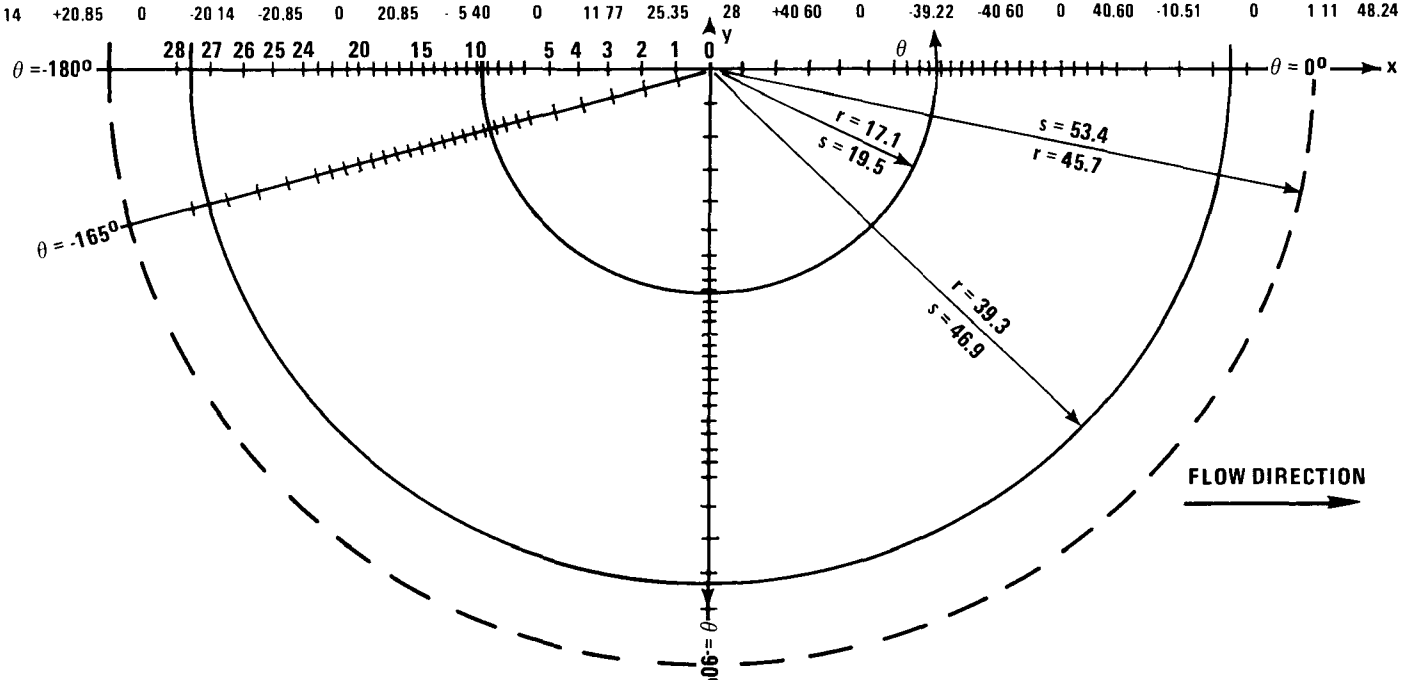

(D) PORT LOCATIONS ON POLYNOMIAL HILL

Figure 7 (continued). Details of polynomial hill model.

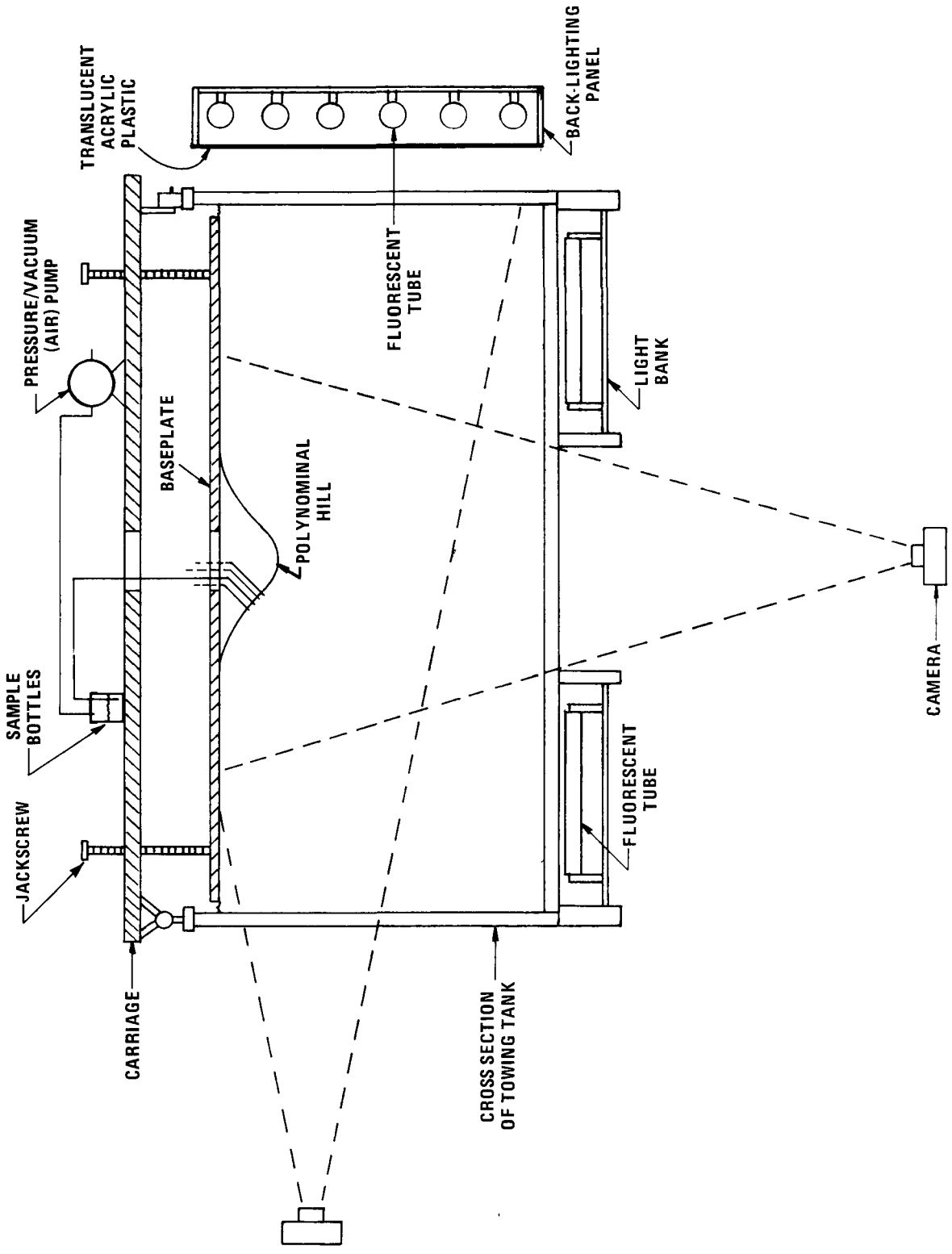

Figure 8. Detail showing suspension of model hill, lighting and photographic arrangement, and sampling and dye injection system.

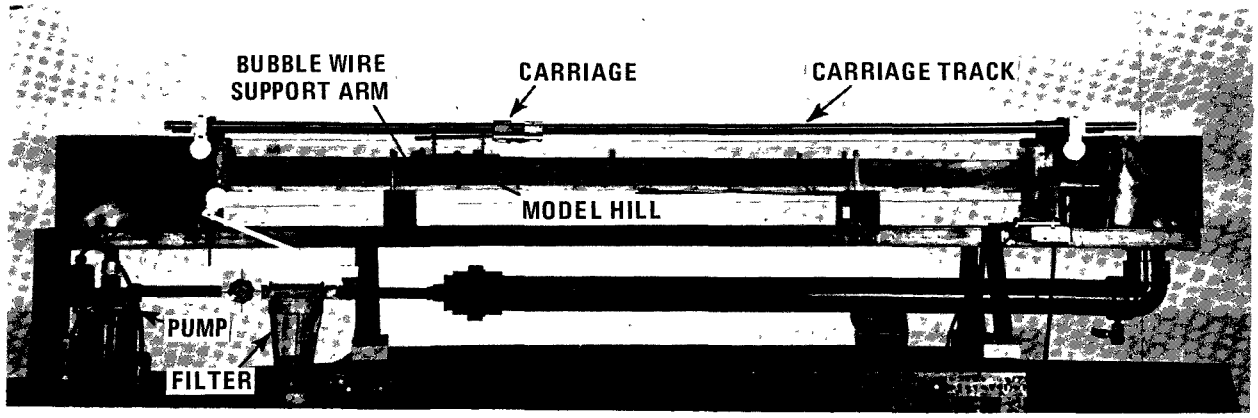

(A) SMALL WATER CHANNEL/STRATIFIED TOWING TANK.

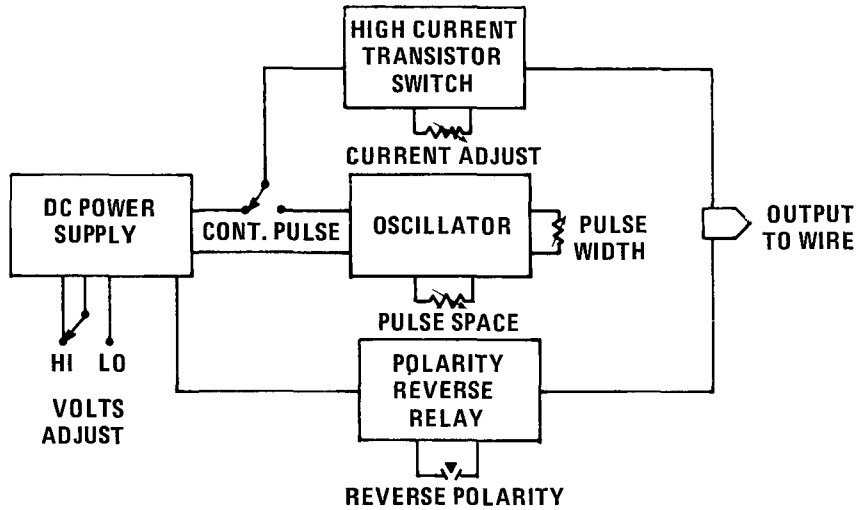

(B) SCHEMATIC DIAGRAM OF CURRENT SOURCE FOR GENERATING HYDROGEN BUBBLES.

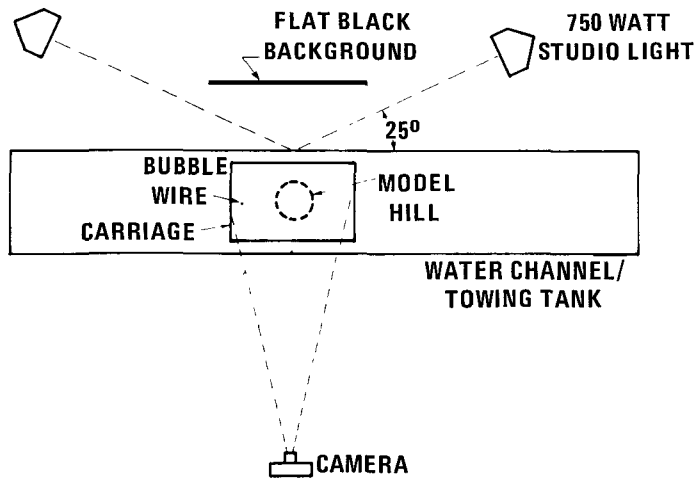

(C) PLAN VIEW OF SET-UP FOR PHOTOGRAPHING HYDROGEN BUBBLES.

Figure 9. Experimental apparatus for work in small towing tank.

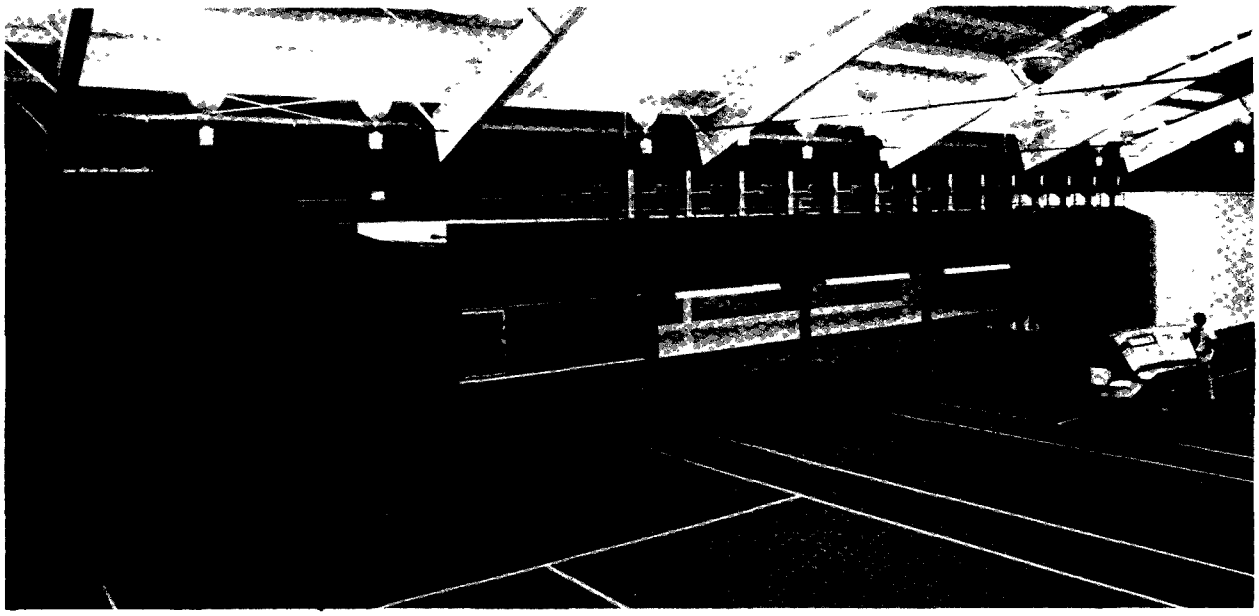

(A) THE EPA METEOROLOGICAL WIND TUNNEL.

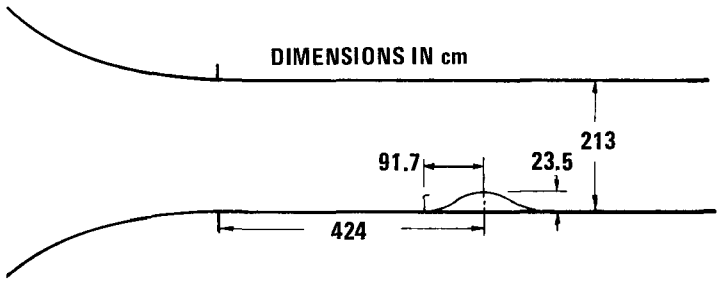

(B) PLACEMENT OF MODEL IN WIND TUNNEL.

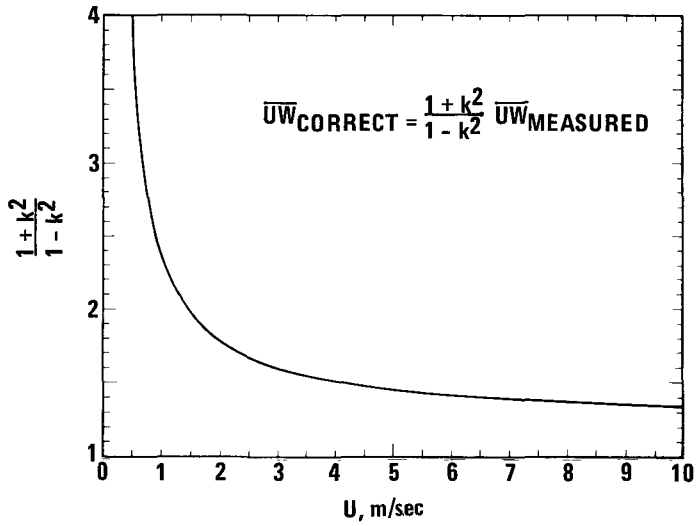

(C) REYNOLDS STRESS CORRECTION FACTOR FOR BOUNDARY LAYER PROBE.

Figure 10. Details of wind tunnel measurements.

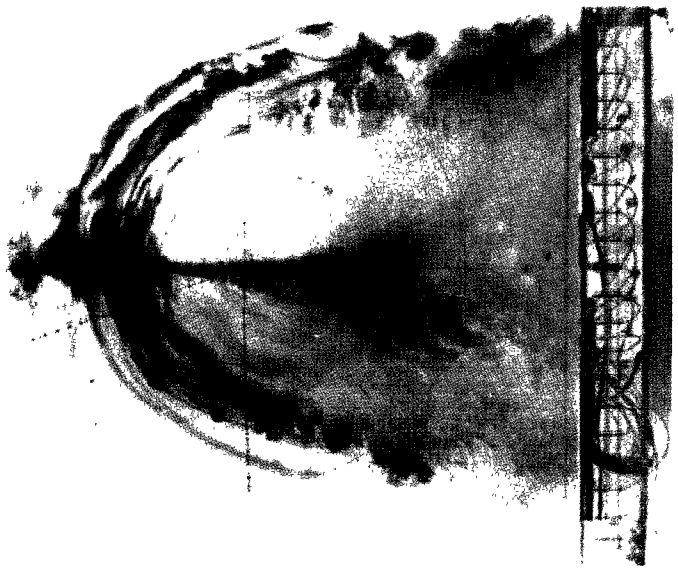

TOP VIEW

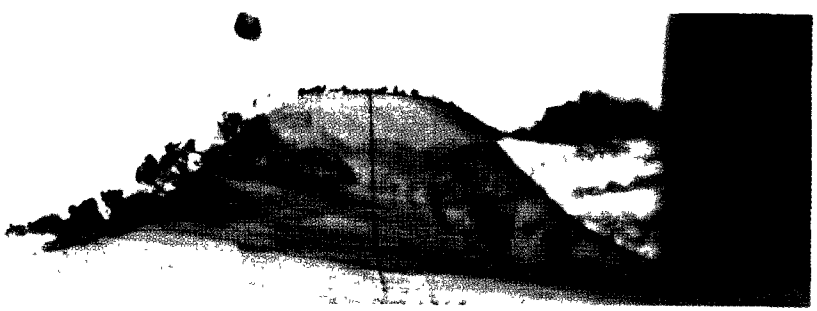

SIDE VIEW

(A) DYE RELEASE FROM 180^0 PORTS, F = 0.2.

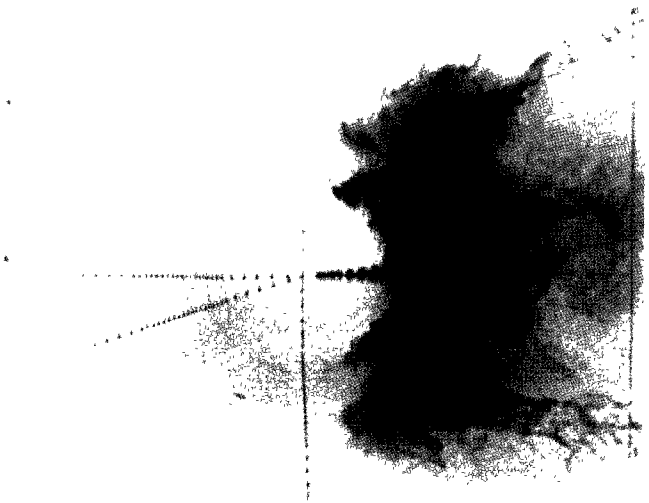

TOP VIEW

SIDE VIEW

(B) DYE RELEASE FROM 0^0 PORTS, F = 0.2.

Figure 11. Visualization of surface flow patterns from injection of tracers.

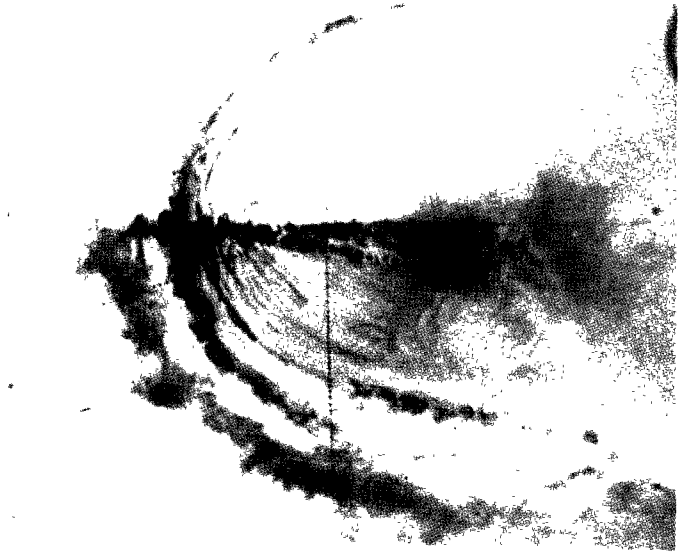

TOP VIEW

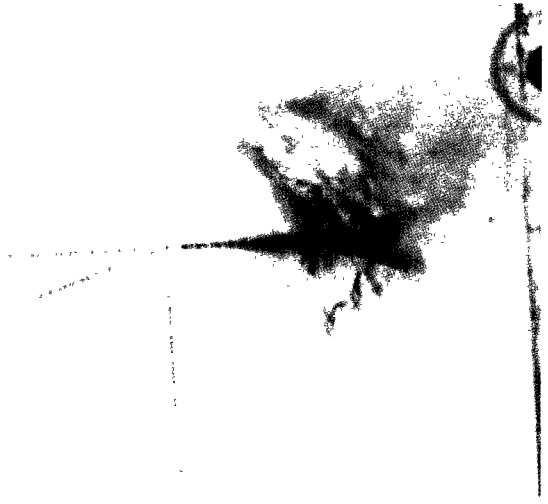

TOP VIEW

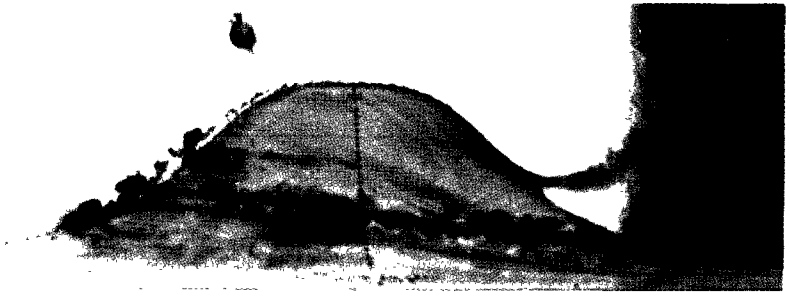

SIDE VIEW

(C) DYE RELEASE FROM 180° PORTS, F = 0.4

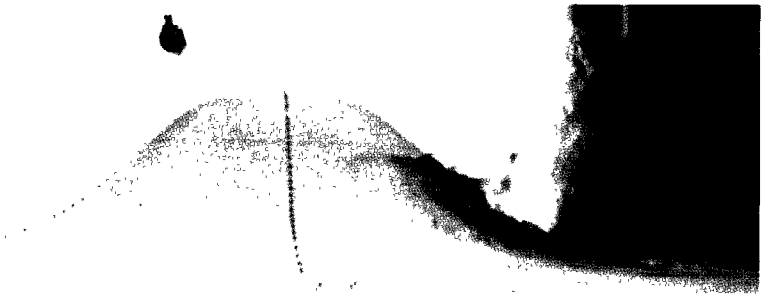

SIDE VIEW

(D) DYE RELEASE FROM 0° PORTS, F = 0.4.

Figure 11 (continued). Visualization of surface flow patterns from injection of tracers.

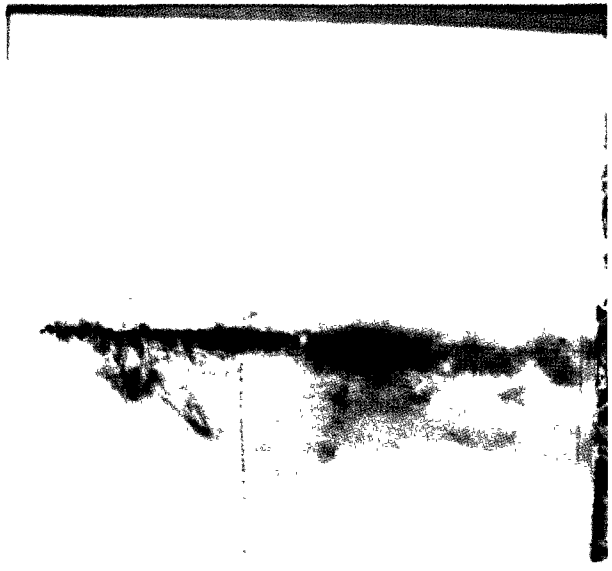

TOP VIEW

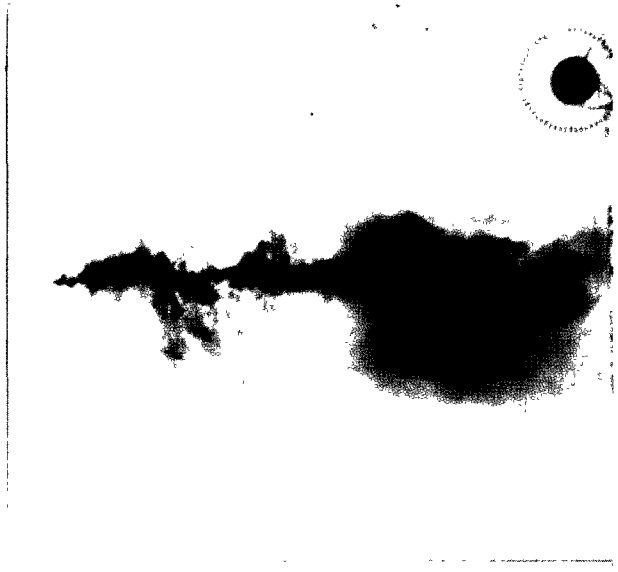

TOP VIEW

SIDE VIEW

(E) DYE RELEASE FROM 180° PORTS, F = 0.9.

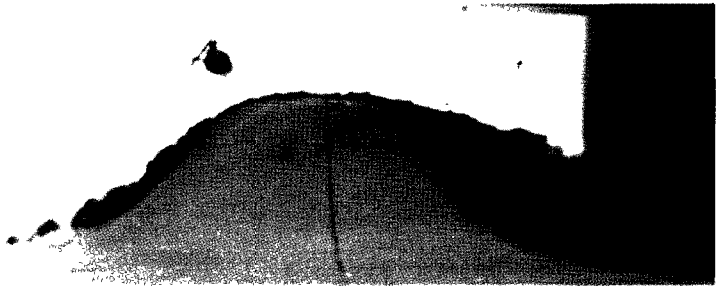

SIDE VIEW

(F) DYE RELEASE FROM 180° PORTS, F = 1.6.

Figure 11 (continued). Visualization of surface flow patterns from injection of tracers.

(G) SMOKE RELEASE FROM 180^{0} PORTS, F = ∞.

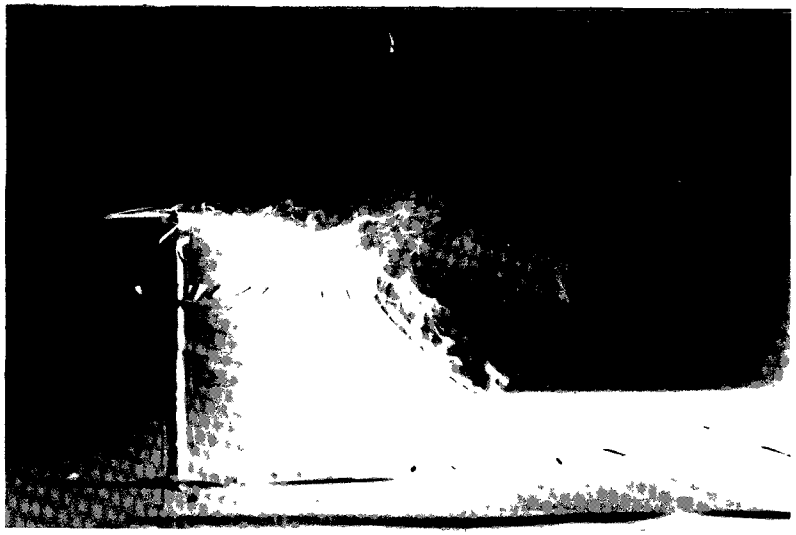

(H) SMOKE RELEASE FROM 0^{0} PORTS, F = ∞.

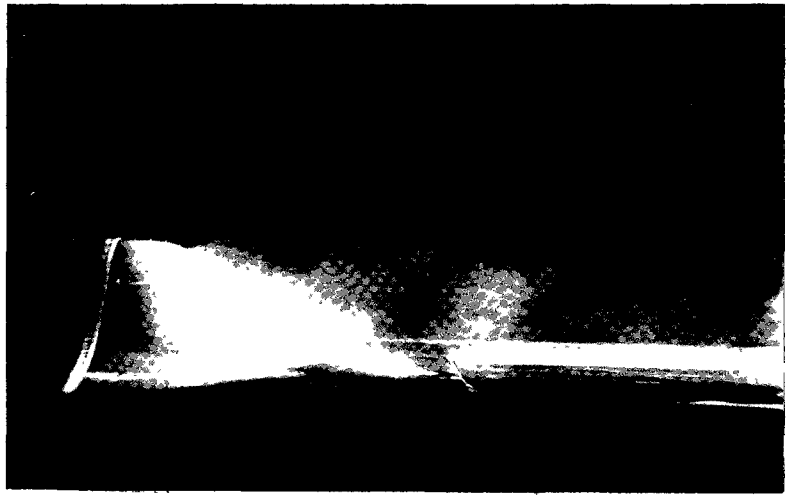

(I) $TiCl_4$ SMOKE AT DOWNWIND BASE OF HILL, F = ∞.

(J) $TiCl_4$ SMOKE AT DOWNWIND BASE OF HILL, F = ∞.

Figure 11 (continued). Visualization of surface flow patterns from injection of tracers.

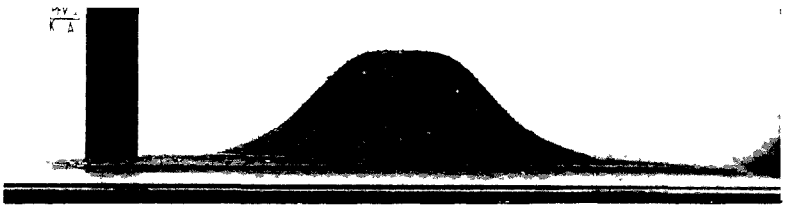

F = 0.2, Re = 5000

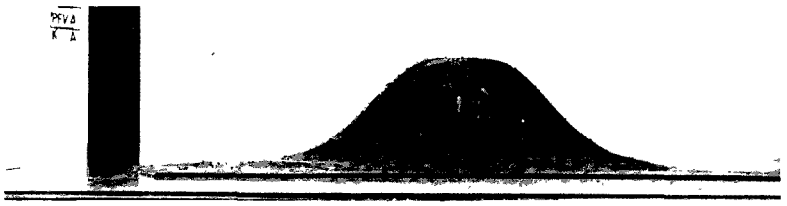

F = 0.4, Re = 10000

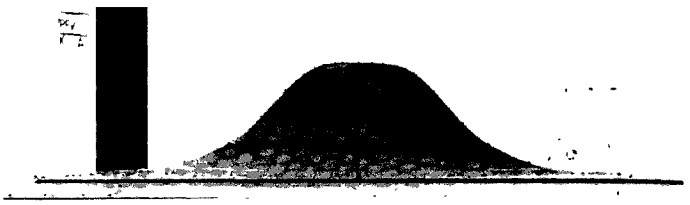

F = 1.0, Re = 25000

F = 1.7, Re = 42600

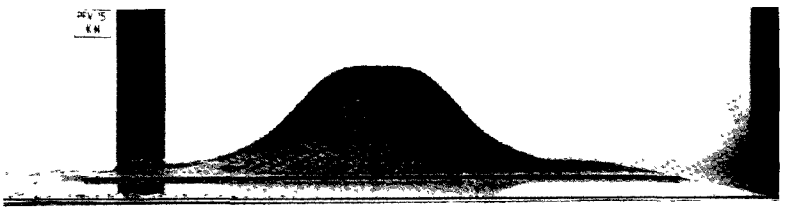

F = ∞, Re = 34400

(A) SIDE VIEWS OF $KMnO_4$ STREAMERS IN LARGE TANK.

Figure 12. Visualization of surface shear stress patterns.

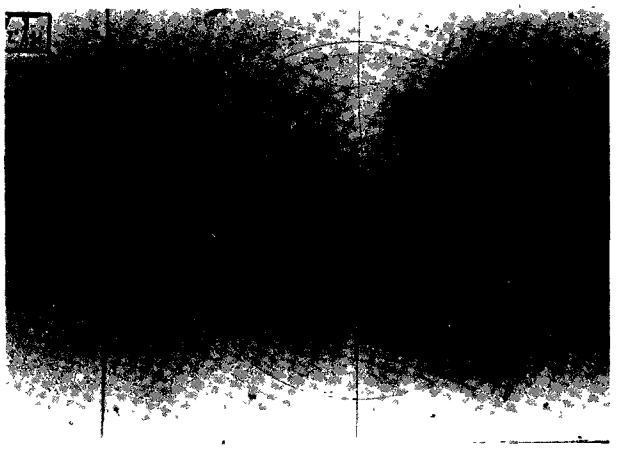

F = 0.2, Re = 5000

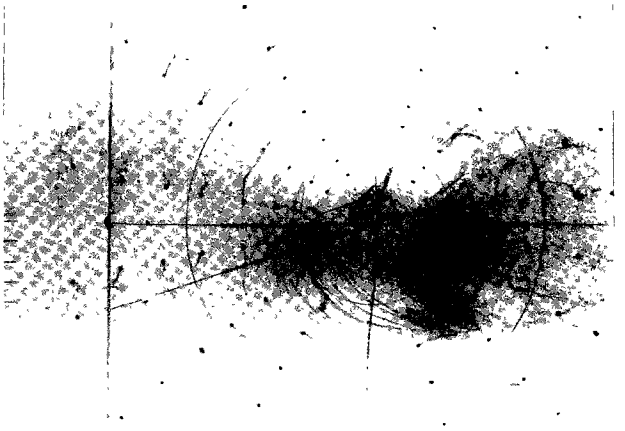

F = 0.4, Re = 10000

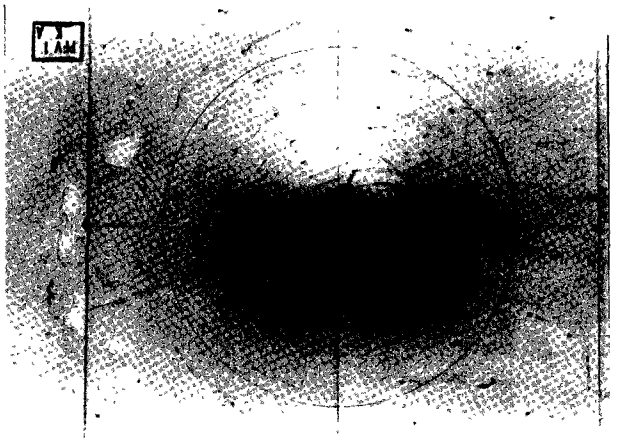

F = 1.0, Re = 25000

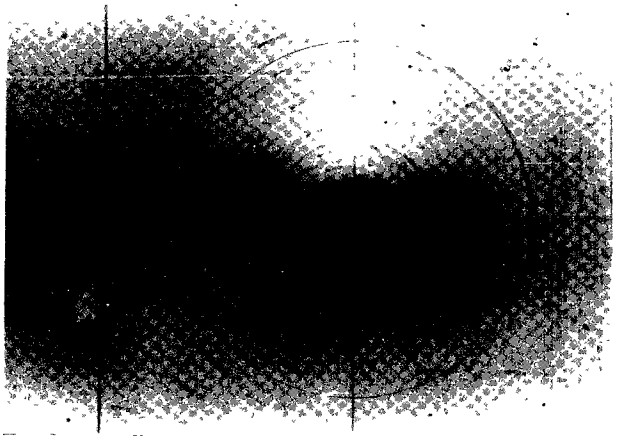

F = 1.7, Re = 42600

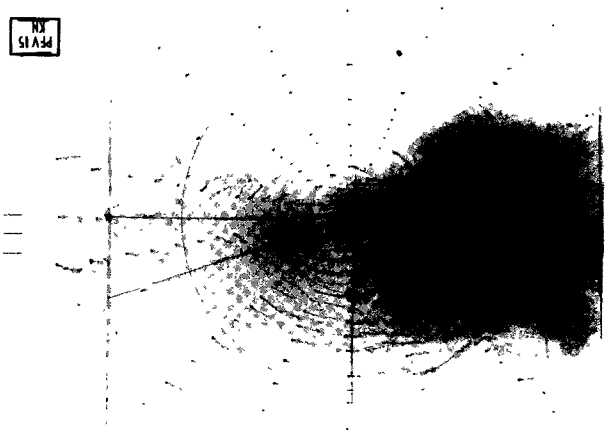

F = ∞, Re = 34000

(B) TOP VIEWS OF $KMnO_4$ STREAMERS IN LARGE TANK

Figure 12 (continued). Visualization of surface shear stress patterns.

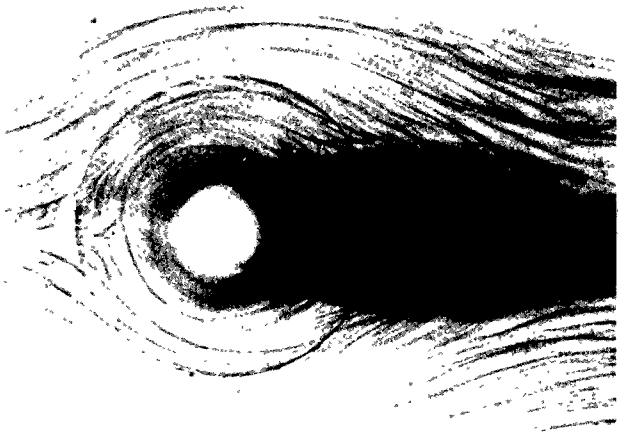

F = 0.2, Re = 160

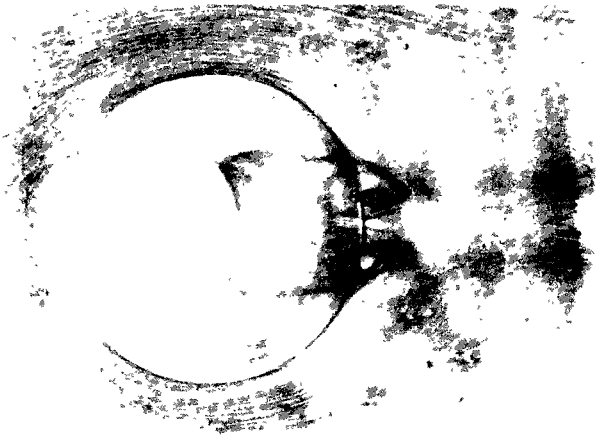

F = 0.4, Re = 400

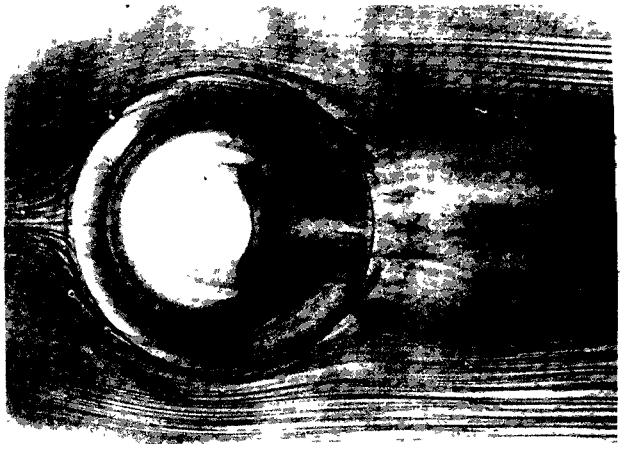

F = 1.0, Re = 800

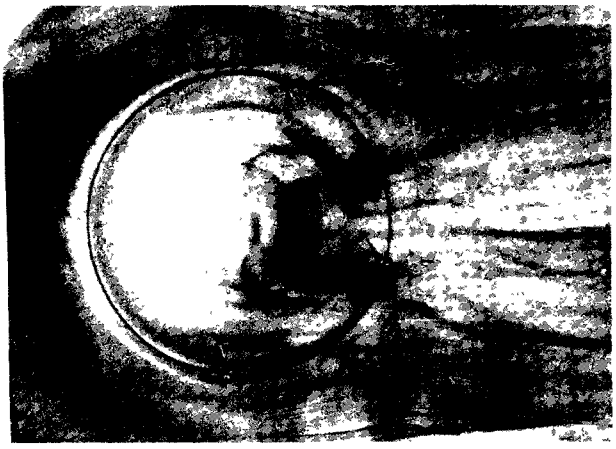

F = 1.7, Re = 1400

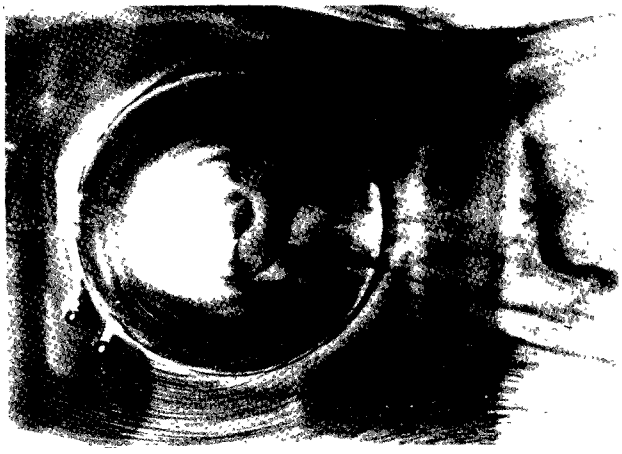

F = ∞, Re = 1000

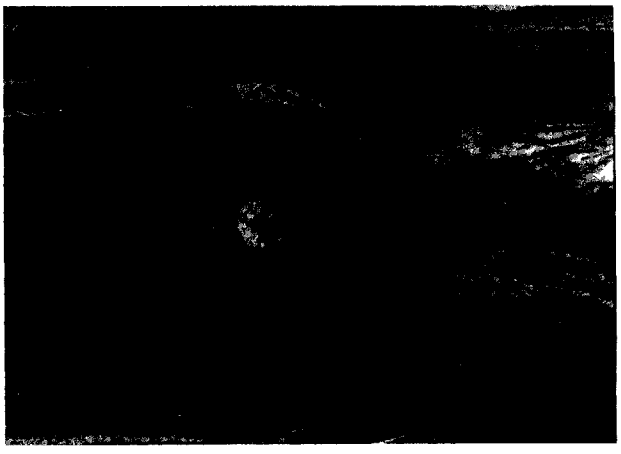

F = ∞, Re = 2000

(C) TOP VIEWS OF GELATIN/DYE AND $KMnO_4$ STREAMERS IN SMALL TANK.

Figure 12 (continued). Visualization of surface shear stress patterns.

(A) F = 0.1, Re = 6870

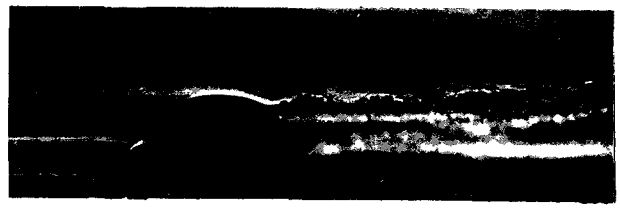

(B) F = 0.2, Re = 13740

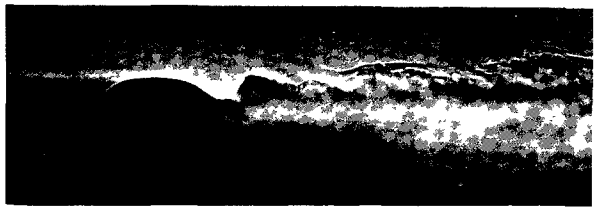

(C) F = 0.3, Re = 20610

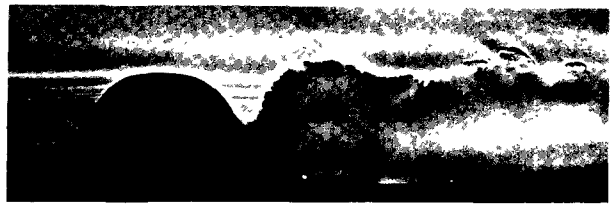

(D) F = 0.4, Re = 27480

(E) F = 0.5, Re = 34400

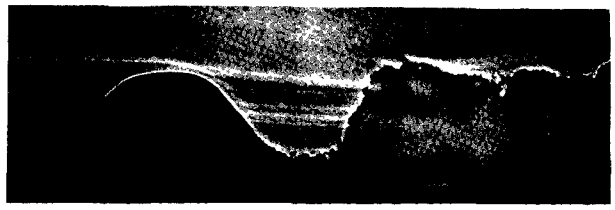

(F) F = 0.6, Re = 41200

(G) F = 0.8, Re = 55000

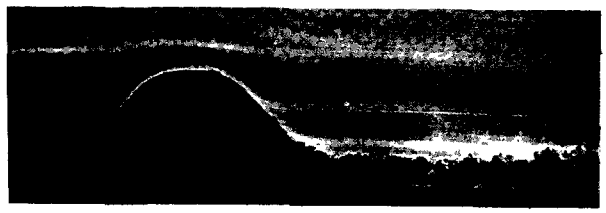

(H) F = 1.0, Re = 68700

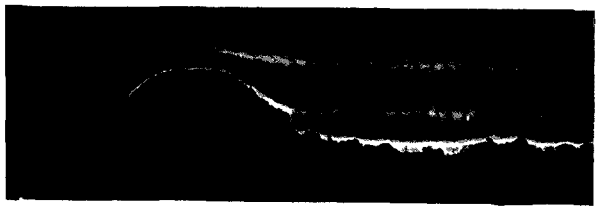

(I) F = 1.2, Re = 81600

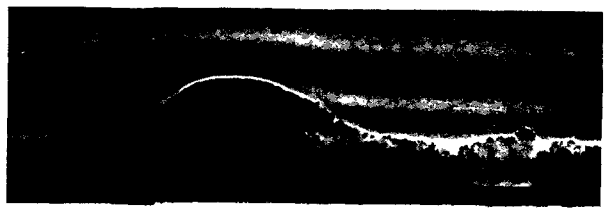

(J) F = 1.7, Re = 117000

Figure 13. Shadowgraphs of flow over hill (N = 1.33 rad/sec).

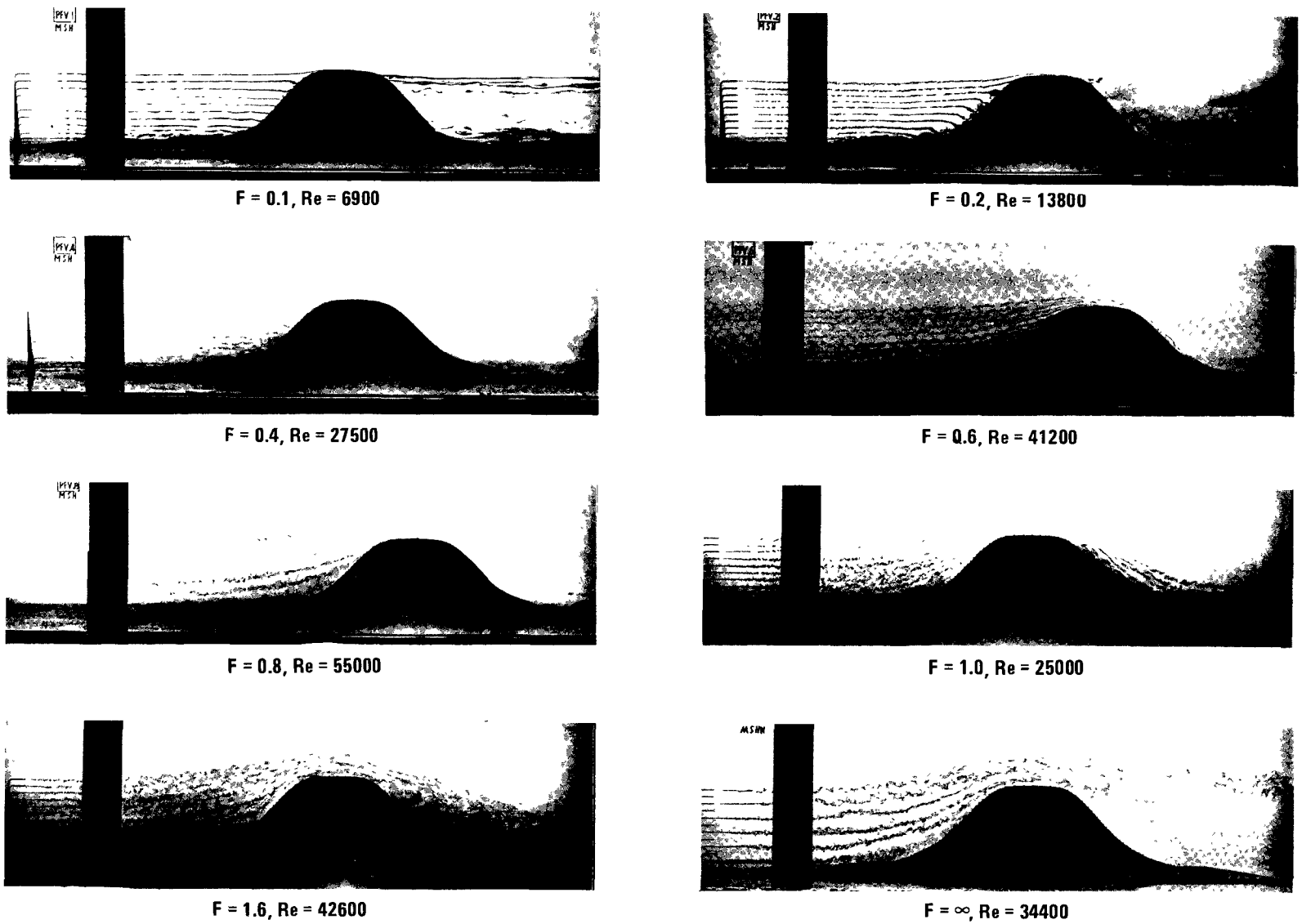

(A) SIDE VIEWS IN LARGE TANK.

Figure 14. Experimental observations of centerplane streamlines from multi-level tracer injection.

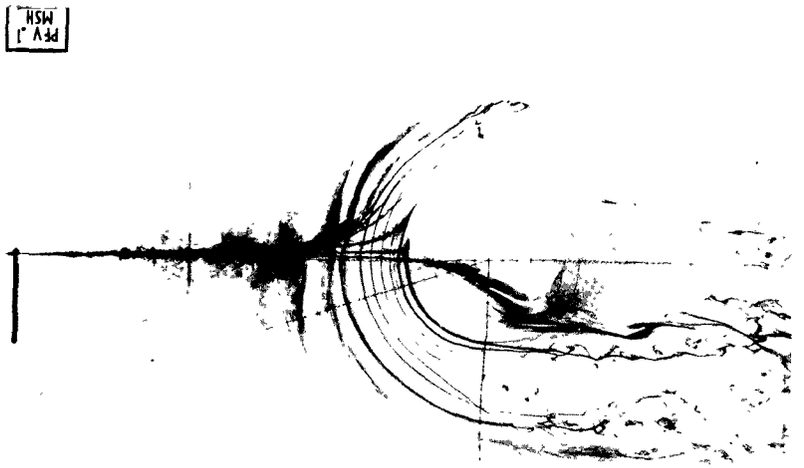

F = 0.1, Re = 6900

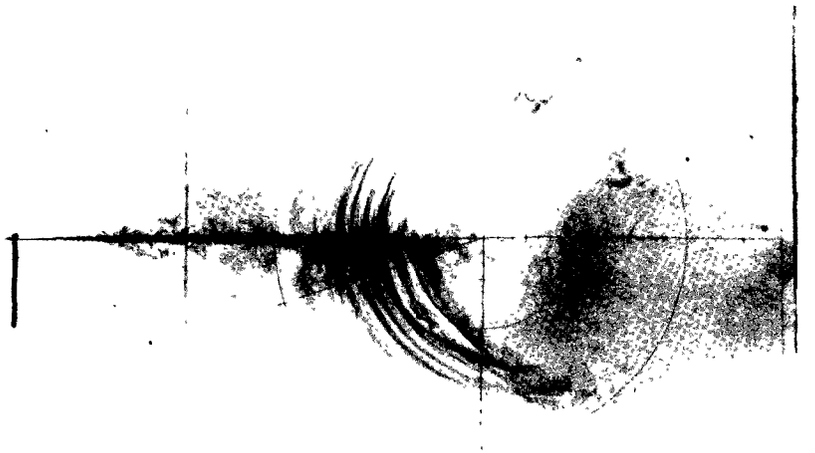

F = 0.2, Re = 13800

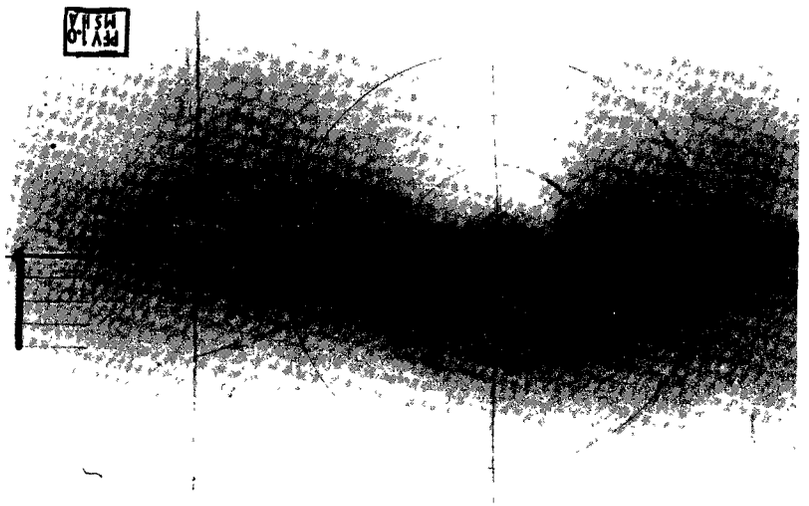

F = 1.0, Re = 25000

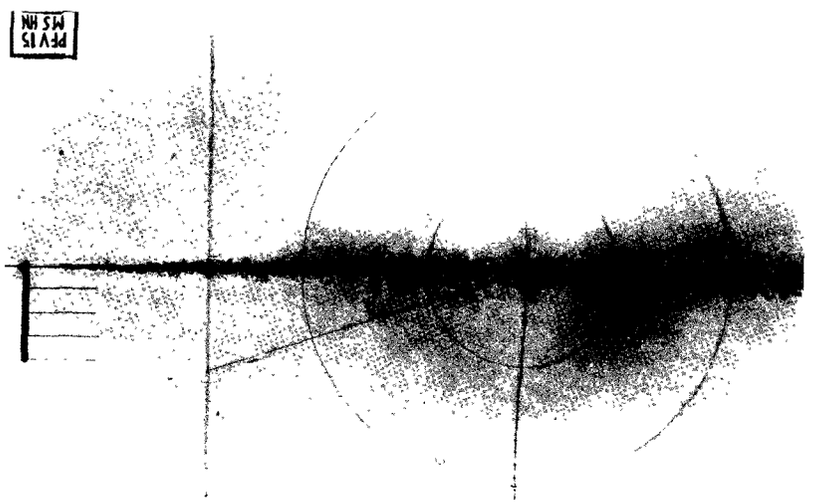

F = ∞, Re = 34400

(B) TOP VIEWS IN LARGE TANK.

Figure 14 (continued). Experimental observations of centerplane streamlines from multi-level tracer injection.

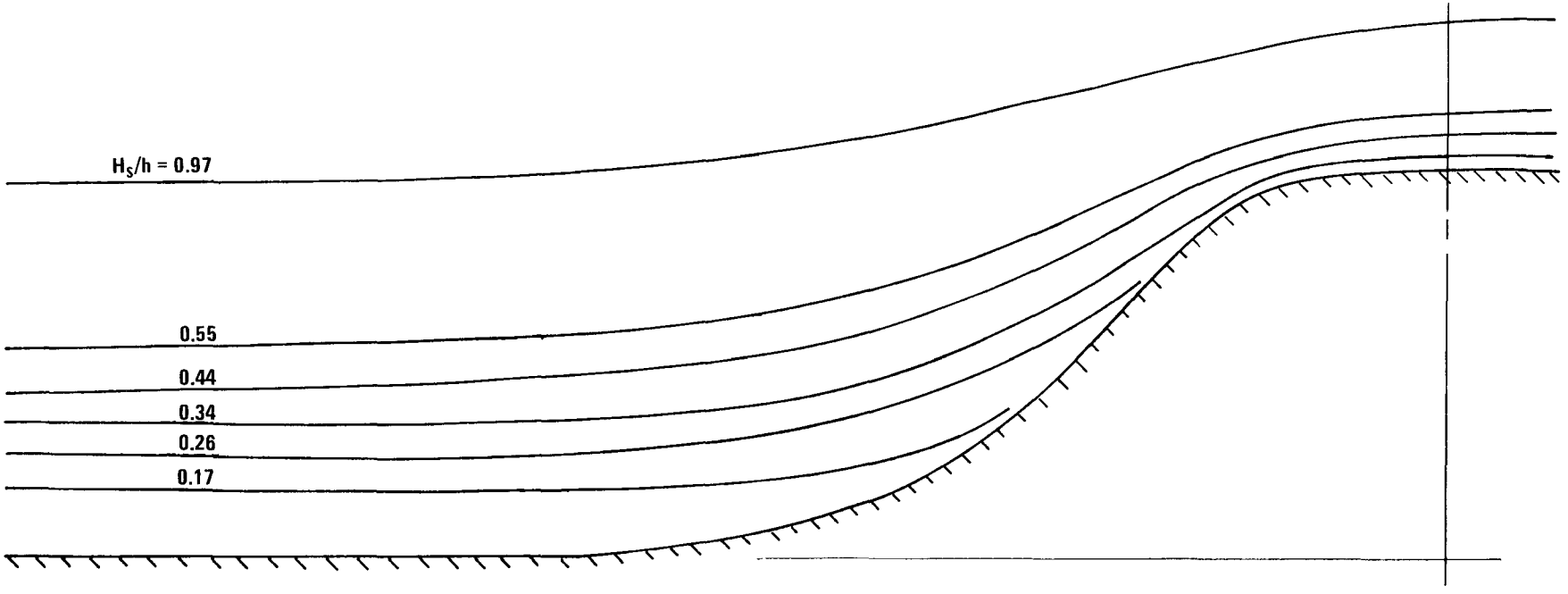

(C) TRACINGS OF SMOKE PLUME CENTERLINES IN WIND TUNNEL, $F = \infty$.

Figure 14(continued). Experimental observations of center plane streamlines from multilevel tracer injection.

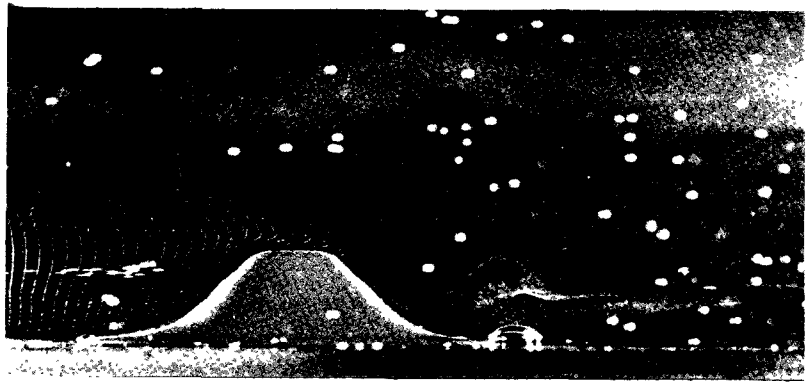

(A) F = 0.4, Re = 1900

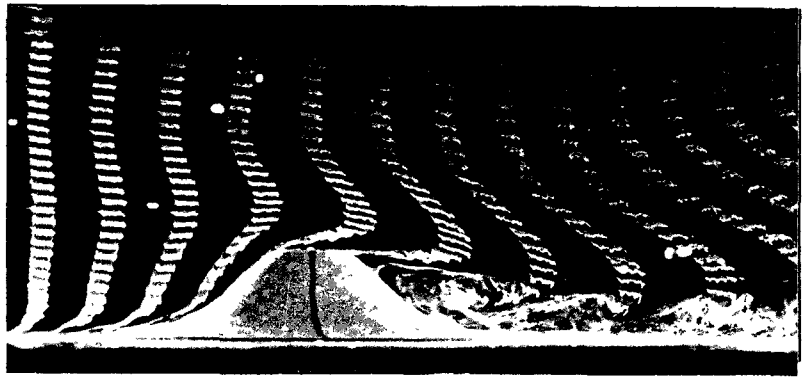

(B) F = 1.0, Re = 1750

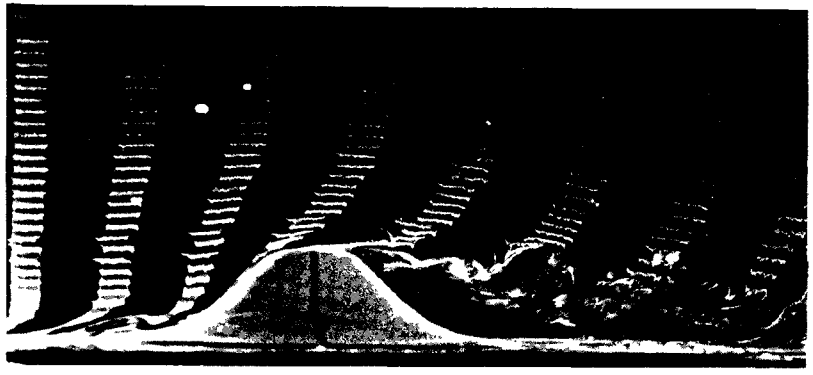

(C) F = 1.7, Re = 3000

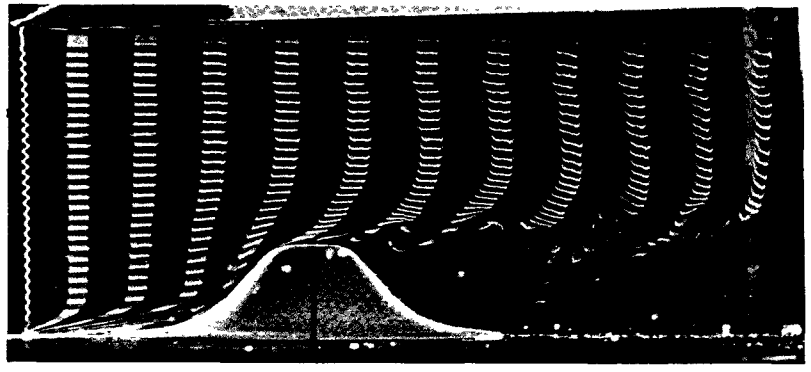

(D) F = ∞, Re = 1900

Figure 15. Hydrogen bubble photographs indicating speed-up over top of hill and the downwind lee wave pattern.

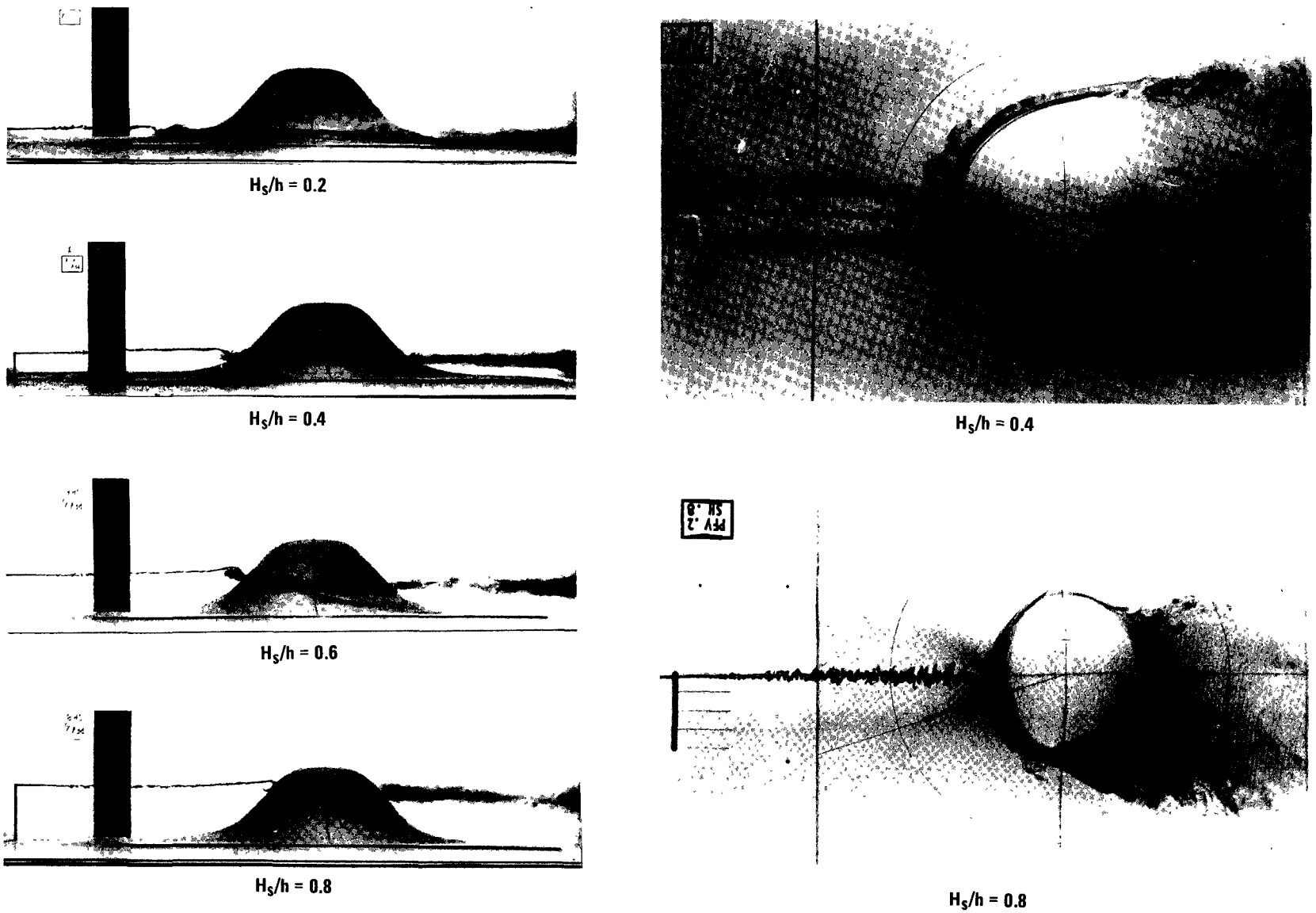

(A) F = 0.2, Re = 13700

Figure 16. Plumes from upwind stacks at various elevations and Froude numbers in large tank.

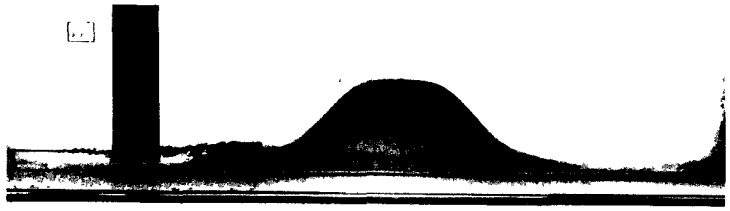

$H_s/h = 0.2$

$H_s/h = 0.4$

$H_s/h = 0.6$

$H_s/h = 0.8$

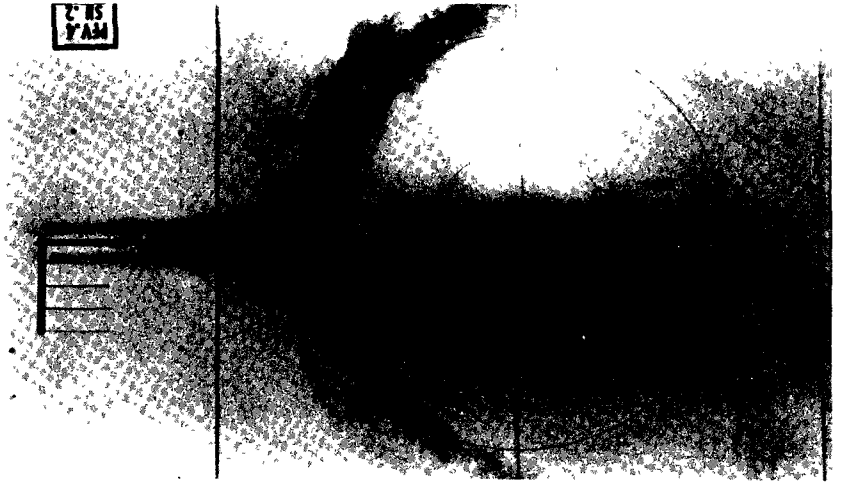

$H_s/h = 0.2$

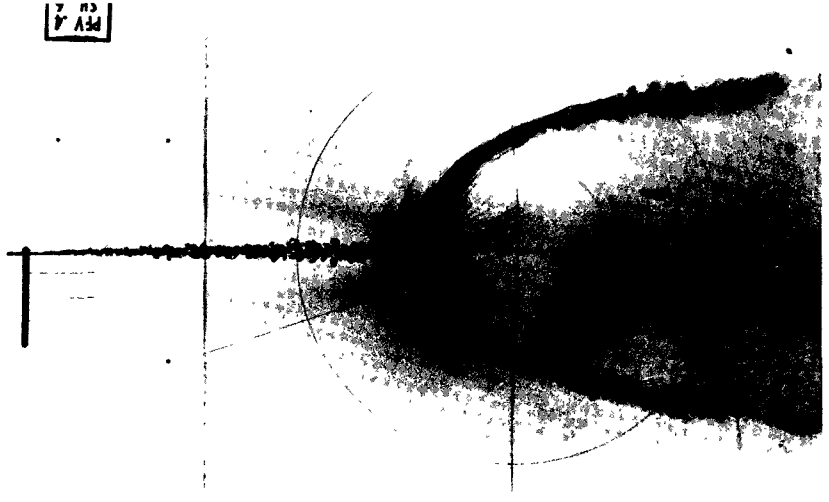

$H_s/h = 0.6$

(B) F = 0.4, Re = 27500

Figure 16 (continued). Plumes from upwind stacks at various elevations and Froude numbers in large tank.

F = 0.6, H_s/h = 0.2, Re = 41200

F = 0.6, H_s/h = 0.4, Re = 41200

F = 0.8, H_s/h = 0.2, Re = 55000

F = ∞, H_s/h = 0.2, Re = 34400

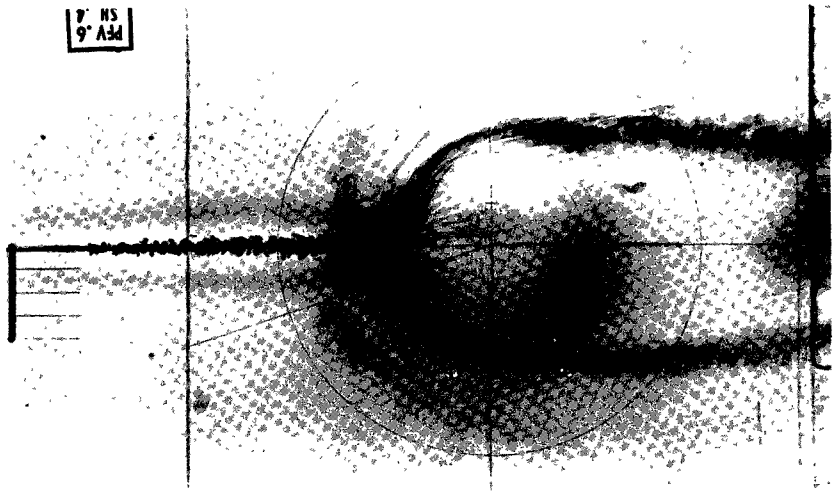

F = 0.6, H_s/h = 0.4, Re = 41200

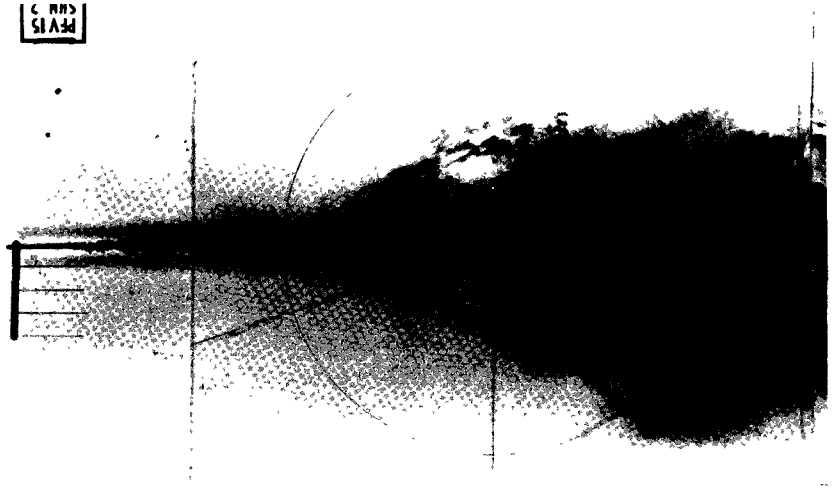

F = ∞, H_s/h = 0.2, Re = 34400

(C) F ≥ 0.6

Figure 16 (continued). Plumes from upwind stacks at various elevations and Froude numbers in large tank.

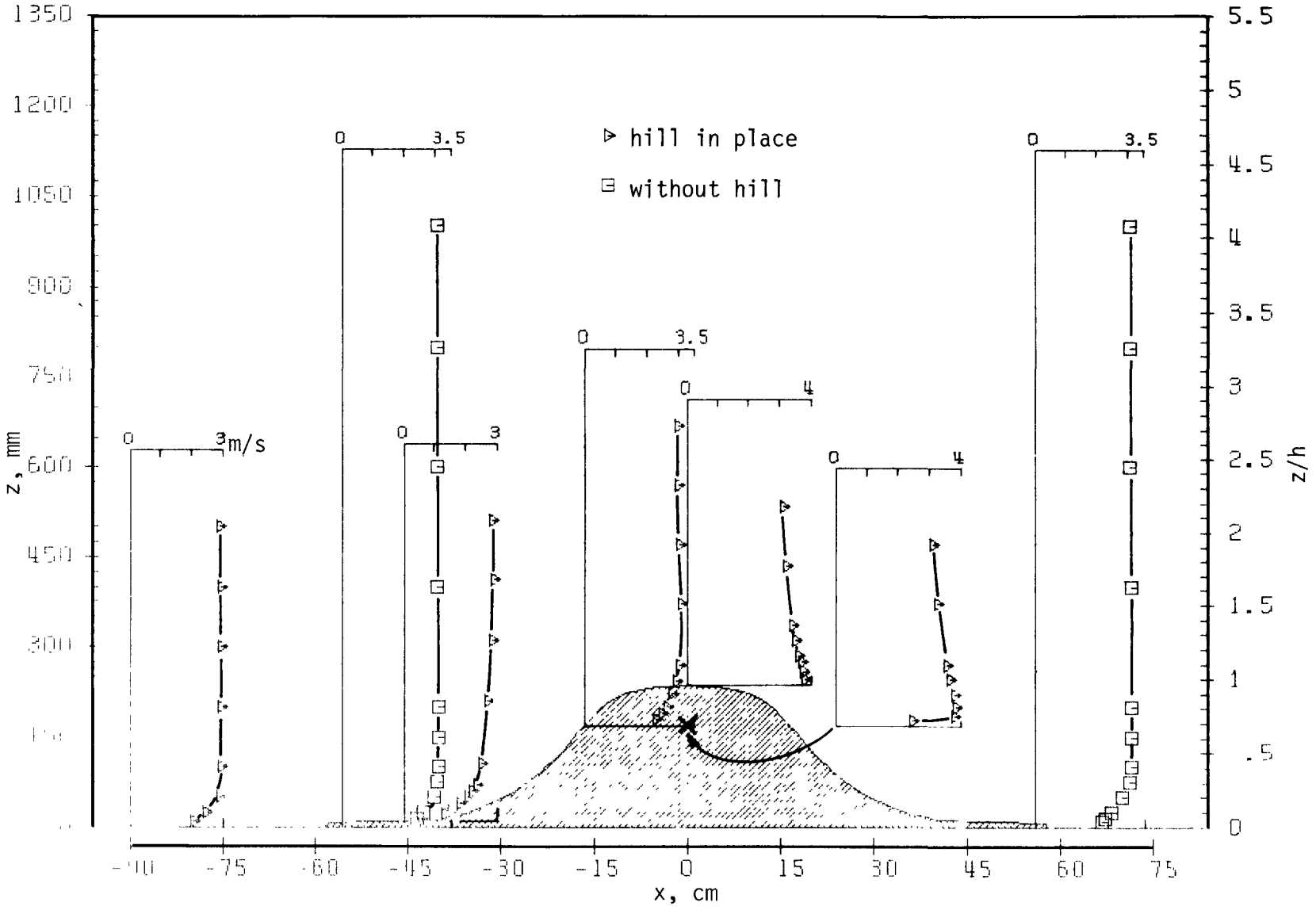

(A) MEAN VELOCITY PROFILES.

Figure 17. Wind tunnel measurements of the flow over and in the absence of the hill.

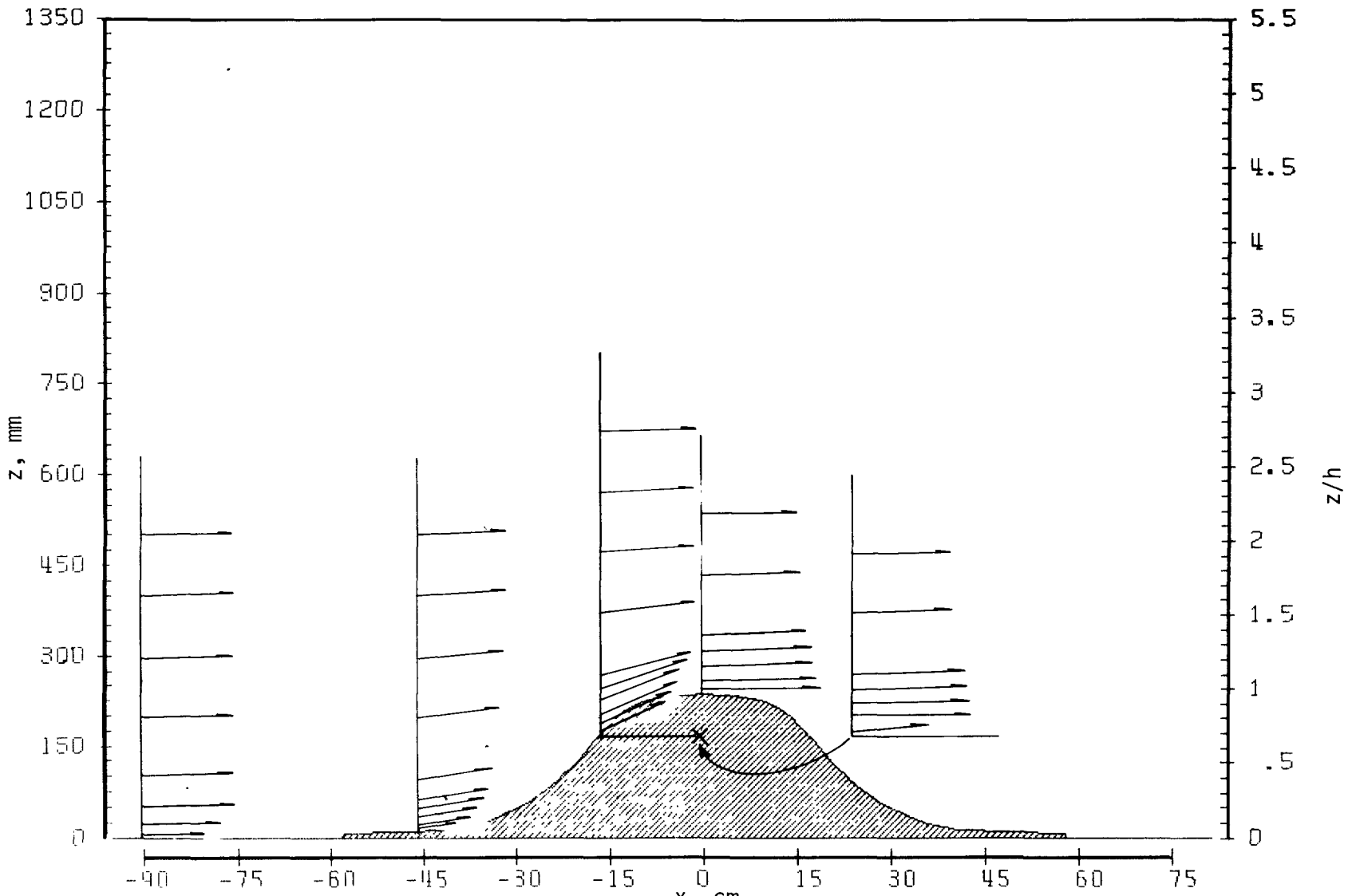

Figure 17 (continued). Wind tunnel measurements of the flow over and in the absence of the hill.

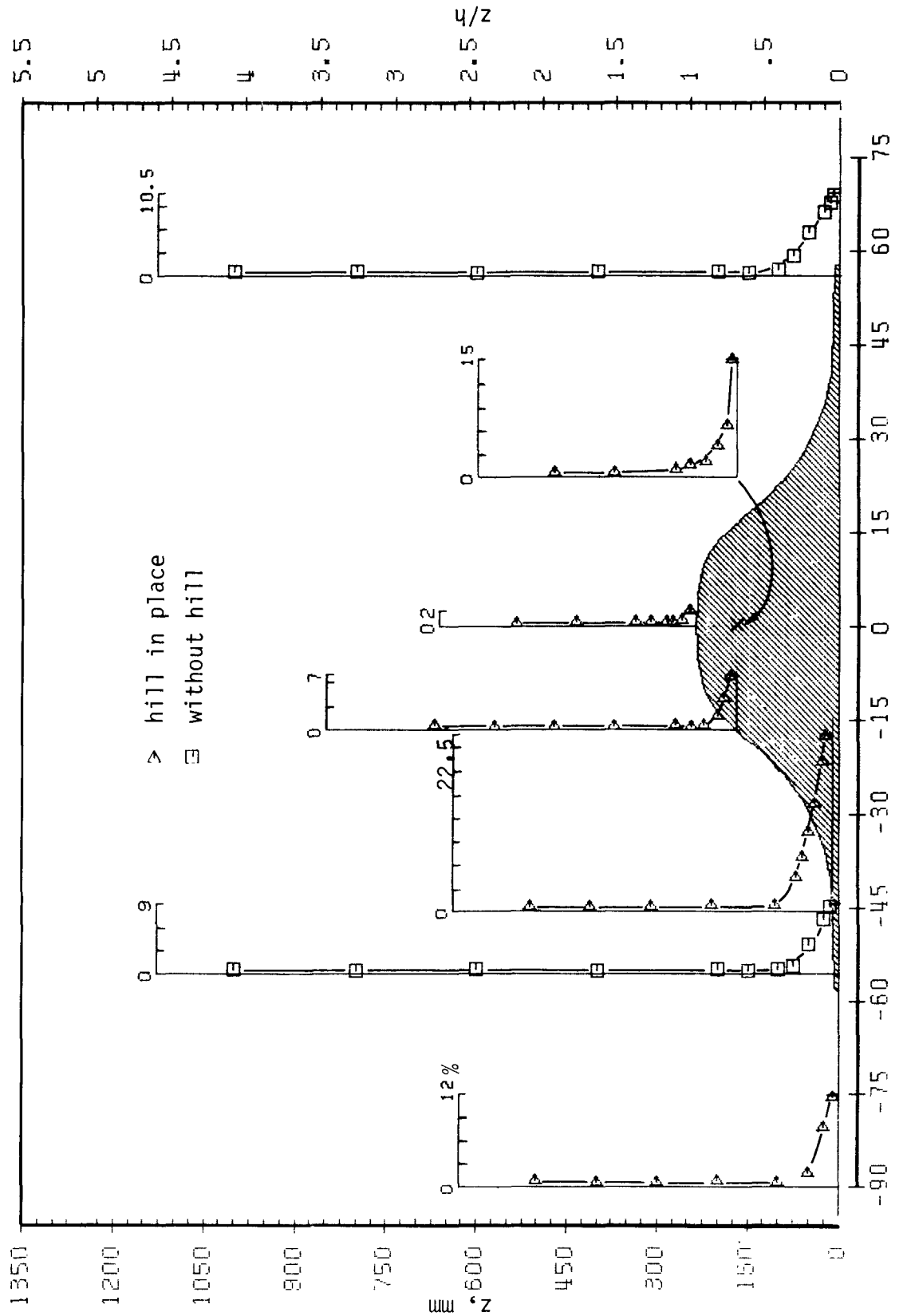

Figure 17 (continued). Wind tunnel measurements of the flow over and in the absence of the hill.

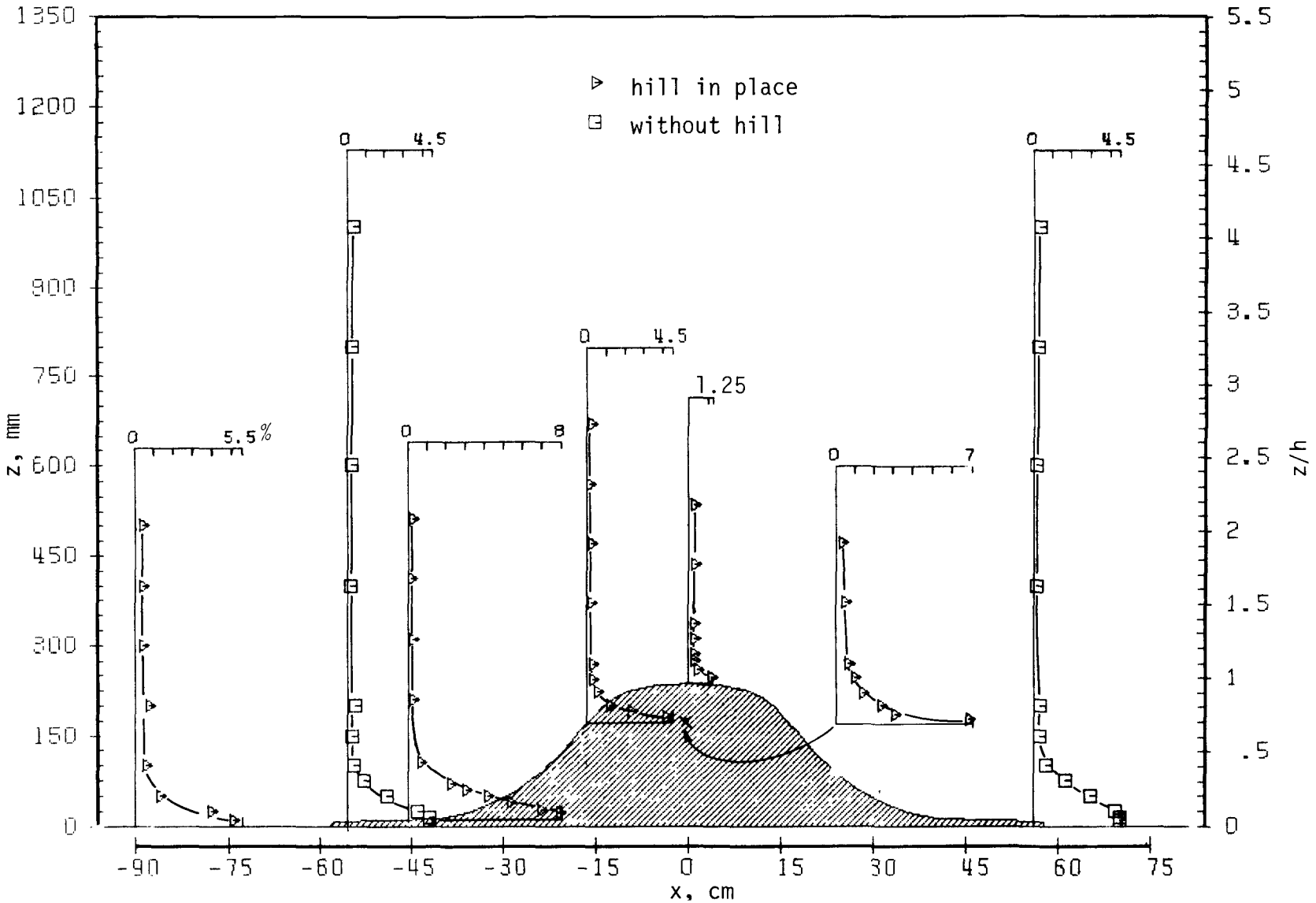

(D) LOCAL VERTICAL TURBULENCE INTENSITY PROFILES.

Figure 17 (continued). Wind tunnel measurements of the flow over and in the absence of the hill.

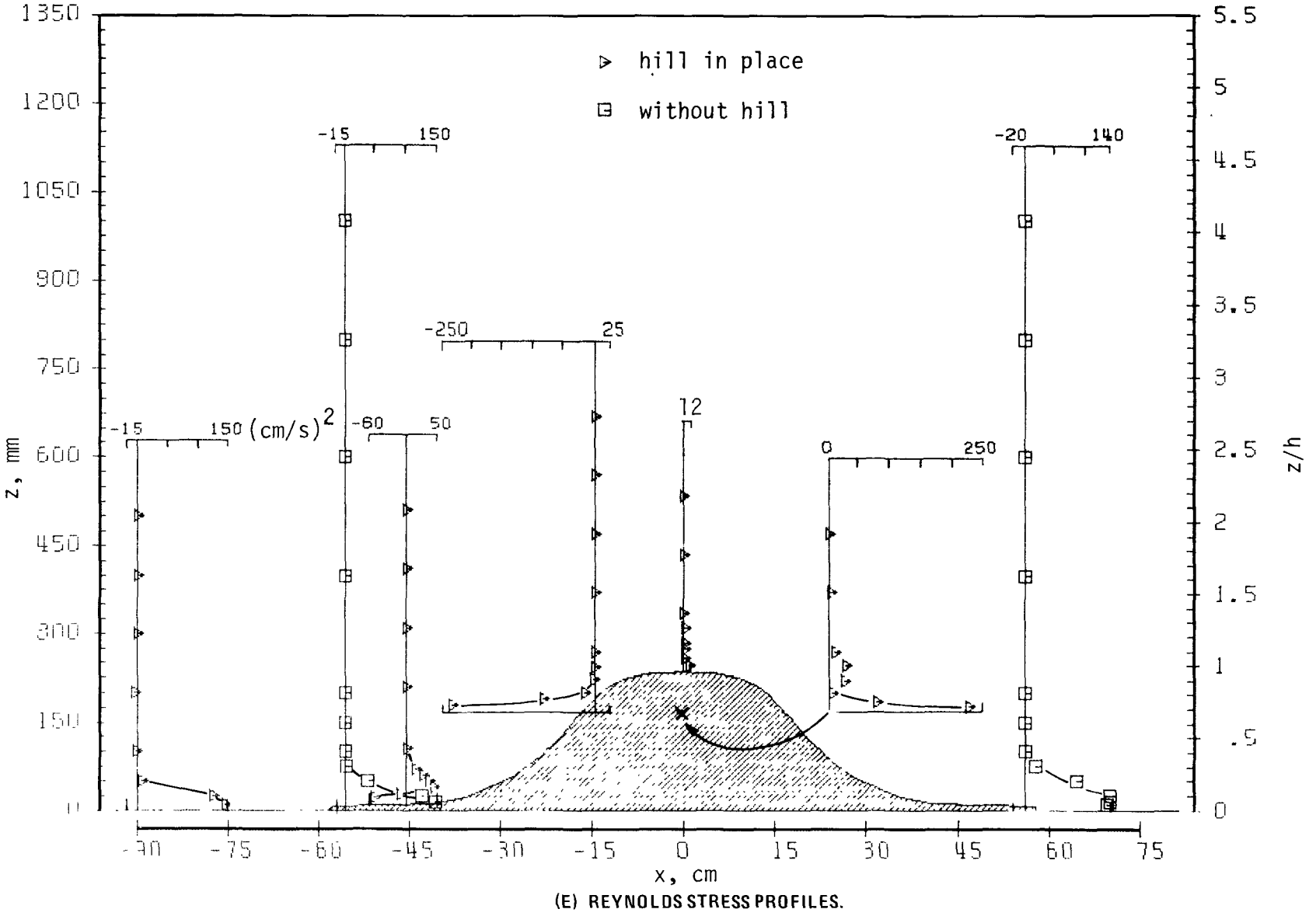

(E) REYNOLDS STRESS PROFILES.

Figure 17 (continued). Wind tunnel measurements of the flow over and in the absence of the hill.

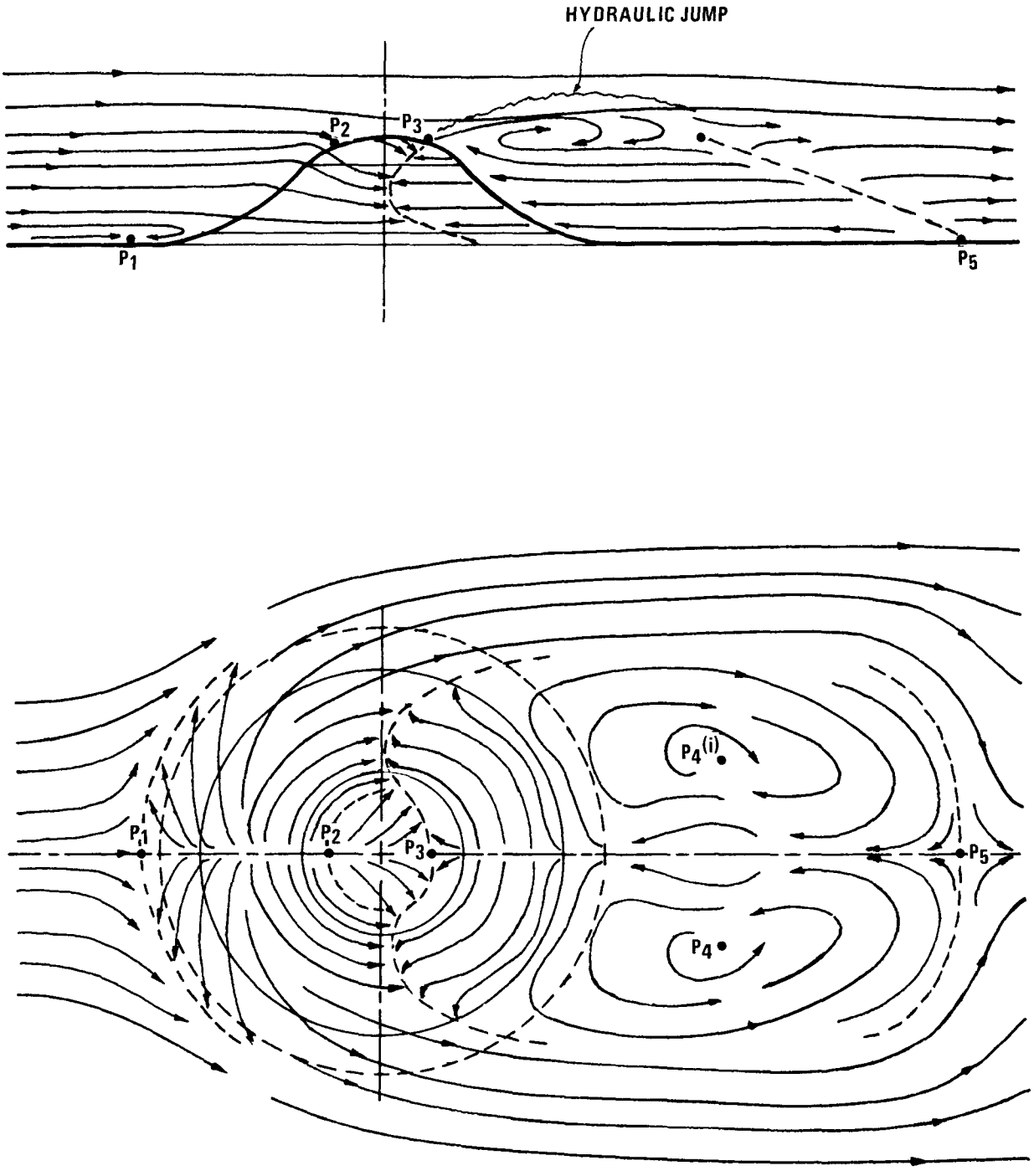

(A) F=0.2

Figure 18. Derived centerplane streamline and surface shear stress patterns.

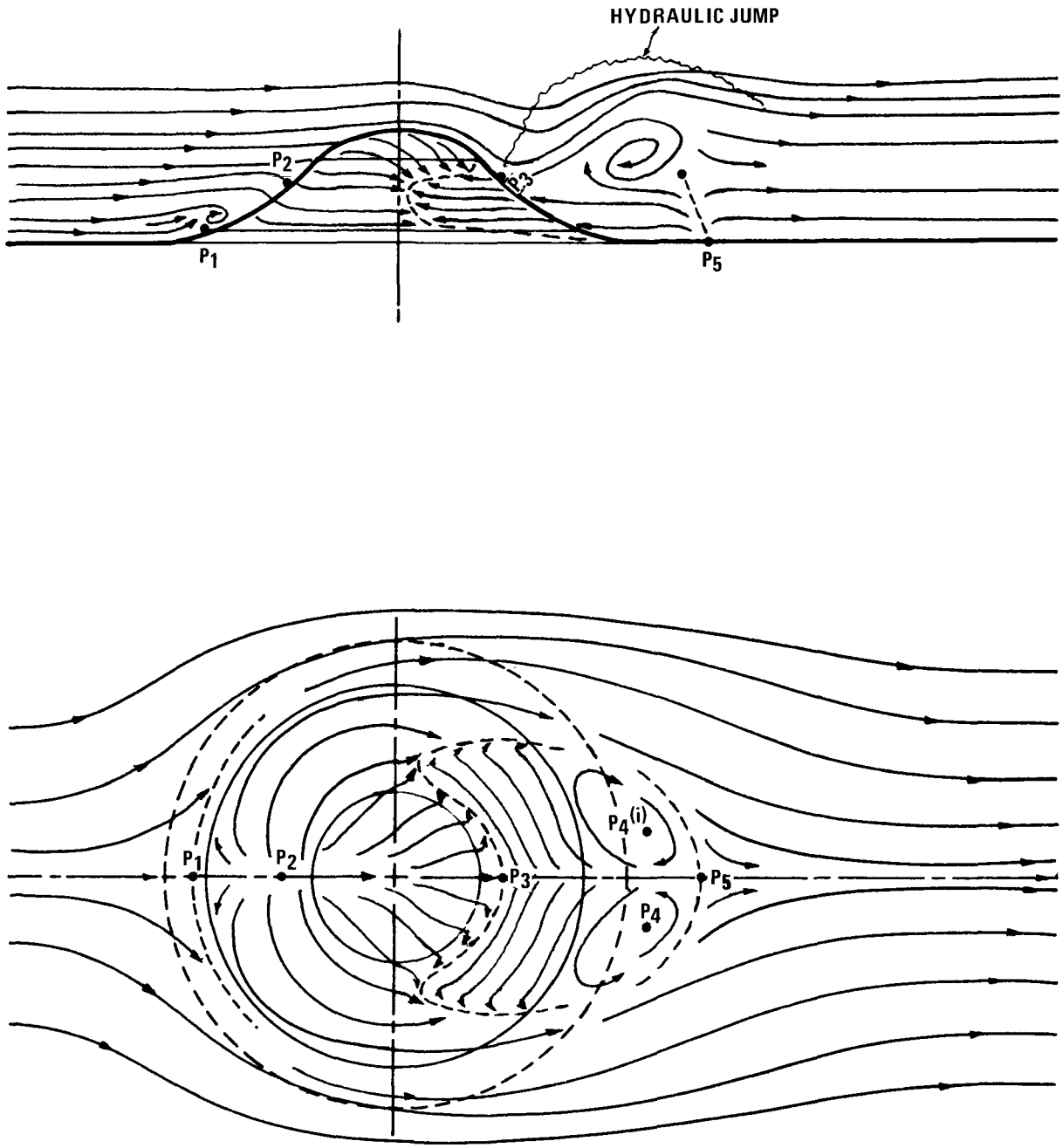

(B) F=0.4

Figure 18 (continued). Derived centerplane streamline and surface shear stress patterns.

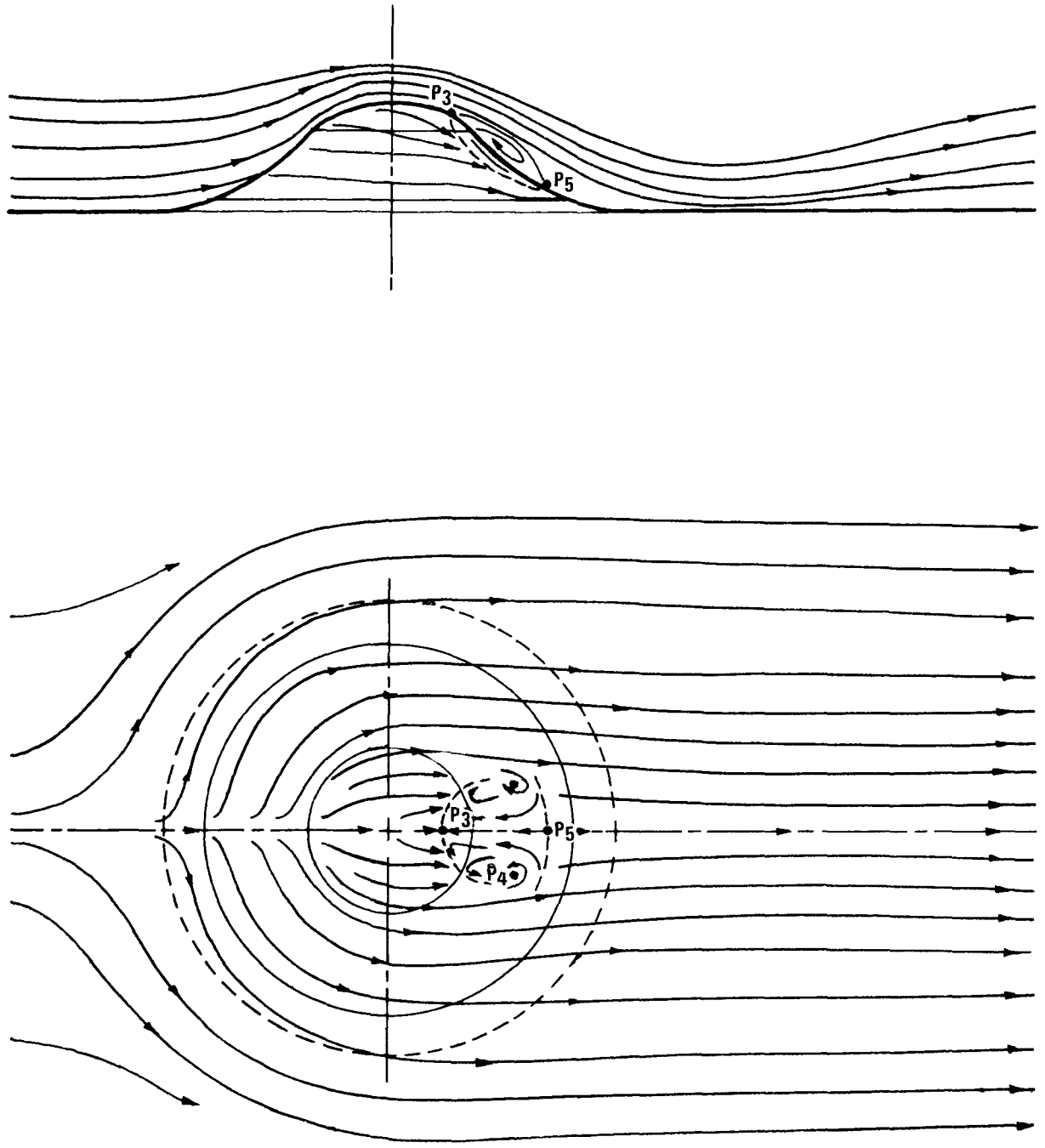

(C) F=1.0

Figure 18 (continued). Derived centerplane streamline and surface shear stress patterns.

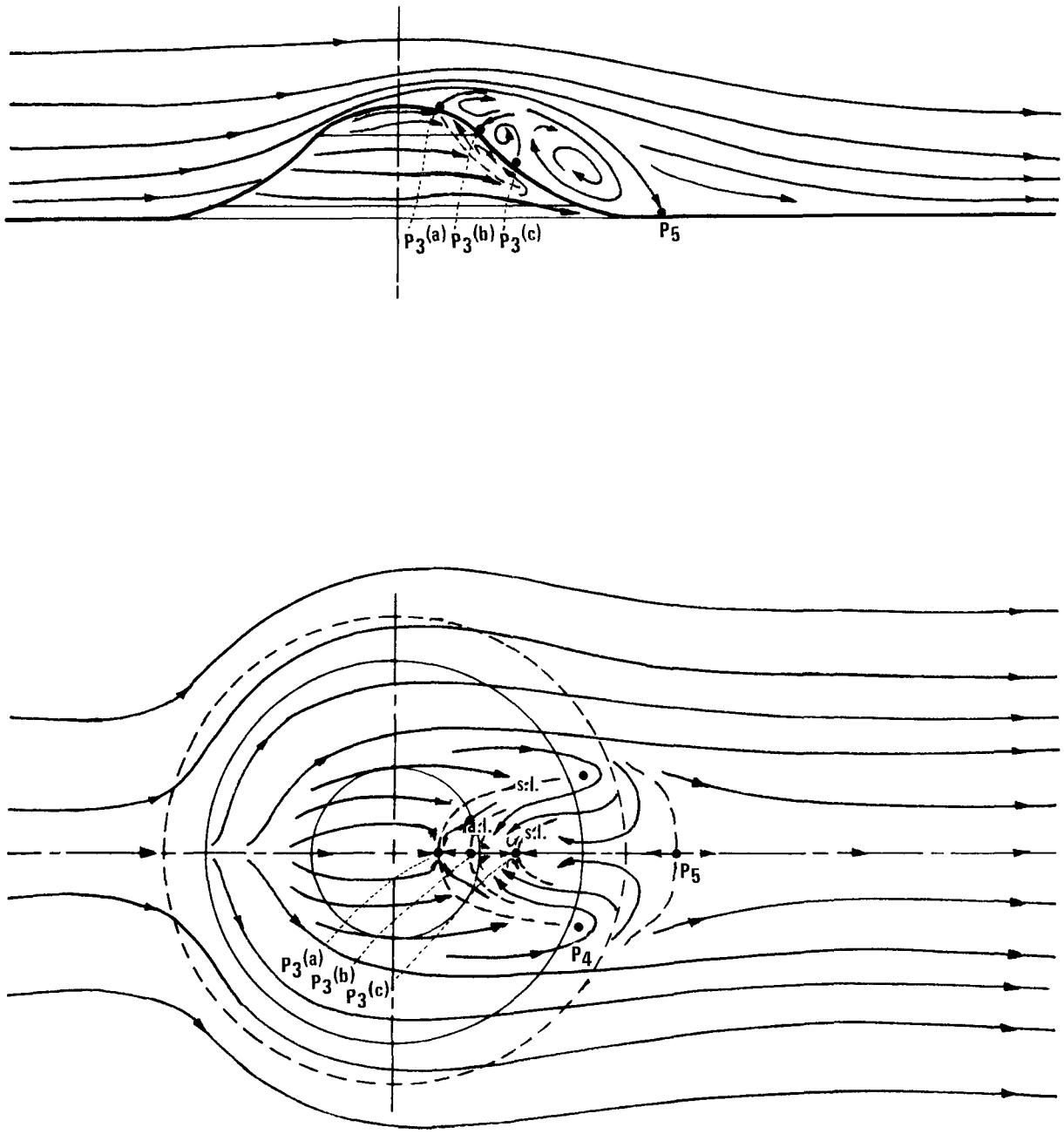

(D) F=1.7

Figure 18 (continued). Derived centerplane streamline and surface shear stress patterns.

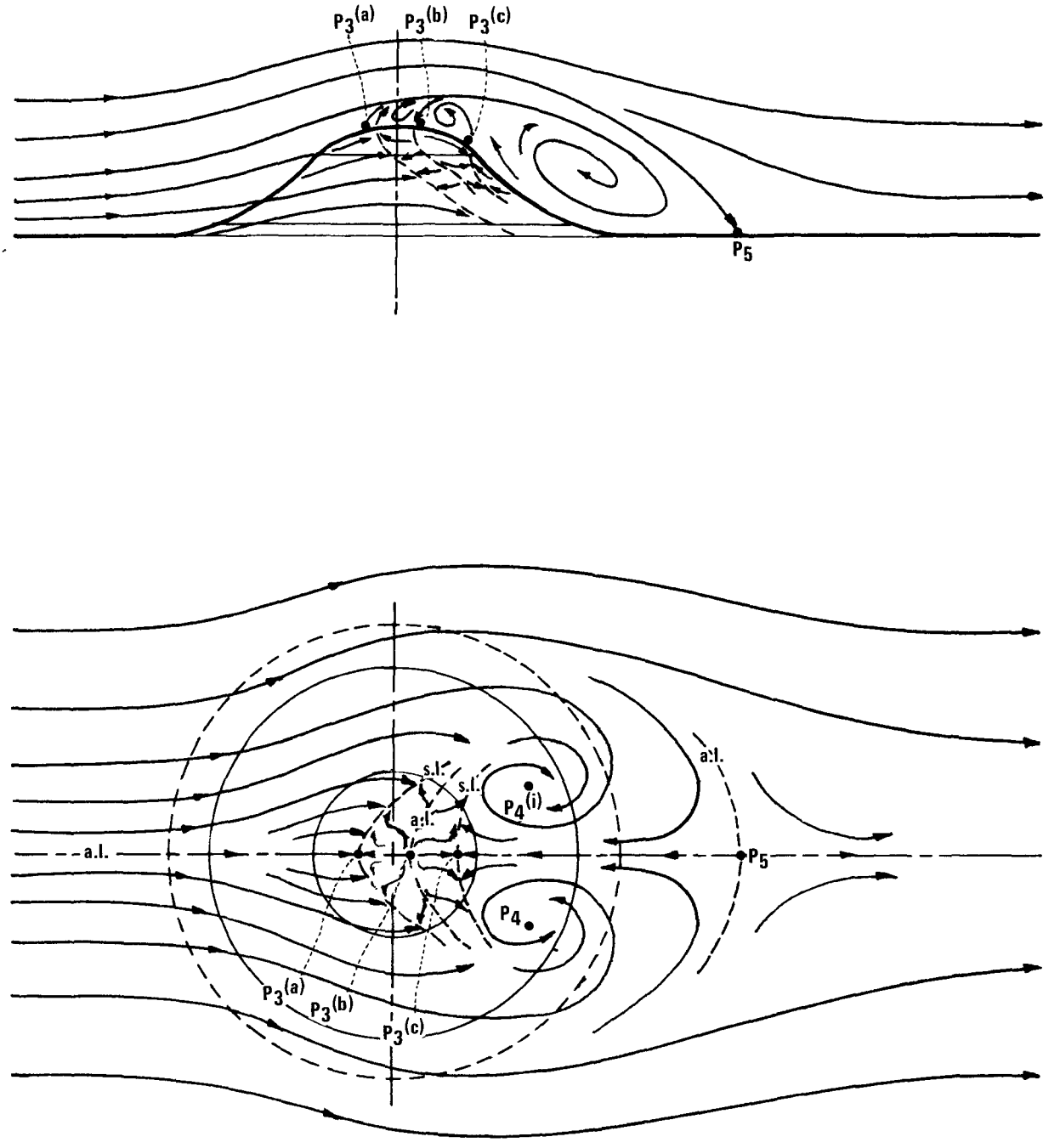

(E) F= ∞

Figure 18 (continued). Derived centerplane streamline and surface shear stress patterns.

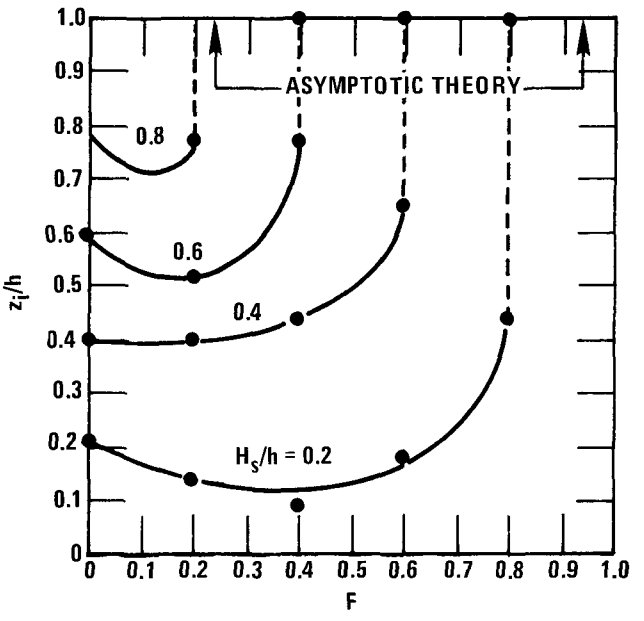

(A) TEST OF HYPOTHESIS $F=1-H_s/h$.

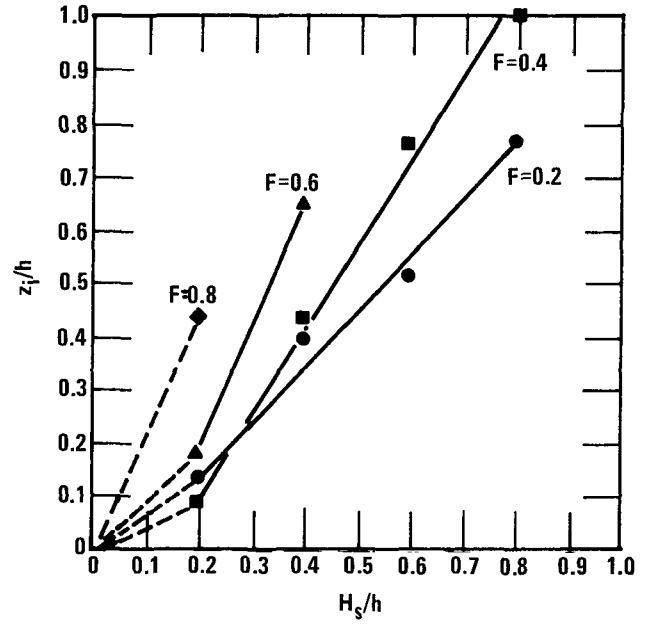

(B) IMPINGEMENT HEIGHT AS A FUNCTION OF SOURCE HEIGHT.

Figure 19. Plume impingement on the hill surface.

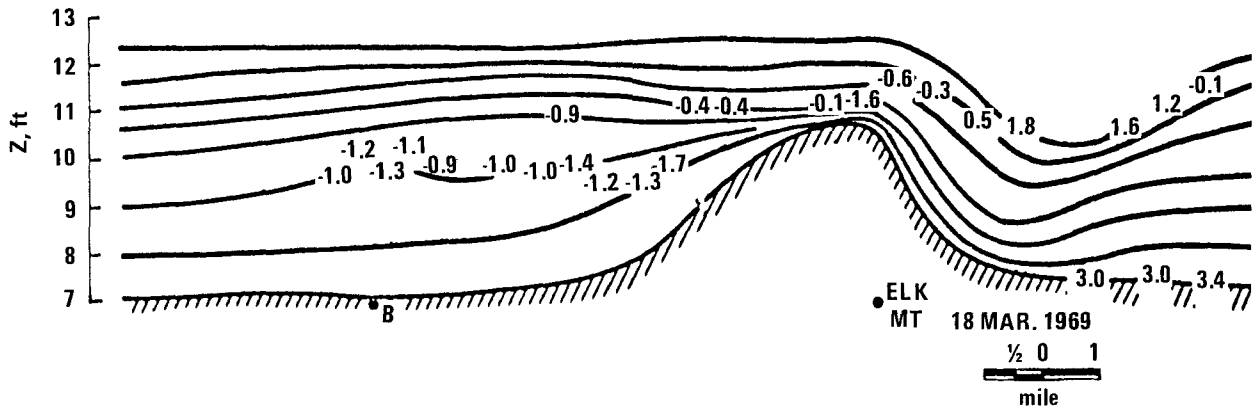

(A) ESTIMATED FROM AIRCRAFT OBSERVATIONS.

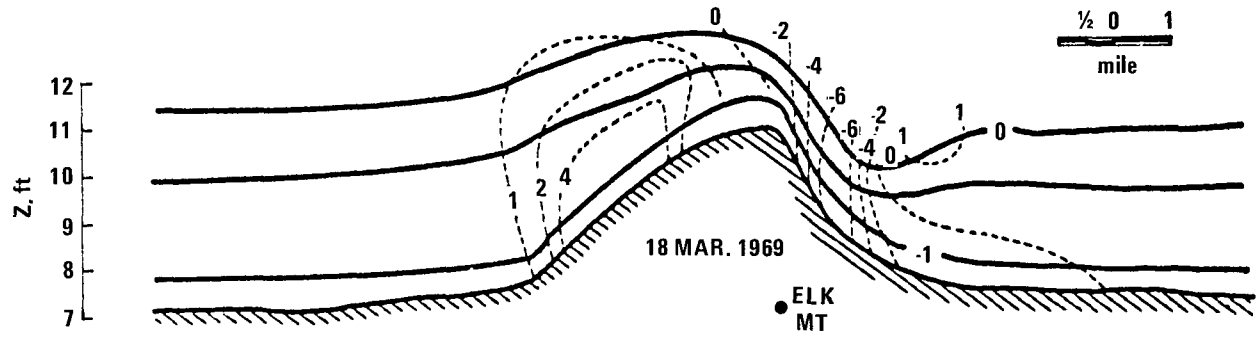

(B) ESTIMATED BY COMPUTER SIMULATION BASED ON SHALLOW WATER MODEL.

Figure 20. Streamline distributions over Elk Mountain, Wyoming (Diagrams taken from Kitabayashi et al., 1971, in turn from Marwitz et al., 1969). $F \simeq 1.0$.

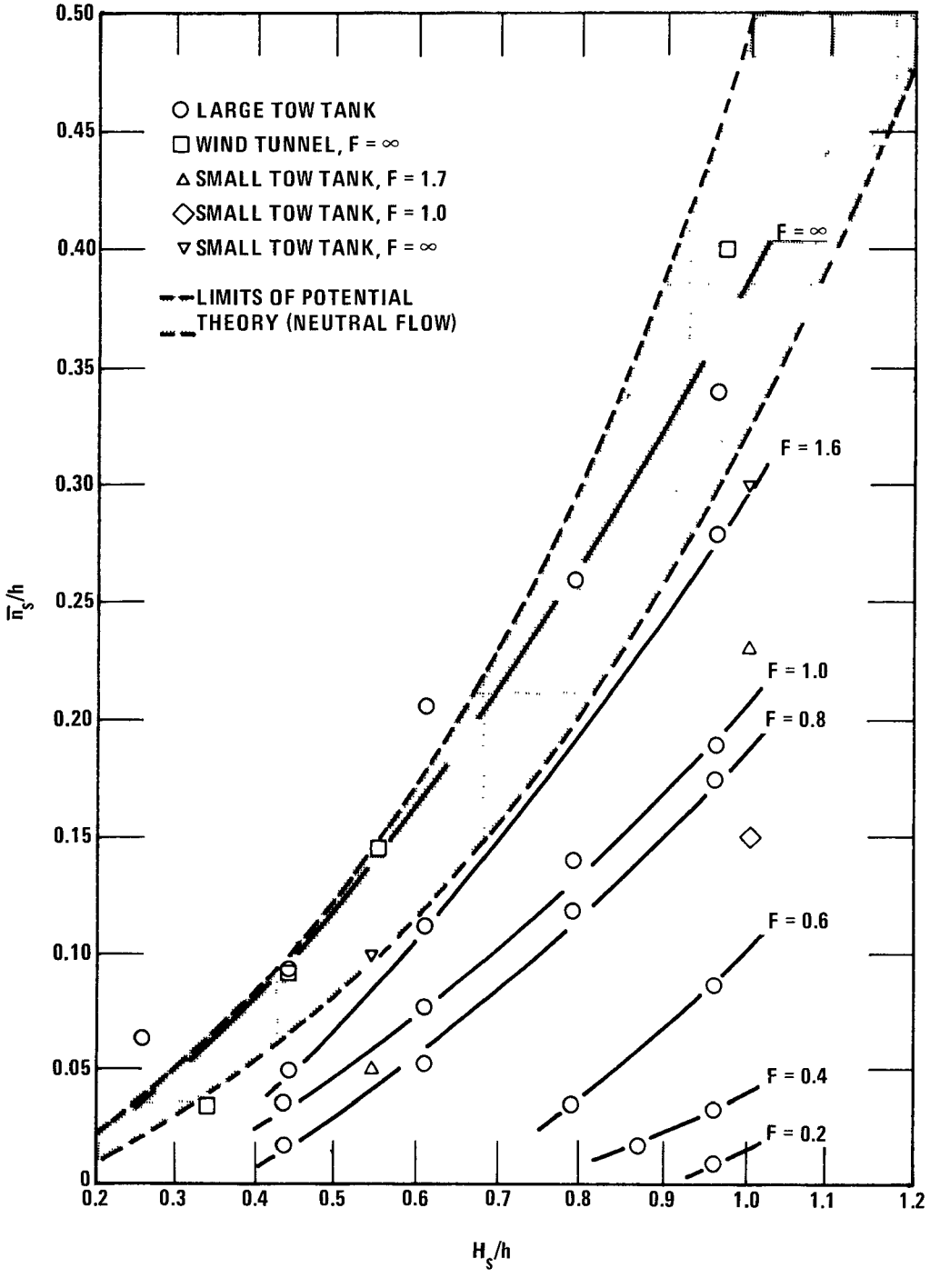

Figure 21. Displacement of streamlines above hill surface.

TECHNICAL REPORT DATA
(Please read Instructions on the reverse before completing)

1. REPORT NO.	2.	3. RECIPIENT'S ACCESSION NO.
EPA-600/4-78-041		

4. TITLE AND SUBTITLE	5. REPORT DATE
FLOW STRUCTURE AND TURBULENT DIFFUSION AROUND A THREE-DIMENSIONAL HILL Fluid Modeling Study on Effects of Stratification Part I. Flow Structure	July 1978 6. PERFORMING ORGANIZATION CODE
7. AUTHOR(S) J.C.R. Hunt[1], W.H. Snyder[2], R.E. Lawson, Jr.[3]	8. PERFORMING ORGANIZATION REPORT NO. Fluid Modeling Report No. 4
9. PERFORMING ORGANIZATION NAME AND ADDRESS Environmental Sciences Research Laboratory Office of Research and Development U.S. Environmental Protection Agency Research Triangle Park, N.C. 27711	10. PROGRAM ELEMENT NO. 1AA603 AB-20 (FY-78) 11. CONTRACT/GRANT NO.
12. SPONSORING AGENCY NAME AND ADDRESS Environmental Sciences Research Laboratory --RTP, NC Office of Research and Development U.S. Environmental Protection Agency Research Triangle Park, N.C. 27711	13. TYPE OF REPORT AND PERIOD COVERED In-house 4/1/77 - 3/31/78 14. SPONSORING AGENCY CODE EPA/600/09

15. SUPPLEMENTARY NOTES
1. University of Cambridge, England. 2. On assignment from National Oceanic and Atmospheric Administration, Dept. of Commerce. 3. Northrop Services, Inc.

16. ABSTRACT

This research program was initiated with the overall objective of gaining understanding of the flow and diffusion of pollutants in complex terrain under both neutral and stably stratified conditions. This report covers the first phase of the project; it describes the flow structure observed over a bell shaped hill (polynomial in cross section) through neutral wind tunnel studies and stably stratified towing tank studies. It verifies and establishes the limits of applicability of Drazin's theory for flow over three-dimensional hills under conditions of small Froude number. At larger Froude number a theory is developed, and largely verified, to classify the types of lee wave patterns and separated flow regions and to predict the conditions under which they will be formed. Flow visualization techniques are used extensively in obtaining both qualitative and quantitative information on the flow structure around the hill. Representative photographs of dye tracers, potassium permanganate, dye streaks, shadowgraphs, surface dye smears, and hydrogen bubble patterns are included. While emphasis centered on obtaining basic understanding of flow around complex terrain, the results are of immediate applicability by air pollution control agencies. In particular, the location of the surface impingement point from an upwind pollutant source can be identified under a wide range of atmospheric conditions. Part II, to be printed as a separate report, will describe the concentration field over the hill resulting from plumes released from upwind stacks and will further quantify the results obtained in Part I.

17. KEY WORDS AND DOCUMENT ANALYSIS

a. DESCRIPTORS	b. IDENTIFIERS/OPEN ENDED TERMS	c. COSATI Field/Group
Air pollution		13B
* Wind(meteorology)		04B
* Wind tunnel models		14B
* Hills		08F
* Atmospheric diffusion		04A
* Stratification		20D
* Flow distribution		

18. DISTRIBUTION STATEMENT	19 SECURITY CLASS *(This Report)*	21. NO. OF PAGES
RELEASE TO PUBLIC	UNCLASSIFIED	96
	20 SECURITY CLASS *(This page)*	22. PRICE
	UNCLASSIFIED	

EPA Form 2220-1 (Rev. 4-77) PREVIOUS EDITION IS OBSOLETE